A Thesis for the Degree of Doctor of Philosophy in Pharmacology

Studies on new bioactive non-ribosomal peptides and polyketides from marine-derived *Streptomyces* spp.

February 2018

Munhyung Bae

Natural Products Science Major, College of Pharmacy
Doctoral Course in the Graduate School
Seoul National University

Studies on new bioactive non-ribosomal peptides and polyketides from marine-derived *Streptomyces* spp.

Under the Direction of Prof. Dong-Chan Oh
Submitted to the Faculty of the Graduate School
Seoul National University

By
Munhyung Bae
Pharmacy in Natural Products Science Major
Doctoral Course in the Graduate School
Seoul National University

Approved as a qualified thesis of Munhyung Bae
For the degree Doctor of Philosophy in Pharmacy
By the committee members
November 2017

CHAIRMAN	Jongheon Shin	(인)
VICE-CHAIRMAN	Ki-Bong Oh	(인)
MEMBER	Sang Kook Lee	(인)
MEMBER	Sang-Jip Nam	(인)
MEMBER	Dong-Chan Oh	(인)

Abstract

Studies on new bioactive non-ribosomal peptides and Polyketides from marine-derived *Streptomyces* spp.

Munhyung Bae
Natural Products Science Major
College of Pharmacy
Doctoral Course in the Graduate School
Seoul National University

During my doctoral course, my research works were concentrated to secondary metabolites derived from marine-bacteria, which have been regarded as a prolific sources for drug discovery. Especially, my targeted compounds were divided into non-ribosomal peptides (Part A) and polyketides (Part B) from marine bacteria.

Part A. Non-ribosomal peptides from marine *Streptomyces* spp.

Nature creates a vast diversity of secondary metabolites by assembling acetate building blocks to polyketides using polyketide synthases (PKSs), by assembling amino acids to peptides using non-ribosomal peptides synthases (NRPSs). Peptide natural products are generally biosynthesized through the NRPSs with amino acids less than 40, showing characteristic UV spectra originated from aromatic amino acids and large molecular ions. Peptide natural products are structurally and biologically diverse due to incorporation of regular and non-proteinogenic amino acids As part of my efforts to search for new bioactive peptides, actinomycete strains were selectively isolated from uncommon marine

environments, intertidal mudflat. The application of a chemical analysis-based discovery strategy using LC/MS chemical profiles allowed us to discover marine *Streptomyces* sp., producing three kinds of structurally novel peptides. Mohangamides A and B, new dilactone-tethered pseudo-dimeric peptides, were discovered from an intertidal mud flat in Buan, Republic of Korea. WS9326F-I, which are new members of WS9326 class, were also obtained from strain SNM55. Additional variation of cultural condition resulted in the discovery of new antibiotic cyclic depsipeptides, hormaomycins B and C. The planar structures of those compounds were determined by 1D and 2D NMR spectroscopy, UV spectroscopy, and mass spectrometry. Mohangamides A and B are first dimeric/pseudo-dimeric peptides of WS9326s class bearing two unusual acyl chains and 14 amino acid residues. WS9326F-I were elucidated as new analogues of WS9326A bearing an unusual acyl chain and 6~7 amino units. Especially, WS9326I incorporates an unprecedented 4-amino-2,4-dihydro-3H-pyarzol-3-one and a sugar-derived moiety. Hormaomycins B and C are the first natural analogues belonging to the hormaomycin peptide class bearing structurally unique units, such as 4-(*Z*)-propenylproline, 3-(2-nitrocyclopropyl)alanine, 5-chloro-1-hydroxypyrrol-2-carboxylic acid, and *β*-methylphenylalanine. Determination of absolute configurations of amino acids were established by derivatization of Marfey's reagents and 2,3,4,6-tetra-O-acetyl-*β*-d-glucopyranosyl isothiocyanatederivatiztion (GITC), followed by LC-MS analysis. The absolute configuration of additional chiral centers of mohangamide A were determined by chemical derivatizations including methanolysis, acetylation, OsO_4 oxidation, and *bis*-benzoyl esterification followed by chromatographic and spectroscopic analyses. The absolute configuration of WS9326I were established by four of chemical steps including acetonide protection, acetylation, acetonide deprotection, and MTPA esterifications. The absolute configurations of hormaomycins B and C were determined by the comparison of ECD spectrum of hormaomycin. Mohangamide A displayed displayed strong inhibitory activity against

Candida albicans isocitrate lyase. WS9326F-I exhibited remarkable antiangiogenic activity. Hormaomycins B and C showed significant antibacterial activity.

Part B. Polyketides from marine *Streptomyces* spp.

Polyketides are any of a large class of diverse compounds that are characterized by more than two carbonyl groups connected by a intervening carbon atoms and generally biosynthesized by PKSs. Especially, NRPS-PKSs hybrid synthase are mega-synthases involved in the biosynthesis of pharmaceutically important natural products such as cyclosporin, rifamycin and erythromycin. Focusing on NRPS and PKS compounds provides better understanding on their biosynthetic mechanisms, contributing massive production and diverse derivatives by combinatorial biosynthesis. As part of my efforts to search for PKS compounds, I collected sediments from uninvestigated environments such as mudflat and volcanic Islands. Mohangic acids were isolated from a *Streptomyces* sp. SNM31 collected from mud flat in Buan, Korea. Comprehensive analysis of spectroscopic data revealed that mohangic acids A-E are new members of *p*-aminoacetophenonic acid class. The relative and absolute configurations of mohangic acids were established by chemical derivatization, application of chiral NMR solvent, and circular dichroism spectroscopy. Mohangic acid E displayed significant quinone reductase induction activity. Further investigation of *Streptomyces* sp. strain isolated from Jeju Island discovered new polyene polyols compounds, succinilenes A-D. Determination of geometry of succinilenes were performed by quantum-mechanics-driven ^{1}H iterative full spin analysis (QM-HiFSA). The absolute configuration of succinilenes were established by chemical derivatizations and chiroptical spectroscopy. Succinilenes showed significant anti-inflammatory activity except succinilene D. Ullengacenes A and B, new benz[*a*]anthracene dimer compounds linked by mono-sulfide bond, were isolated from sediment in

Ul-leungdo, Korea. The exact components of compounds were identified by energy dispersive X-ray experiments. The absolute configuration of ullengacenes were determined by combination of ECD calculations and DP4 calculations. Ullengacene A exhibited quinone reductase induction activity while ullengacene B displayed remarkable antiangiogenic activity.

Key words; marine bacteria, non-ribosomal peptides, polyketides

Student number:2013-30506

List of Contents

Abstract in English I
List of Contents V
Introduction 1
Part A. Non-ribosomal peptides from marine *Streptomyces* spp.
I. Mohangamides A and B, dilactone-tethered pseudo-dimeric peptides inhibiting *Candida albicans* isocitrate lyase. 6
II. WS9326F-I, antiangiogenic peptides belonging to WS9326 peptide class 18
III. Hormaomycins B and C: antibiotic cyclic depsipeptides from a marine mudflat-derived *Streptomyces* sp. SNM55 38

Part B. Polyketides from marine *Streptomyces* spp.
I. Mohangic acids A-E, *p*-aminoacetophenonic acids from a marine mudflat-derived *Streptomyces* sp. SNM31 74
II. QM-HiFSA-aided structure determination of succinilenes A-D, triene polyols from a marine-derived *Streptomyces* sp. SAK1 92
III. Ullengacenes A and B, dimeric benz[*a*]anthracenes linked by a mono-sulfide bond derived from volcanic island *Streptomyces* sp. SUD119. 106
Summary 146
References 154
Appendix: NMR Spectroscopic Data 160
Abstract in Korean 181
Publication List 183
Permissions for Republication of the Published Papers in Thesis 185
Acknowledgements 187

Introduction

Over the past several decades, natural products derived from microbes have served as the most efficient natural source for drug discovery and development because of relatively convenient production of lead compounds by microbial cultivation.[1] Despite the previous success of microbial natural products, the constant clinical need for bioactive compounds with structural novelty has led natural product chemists to search for chemically prolific microorganisms such as actinomycetes that inhabit relatively uninvestigated environments.[2] Marine ecosystems, covering 70% of the surface of the earth and possessing great biological diversity, have been regarded as under-investigated sources of microorganisms with biosynthetic machinery for bioactive secondary metabolites.[3] Although only a small portion of marine microbes have been chemically studied because of limited accessibility and technical problems, the discovery of promising drug leads, including an anticancer drug candidate, salinosporamide A,[4] and an antibiotic drug candidate, thiocoraline,[5] from marine actinomycetes has revealed that marine actinomycetes are particularly prolific in their production of structurally and biologically unique secondary metabolites with pharmaceutical potential.

The most of secondary metabolites produced by microbes were synthesized by two biosynthetic pathways. One is polyketide synthases (PKSs) which assemble acetate building blocks to polyketides and the other

is non-ribosomal peptides sythases (NRPSs) which assemble amino acids to peptides. Non-ribosomal peptide products are structurally and biologically diverse due to incorporation of regular and non-proteinogenic amino acids. Vancomycin are the representative peptide compound treated as most important antibiotic against penicillin-resistant pathogenic bacteria.[6] Polyketide are any of a large class of diverse compounds that are characterized by more than two carbonyl groups by intervening carbon atoms and generally biosynthesized by PKSs. Interestingly, non-ribosomal peptide synthase and polyketide synthase are sometimes incorporated as NRPS-PKS hybrid synthases. These are mega-synthases involved in the biosynthesis of pharmaceutically important natural products such as cyclosporine,[7] rifamycin,[8] and erythromycin.[9] Therefore, Focusing on NRPS and PKS compounds provides better understanding on their biosynthetic mechanisms, contributing massive production and diverse derivatives by combinatorial biosynthesis.

As part of my efforts to discover new bioactive compounds from marine microorganisms, we isolated actinomycete strains from the intertidal mudflat in Buan and volcanic Islands including Jeju and Ul-lengdo, Republic of Korea and studied their chemical profiles by LC/MS. In search for structurally novel compounds, de-repeplication step was performed by utilizing UV spectra. Woodward's rule may calculate λ_{max} values from chromophores but it is difficult to predict the shapes of UV spectra. Even λ_{max} values of two compounds are identical, these are completely different

compounds if the shapes of UV spectra are different. According to dereplication based on shapes of UV spectra and compounds data base, I discovered six class of novel peptides and polyketides.

Here, I report the structural elucidation based on the spectroscopic data, the determination of absolute configuration, and the biological activities of those compounds.

Part A

Non-ribosomal peptides from marine *Streptomyces* spp.

I. Mohangamides A and B, dilactone-tethered pseudo-dimeric peptides inhibiting *Candida albicans* isocitrate lyase

I. I. Results and discussion

Mohangamide A (**1**) was isolated as a white powder (yield: 0.7 mg/L). The molecular formula of **1** was determined to be $C_{107}H_{139}N_{17}O_{26}$ by ^{1}H and ^{13}C nuclear magnetic resonance (NMR) (Table 1) and high-resolution fast atom bombardment MS (HRFAB-MS) data (observed [M]+ ion at m/z 2078.0071, calculated [M]+ ion at 2078.0077). Careful analysis of the complicated 2D NMR spectra, including COSY, TOCSY, HSQC, and HMBC, clarified the existence of ΔMe tyrosine,[10] two leucine, two phenylalanine, two asparagine and two serine residues.

The amino acid composition was identical to that of WS9326A but was doubled, indicating that mohangamide A (**1**) possibly possessed a dimeric feature of WS9326A. Despite its dimeric feature, the ^{1}H and ^{13}C NMR spectra of **1** indicated asymmetric portions of the molecule because the numbers of ^{1}H and ^{13}C peaks were not half of the numbers of atoms indicated in its molecular formula. One of the asymmetric por-tions was elucidated as 3-[2-(1(*Z*)-pentenyl)phenyl]-2(*E*)-propenoic acid.[11] The last partial structure, which is an unu-sual acyl chain, was established by further 2D NMR analyses. First, based on COSY, a C5 (C-63 to C-67) chain was easily constructed. Additional ^{1}H-^{1}H correlations between H-63 and H-62 secured the connectivity of the chain to C-62. The H-61/H-62 correlation extended this partial structure to C-61. These connectivities were also supported by TOCSY from H-61 to H-67. The COSY correlations be-tween H-56 and H-57 verified that C-56 is located adja-cent to C-57. The ^{1}H-^{1}H

coupling constant (8.5 Hz) of the doublet olefinic signals (H-59 and H-60) secured their con-nectivity and indicated that they belong to a six-membered ring, not a linear chain. Further analysis of the HMBC spectrum assigned the dihydropyridine moiety and con-nected the amide carbon (C-55) to the ring through C-56 and C-57 (Figure 1). The double bond geometries in the acyl chain were established as 57*E*, 59*Z*, and 63*Z* by H-57/H-59 and H-63/H-64 NOESY and ROESY correlations.[12]

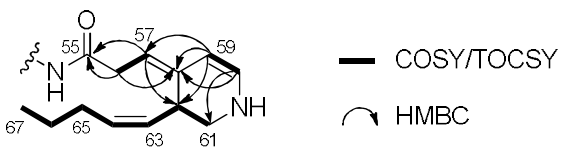

Figure 1. Key ^{1}H-^{1}H COSY/TOCSY and HMBC correlations of the acyl chain bearing dihydropyridine.

Once the partial structures were elucidated, I analyzed the HMBC correlations to connect the amino acids and the acyl chains. The sequence of the amino acids, -Thr-ΔMeTyr-Leu-Phe-Thr-Asn-Ser-, was repeated. The first acyl chain, 3-[2-(1(*Z*)-pentenyl)phenyl]-2(*E*)-propenoic acid, was connected to ^{1}Thr by the HMBC correlation from 16-NH to C-1. Similarly to the sequence of the first mole-cule half, the other acyl chain bearing dihydropyridine was assigned next to ^{8}Thr by the HMBC correlation from 69-NH to C-55, which completed two acyl chain-Thr-ΔMeTyr-Leu-Phe-Thr-Asn-Ser- substructures. These two substruc-tures were assembled through two ester linkages at ^{1}Thr-^{14}Ser and ^{7}Ser-^{8}Thr based on the H-17/C-105 and H-70/C-52 HMBC couplings, thus finalizing the planar structure of

mohangamide A (**1**). The structure was further confirmed by full NMR assignment of the methanolysis products, **3a** and **3b**. The absolute configurations of the amino acids in **1** were determined using the advanced Marfey's method.[13] Phenylalanine possessed a D-configuration, whereas the other residues (Thr, Leu, Asn, and Ser) corresponded to L-amino acids. Futher analysis by 2,3,4,6-tetra-O-acetyl-*β*- D-glucopyranosyl isothiocyanate (GITC) derivatization[14] of **1** disclosed that mohangamide A contains two allo- L-Thr and L-Thr (see Table 3). These L-Thr and allo- L-Thr units were distinguished by *J*-based configuration analyses (Figure 2).[15]

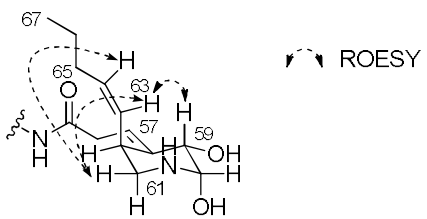

Figure 2. Key ROESY correlations of piperadine in **5**.

Although I determined the absolute configuration of the amino acids of **1**, the stereochemistry of the asymmetric carbon at C-62 in the dihydropyridine ring required fur-ther identification. Thus I designed a four-step derivatization procedure of **1** (Scheme 1). First, mohangamide A (**1**) was subjected to methanolysis to yield products **3a** and **3b**, which were utilized to confirm the planar structure of **1** *vide supra*. Product **3b**, which bears the C-62 stereogenic center, was acetylated. The major product, tetraacetate **4**, deprived of hydroxyl groups, was then oxidized by using OsO_4[16] to introduce vic-inal diol groups into the double bond in the

dihydropyridine ring. After 3 hours, the major product (compound **5**) was obtained, in which original olefinic methines in the dihy-dropyridine ring were replaced with vicinal hydroxyl groups [δ_C59 71.4-δ_H59 3.91; δC60 73.4-δH60 3.78].

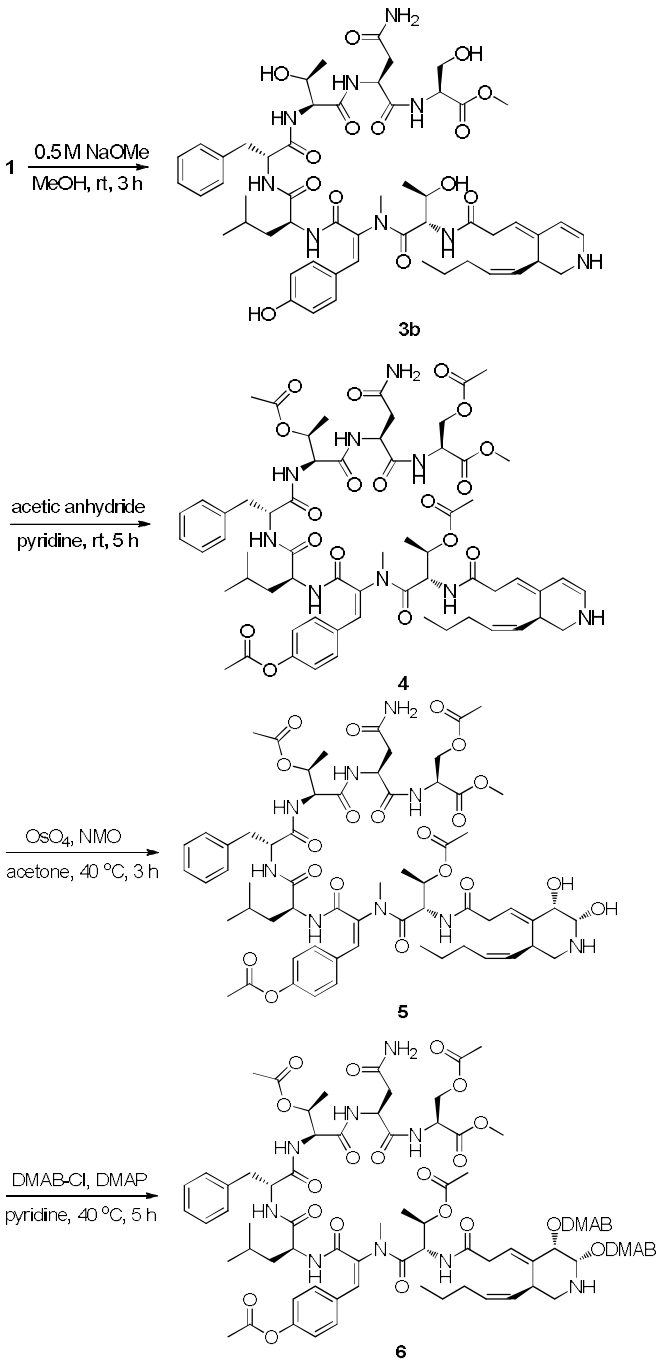

Scheme 1. A four-step derivatization scheme to determine the absolute configuration of dihydropyridine in **1**.

The relative configurations of the ring in **5** were established as 59*S**, 60*S**, 62*S** by analyzing the ROESY data (Figure 2). Finally, I derivatized the introduced diol in 5 with 4-(dimethylamino) benzoyl chloride (DMAB-Cl) to form a DMAB diester and induce exciton coupling in circular dichroism (CD).[17] The CD spectrum of **6** exhibited a negative bisignate signal and established the anticlockwise configuration of the diol (Figure 3). Therefore, the absolute configurations of the stereogenic centers in the ring of **5** were determined as 59*S*, 60*S*, and 62*S* and were finally assigned as 62*S* in mohangamide A (**1**).

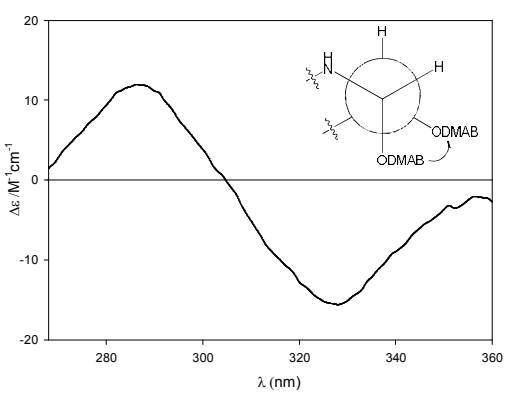

Figure 3. The exciton coupling CD spectrum of **6** to determine the absolute configuration of C-62 in **1**.

Mohangamide B (**2**) was obtained as a white powder (yield: 0.4 mg/L). The molecular formula, $C_{106}H_{139}N_{17}O_{26}$, was determined based on

^{1}H and ^{13}C spectroscopic data (Table 2) and HRFAB-MS (observed [M+Na]+ ion at m/z 2088.9971, calculated [M+Na]+ at 2088.9975). The planar structure of **2** was determined by careful comparison of the 1D and 2D NMR data of **1** and **2**, which revealed that the ^{8}Thr and ^{9}ΔMeTyr residues in **1** were respectively replaced by ^{8}Ser and ^{9}N-MeTyr in **2**. Determination of the absolute configuration of the amino acids in **2** was conducted using the same procedure as for **1**. The absolute configurations of the amino acid units commonly existing in **1** and **2** were identical. Different units, such as ^{8}Ser and ^{9}N-MeTyr, were determined to be the L-form. The absolute configuration of the dihydropyridine ring was determined to be the same as **1** based on the identical ^{1}H and ^{13}C NMR chemical shifts, ^{1}H-^{1}H coupling constants and their common biosynthetic origin.

The structures of the mohangamides are unique in several ways. In my comprehensive literature search, comparable or similar structures to that of the unusual acyl chain-bearing dihydropyridine discovered in **1** and **2** could not be found. Moreover, the dilactone-tethered, pseudo-dimeric feature is extremely rare. To my best knowledge, the only class of peptide dimer natural products connected with dilactone is echinomycin and its analogues.[18] Furthermore, the mohangamides bear 14 amino acid units, whereas the echinomycin class incorporates ten amino acids in total. Therefore, the mohangamides are the largest characterized dilactone-tethered, dimeric cyclic peptides. For echinomycin, its biosynthetic modules iterate the synthesis of two peptide chains, and the terminal thioesterase

domain catalyzes the dimerization of the peptide chain and concomitant cyclization.[19] Therefore, dimeric peptides have not been detected together with their monomers. Surprisingly, the mohangamides were discovered with their monomer WS9326A, which is unprecedented and intriguing regarding the specificity of iteration and the function of thioesterase in nonribosomal peptide biosynthesis.

The biological activities of the mohangamides were pri-marily evaluated against *C. albicans* ICL. Mohangamide A (1) displayed significant inhibition against ICL with an IC_{50} value of 4.4 μM, which was three times more potent than the positive control, 3-nitropropionate (IC_{50} = 14.1 μM). Mohangamide B (**2**) exhibited moderate ICL inhibition (IC_{50} = 20.5 μM). Interestingly, the monomeric compound WS9326A, methanolysis products **3a** and **3b** and tetraacetate (**4**) did not inhibit ICL (IC_{50} > 100 μM), indicating that the dimeric feature is required for ICL inhibition. Overall, my evaluation suggests that the mohangamides could represent the first peptide class of ICL inhibitors, as peptide-derived compounds have not been reported to inhibit ICL.

I further investigated the biological activities of **1** and **2** in cell-based antifungal assays against *C. albicans*, *Aspergillus fumigatus*, *Trichophyton rubrum*, and *T. mentagrophytes*. However, these compounds did not show sig-nificant antifungal activity when the fungi were fed glucose. Interestingly, mohangamide A (**1**) inhibited *C. albicans* grown on acetate, which indicates that the ICL is crucial in the proliferation of the fungus on

C2 substrates (Figure 4).

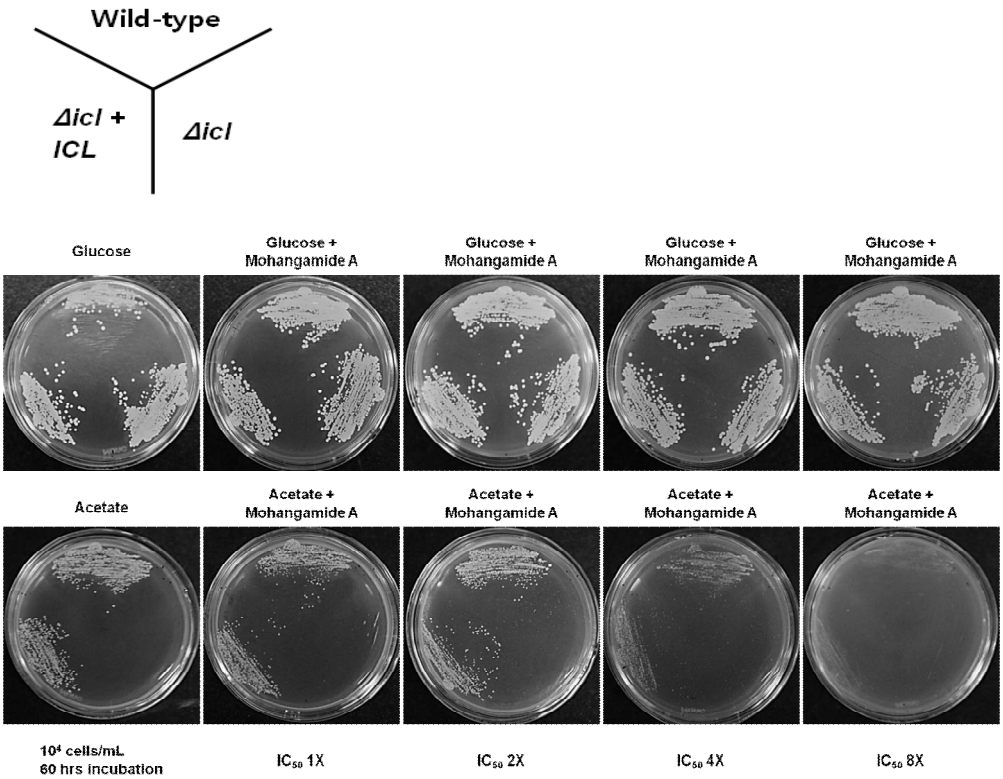

Figure 4. Inhibitory activity of mohangamide A against the growth of *C. albicans* wild-type and Δ*icl* mutants. *C. albicans* strain SC5314 (wild-type), MRC10 (Δ*icl*), and MRC11 (Δ*icl* + *ICL*) were grown in a 6.7% YNB containing 2% glucose for 24 h at 28 °C, collected by centrifugation, and washed twice with sterile distilled water.* Cells (104 cells/mL) were cultured on YNB agar plates containing the indicated carbon source (2% glucose or 2% sodium acetate) with or without mohangamide A for 60 h at 28 °C.

*It is widely known that a number of "macromolecules', primarily microbes and their toxins, manage to enter the organism through cell physical barriers by endocytotic mechanisms. For the mechanisms of macromolecule delivery, please see the review papers:

- Belting, M.; Sandgren, S.; Wittrup, A. Nuclear delivery of macromolecules: barriers and carriers. *Advanced Drug Delivery Reviews* **2005**, *57*, 505-527.

- Conner, S. D.; Schimid, S. L. Regulated portals of entry into the cell. *Nature* **2003**, *422*, 37-44.

Yeasts also have endocytotic mechanism. Please see the review paper:

- Boettner, D. R.; Chi, R. J.; Lemmon, S. K. Lessons from yeast for clathrin-mediated endocytosis. *Nature Cell Biology* **2012**, *14*, 2-10.

The fact that mohangamide A inhibited the *Candida* mutant and wild type strains on acetate also indicates its internalization to the cells.

The mohangamides did not display antibacterial activity against *Staphylococcus aureus*, *Bacillus subtilis*, *Kocuria rhizophila*, *Salmonella enterica*, *Proteus hauseri*, or *Escherichia coli*. In addition, the mohangamides showed no cytotoxicity against the tested human carcinoma cell lines, A549, HCT116, SNU638, K562, SK-HEP1, or MDA-MB231.

In conclusion, I discovered mohangamides A and B (**1**-**2**) as inhibitors of *C. albicans* ICL from a marine actinomycete *Streptomyces* sp. derived from an intertidal mud flat. Mohangamides are structurally novel and biosynthetically interesting because they possess a unique dihydro-pyridine acyl chain and a dilactone-tethered, dimeric cyclic peptide structure discovered along with a monomeric structure.

Table 1. ^{1}H and ^{13}C NMR Data of **1** in DMSO-d_6[a]

No.	δ_H, mult (J in Hz)	δ_C	No.	δ_H, mult (J in Hz)	δ_C
1	–	171.5, s	55	–	171.6, s
2	6.94, 1H, d (15.0)	125.8, d	56	2.83, 1H, m	34.5, t
3	7.30, 1H, m	129.3, d		3.08, 1H, m	
4	–	141.5, s	57	5.10, 1H, m	119.5, d
5	7.28, 1H, m	126.7, d	58	–	137.2, s
6	7.15, 1H, t (7.5)	126.8, d	59	6.39, 1H, d (8.5)	124.2, d
7	7.09, 1H, t (7.5)	126.0, d	60	5.83, 1H, d (8.5)	132.8, d
8	6.99, 1H, d (7.5)	129.7, d	61	2.88, 2H, brs	36.5, t
9	–	137.1, s	62	3.03, 1H, m	37.5, d
10	6.31, 1H, d (10.5)	129.3, d	63	5.17, 1H, m	132.3, d
11	5.63, 1H, m	132.7, d	64	5.18, 1H, m	129.2, d
12	1.95, 1H, m	30.5, t	65	1.85, 2H, m	29.3, t
	2.03, 1H, m		66	1.23, 2H, m	22.5, t
13	1.35, 2H, m	22.8, t	67	0.77, 3H, t (7.5)	22.3, q
14	0.83, 3H, t (7.5)	14.3, q	68	–	169.7, s
15	–	169.7, s	69	5.19, 1H, d (8.0)	53.5, d
16	5.22, 1H, d (8.0)	53.4, d	69-NH	8.37, 1H, brs	
16-NH	8.39, 1H, brs		70	4.91, 1H, m	73.6, d
17	4.97, 1H, m	73.7, d	71	1.08, 3H, d (6.0)	17.2, t
18	1.11, 3H, d (6.0)	17.0, q	72	2.98, 3H, s	34.5, t
19	2.97, 3H, s	34.7, q	73	–	166.1, s
20	–	166.2, s	74	–	129.0, s
21	–	128.9, s	75	6.00, 1H, s	132.2, d
22	5.99, 1H, s	132.0, d	76	–	123.5, s
23	–	123.3, s	77	7.24, 1H, d (8.0)	132.4, d
24	7.35, 1H, d (8.0)	132.3, d	78	6.62, 1H, d (8.0)	115.4, d
25	6.60, 1H, d (8.0)	115.5, d	79	–	158.4, s
26	–	158.5, s	80	6.62, 1H, m	115.4, d
27	6.60, 1H, m	115.5, d	81	7.24, 1H, m	132.4, d
28	7.35, 1H, m	132.3, d	82	–	172.4, s
29	–	172.6, s	83	4.04, 1H, m	54.2, d
30	4.07, 1H, m	54.0, d	83-NH	9.22, 1H, brs	
30-NH	9.23, 1H, brs		84	1.25, 2H, m	39.6, t
31	1.26, 2H, m	39.5, t	85	0.87, 1H, m	23.4, d
32	0.87, 1H, m	23.6, d	86	0.67, 3H, d (7.0)	23.4, q
33	0.65, 3H, d (7.0)	23.2, q	87	0.74, 3H, d (7.5)	22.4, q
34	0.75, 3H, d (7.5)	22.2, q	88	–	170.6, s
35	–	170.7, s	89	4.33, 1H, m	56.4, d
36	4.35, 1H, m	56.5, d	89-NH	9.13, 1H, brs	
36-NH	9.18, 1H, brs		90	2.75, 1H, m	36.7, t
37	2.72, 1H, m	36.9, t		3.28, 1H, m	
	3.26, 1H, m		91	–	139.3, s
38	–	139.5, s	92	7.31, 1H, m	129.6, d
39	7.32, 1H, m	129.5, d	93	7.26, 1H, m	128.6, d
40	7.27, 1H, m	128.5, d	94	7.19, 1H, m	126.3, d
41	7.20, 1H, m	126.5, d	95	7.26, 1H, m	128.6, d
42	7.27, 1H, m	128.5, d	96	7.31, 1H, m	129.6, d
43	7.32, 1H, m	129.5, d	97	–	170.4, s
44	–	170.5, s	98	4.27, 1H, m	57.5, d
45	4.32, 1H, m	57.7, d	98-NH	7.61, 1H, brs	
45-NH	7.59, 1H, brs		99	4.14, 1H, m	68.5, d
46	4.20, 1H, m	68.6, d	100	0.58, 3H, m	22.2, q
47	0.56, 3H, m	22.3, q	101	–	171.9, s
48	–	172.0, s	102	4.41, 1H, m	51.2, d
49	4.46, 1H, m	51.3, d	102-NH	8.27, 1H, brs	
49-NH	8.32, 1H, brs		103	2.40, 2H, m	36.9, t
50	2.42, 2H, m	37.2, t	104	–	171.7, s
51	–	171.6, s	105	–	169.3, d
52	–	169.5, s	106	4.29, 1H, m	56.0, d
53	4.38, 1H, m	55.7, d	106-NH	8.26, 1H, brs	
53-NH	8.44, 1H, brs		107	2.97, 2H, m	61.1, t
54	3.26, 2H, m	61.4, t			

[a] ^{1}H and ^{13}C NMR were recorded at 900 and 225 MHz, respectively.

Table 2. ^{1}H and ^{13}C NMR Data of **2** in DMSO–d_6[a]

No.	δ_H, mult (J in Hz)	δ_C	No.	δ_H, mult (J in Hz)	δ_C
1	–	172.7, s	55	–	172.5, s
2	6.83, 1H, d(15.0)	125.8, d	56	2.78, 1H, m	36.5, t
3	7.24, 1H, m	127.3, d		3.08, 1H,	
4	–	141.6, s		dd (16.0, 8.0)	
5	7.17, 1H, d (7.5)	129.2, d	57	5.24, 1H, m	118.9, d
6	7.14, 1H, m	129.9, d	58	–	137.0, s
7	7.07, 1H, t (7.5)	125.9, d	59	6.26, 1H, d (8.0)	124.7, d
8	6.98, 1H, d (7.5)	126.9, d	60	5.76, 1H, d (8.0)	132.8, d
9	–	137.2, s	61	2.86, 2H, m	36.2, t
10	6.29, 1H, d (10.5)	129.3, d	62	2.97, 1H, m	37.6, d
11	5.60, 1H, m	132.8, d	63	5.08, 1H,	132.3, d
12	1.98, 1H, m	30.5, t		dd (10.5, 6.5)	
	2.03, 1H, m		64	5.13, 1H, m	129.3, d
13	1.33, 2H, m	22.8, t	65	1.83, 2H, m	37.3, t
14	0.82, 3H, t (7.5)	23.8, q	66	1.18, 2H, m	29.4, t
15	–	169.7, s	67	0.76, 3H, t (7.5)	22.8, q
16	5.17, 1H, d (8.0)	53.4, d	68	–	170.4, s
16-NH	8.37, 1H, brs		69	4.99, 1H, d (8.0)	48.5, d
17	4.91, 1H, m	73.5, d	69-NH	8.73, 1H, brs	
18	1.07, 3H, d (6.0)	16.9, q	70	2.00, 1H, m	73.6, d
19	2.94, 3H, s	34.7, q		3.77, 3H, d (6.0)	17.2, q
20	–	170.0, s	71	2.60, 3H, s	28.9, q
21	–	129.2, s	72	–	169.3, s
22	5.96, 1H, s	132.0, d	73	5.41, 1H, m	61.9, d
23	–	123.3, s	74	2.92, 2H, m	33.2, t
24	7.24, 1H, m	132.5, d	75	–	123.3, s
25	6.58, 1H, d (7.5)	115.5, d	76	7.03, 1H, d (7.5)	132.6, d
26	–	158.5, s	77	6.61, 1H, d (7.5)	115.2, d
27	6.58, 1H, d (7.5)	115.5, d	78	–	158.5, s
28	7.24, 1H, m	132.3, d	79	6.61, 1H, d (7.5)	115.2, d
29	–	173.0, s	80	7.03, 1H, d (7.5)	132.6, d
30	4.03, 1H, m	54.1, d	81	–	170.6, s
30-NH	9.15, 1H, brs		82	4.33, 1H, m	50.5, d
31	1.24, 2H, m	29.6, t	82-NH	8.90, 1H, brs	50.5, d
32	0.85, 1H, m	23.9, d	83	1.23, 2H, m	39.2, t
33	0.63, 3H, d (7.0)	23.4, q	84	1.18, 1H, m	24.4, d
34	0.75, 3H, d (7.5)	22.5, q	85	0.70, 3H, d (7.0)	22.8, q
35	–	170.7, s	86	0.70, 3H, d (7.0)	22.8, q
36	4.33, 1H, m	56.5, d	87	–	170.8, s
36-NH	9.11, 1H, brs		88	4.57, 1H, m	53.9, d
37	2.69, 1H, m	36.8, t	88-NH	8.07, 1H, brs	
	3.25, 1H, m		89	2.80, 1H, m	36.5, t
38	–	139.5, s		3.22, 1H, m	
39	7.32, 1H, m	129.8, d	90	–	138.5, s
40	7.26, 1H, m	128.5, d	91	7.31, 1H, m	129.8, d
41	7.20, 1H, m	126.5, d	92	7.25, 1H, m	128.6, d
42	7.26, 1H, m	128.5, d	93	7.20, 1H, m	126.3, d
43	7.32, 1H, m	129.8, d	94	7.25, 1H, m	128.6, d
44	–	170.4, s	95	7.31, 1H, m	129.8, d
45	4.27, 1H, m	57.6, d	96	–	171.3, s
45-NH	7.58, 1H, brs		97	4.38, 1H, m	57.5, d
46	4.13, 1H, m	68.6, d	97-NH	6.83, 1H, brs	
47	0.57, 3H, d (5.0)	22.3, t	98	4.14, 1H, m	68.5, d
48	–	172.0, s	99	0.94, 3H, m	21.2, q
49	4.39, 1H, m	51.3, d	100	–	172.4, s
49-NH	8.26, 1H, brs		101	4.69, 1H, m	51.8, d
50	2.38, 2H,	37.2, t	101-NH	8.81, 1H, brs	
	dd (14.5, 9.0)		102	2.54, 2H, m	37.0, t
51	–	171.8, s	104	–	169.4, s
52	–	169.5, s	105	4.36, 1H, m	57.0, d
53	4.26, 1H, m	55.9, d	105-NH	8.35, 1H, brs	
53-NH	8.25, 1H, brs		106	3.60, 2H, m	61.3, t
54	2.90, 2H, m	61.5, t			

[a] ^{1}H and ^{13}C NMR were recorded at 900 and 225 MHz, respectively.

Table 3. LC/MS analysis of the FDAA derivatives of mohangamides A and B (**1** and **2**).

Mohangamide A (**1**)				Mohangamide B (**2**)			
Amino acid	Elution order	t_{RL} (min)	t_{RD} (min)	Amino acid	Elution order	t_{RL} (min)	t_{RD} (min)
Thr (L)	L → D	10.5	13.0	Thr (L)	L → D	10.5	13.0
Leu (L)	L → D	25.0	29.0	Leu (L)	L → D	25.0	29.0
Phe (D)	D → L	28.4	25.0	Phe (D)	D → L	28.4	25.0
allo Thr (L)	L → D	9.9	11.7	*allo* Thr (L)	L → D	9.9	11.7
Asp (L)	L → D	10.8	11.4	Asp (L)	L → D	10.8	11.4
Ser (L)	L → D	9.7	10.0	Ser (L)	L → D	9.7	10.0
				N-MeTyr (L)	L → D	9.7	9.9

II. WS9326F-I, antiangiogenic peptides belonging to WS9326 peptide class

II. I. Results and discussion

WS9326F (**7**) was obtained as a white powder, having the molecular formula as $C_{53}H_{68}N_8O_{13}$ (unsaturation number: 24) determined by HR-FAB mass spectroscopy (obsd $[M+H]^+$ at *m/z* 1025.4983, calcd $[M+H]^+$ 1025.4984), and ^1H and ^{13}C NMR data (Table 4). The ^1H NMR spectrum showed a highly analogous pattern of WS9326A, including six NH signals (δ_H 9.18, 9.17, 8.90, 8.56, 8.51, and 7.28) and seven α-proton signals (δ_H 5.52, 5.33, 4.81, 4.70, 4.43, 4.41, and 4.33). The ^{13}C NMR spectrum indicated that there exist nine carbonyl signals (δ_C 172.2, 171.4, 170.7, 170.3, 170.2, 169.7, 169.4, 166.4, and 166.3) and ten carbons in the resonance region of α–carbons or oxygenated carbons (69.2, 63.7, 61.6, 60.8, 56.9, 56.1, 56.0, 52.8, 51.1, and 48.1).

Because the major metabolite, WS9326A was already reported previously, the planar structure of WS9326F (**7**) was assigned by careful comparison of 1D and 2D NMR spectra including COSY, HSQC, HMBC, and TOCSY between with those of WS9326A. In addition, comparing their molecular formulae ($C_{53}H_{68}N_8O_{13}$ for **7**) and ($C_{54}H_{68}N_8O_{13}$ for WS9326A) clearly indicated that WS9326F (**7**) possesses one carbon and two hydrogen atoms less than WS9326A. Detailed analysis of the NMR spectra of **7** revealed that one methyl group and one double bond are mixing, thus accounting for the difference between **7** and WS9326A. After 1-bond C-H correlations were completely assigned based on the HSQC NMR spectrum, COSY, HMBC, and TOCSY NMR spectra were analyzed to elucidate seven

amino acid units and one acyl chain. WS9326F was revealed to incorporate two serine, an *N*-Me-tyrosine, a leucine, a phenylalanine, a threonine, and an asparagine units as well as 3-[2-(1(*Z*)-pentenyl)phenyl]-2(*E*)-propenoic acid. These units accounted for 23 of 24 double bond equivalents deduced from the molecular formula with three aromatic rings (12 equivalents), two double bonds (two equivalents), nine carbonyl functional groups (9 equivalents). Therefore the structure of **7** must possess an additional ring to explain the last double bond equivalent.

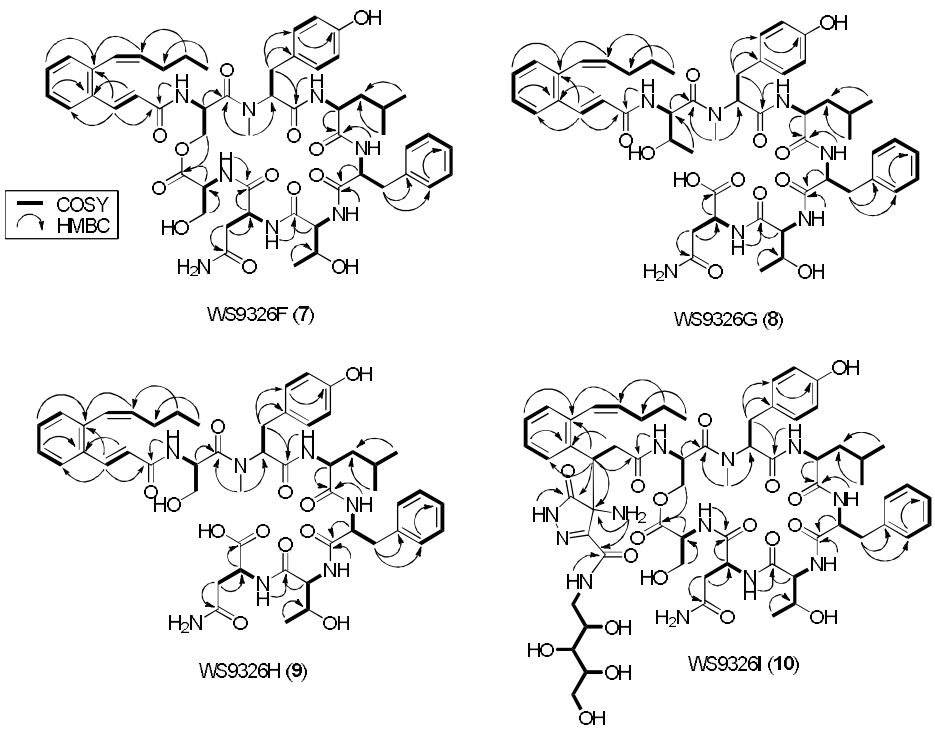

Figure 5. Key COSY and HMBC correlations for the structures elucidations of **7**-**10**.

Even though the amino acid sequence of **7** was expected to be similar to that of WS9326A, the existence of two serine units, one of which replaced a

threonine, required a comprehensive analysis of HMBC correlations to determine the sequence of the seven amino acid residues and the acyl chain (Figure 4). First, 16-NH (δ_H 9.17) of Ser-1 showed an HMBC correlation with the C-1 carbonyl carbon (δ_C 166.4). The olefinic protons (H-2; δ_H 6.44, H-3; δ_H 7.77) belonging to 3-[2-(1(*Z*)-pentenyl)phenyl]-2(*E*)-propenoic acid (PPPA) also displayed clear cross peaks with C-1 in the HMBC spectrum, indicating that the acyl group is connected directly to Ser-1. Furthermore the α–proton of Ser-1 (δ_H 5.33) showed an HMBC correlation with C-15 (δ_C 170.2; carbonyl carbon of Ser-1), which also correlated with *N*-Me protons (H_3-18; δ_H 2.62) of *N*-Me-Tyr in the HMBC spectrum, establishing the connectivity between Ser-1 and *N*-Me-Tyr. The amino acid residue next to N-Me-Tyr was assigned as Leu based on the HMBC correlation from 29-NH (δ_H 9.18; the amide proton of Leu) and H-20 (δ_H 5.52; α-proton of *N*-Me-Tyr) to C-19 (δ_C 166.3; the amide carbon of *N*-Me-Tyr). The Phe unit was connected to Leu on the basis of the HMBC correlation from the amide proton of Phe (35-NH; δ_H 8.56) and the α-proton of Leu (H-29; δ_H 4.33) to the carbonyl carbon of Leu (C-28; δ_C 169.4). The HMBC signals from 44-NH (the amide proton of Thr; δ_H 7.28) and H-35 (the α-proton of Phe; δ_H 4.81) to C-34 (the amide carbon of Phe; δ_C 170.3) clarified the sequence from Phe to Thr. The 2-bond $^{1}H–^{13}C$ coupling from 48-NH (δ_H 8.90) and H-44 (δ_H 4.41) to C-43 (δ_C 170.7) established the connectivity Asn next to Thr. Further analysis of HMBC NMR data elucidated the connectivity between Asn and Ser-2 based on the HMBC correlation from NH of Ser-7 at δ_H 8.51

and the α–proton of Asn-6 at δ_H 4.70 to the amide carbon of Asn-6 (C-47; δ_C 172.2). Finally, Ser-2 was revealed to cyclize the peptide chain to Ser-1 by an ester linkage based on the HMBC signals from H_2-17 (δ_H 3.80; δ_H 1.97) to C-51 (δ_C 169.7), thus completing the planar structure of WS9325F (**7**).

WS9326G (**8**) was isolated as a white powder. The molecular formula of **8** was established as $C_{51}H_{65}N_7O_{12}$ based on the analysis of HRFAB mass spectroscopic data (obsd $[M+Na]^+$ at *m/z* 990.4598, calcd $[M+Na]^+$ 990.4589) along with the NMR spectra (Table4). The difference between the molecular formulae of **7** and **8** was C_2H_3NO, which could not be explained simply by the disappearance of an amino acid. The comparing analysis of 1D and 2D NMR data including HSQC, COSY, TOCSY, and HMBC spectra of **7** and **8** identified two Thr, ΔN-Me-Tyr, Leu, Phe, and Asn residues as well as 3-[2-(1(*Z*)-pentenyl)phenyl]-2(*E*)-propenoic acid (PPPA) in WS9326G (**2**). The sequence of the amino acids and the acyl chain was assigned based on HMBC correlations. Therefore the structure of WS9326G (**2**) was determined as a linear peptide with the sequence of PPPA, Thr, ΔN-Me-Tyr, Leu, Phe, Thr, and Asn. The structural difference of **8** compared with **7** was originated from the replacement of Ser-1 and N-Me-Tyr in **7** with Thr and ΔN-Me-Tyr and the loss of Ser-2 from **8**.

WS9326H (**9**) was isolated as a white powder, of which molecular formula, $C_{50}H_{63}N_7O_{12}$, was assigned by the analysis of HRFAB mass spectroscopic data (obsd $[M+Na]^+$ at *m/z* 976.4438, calcd $[M+Na]^+$ 976.4432) and ^1H and ^{13}C NMR spectra (Table1). The difference in the

molecular formulae of **8** and **9** was just CH_2, which indicated a loss of methyl or methylene group. By extensive comparison of COSY, HSQC, HMBC, and TOCSY, one of the methyl groups in the two Thr units in **8** disappeared and an additional methylene group (δ_H 3.53, δ_H 3.74; δ_C 61.2) showed up instead, proving that one of the threonines of **2** was replaced with Ser in **9**. Further analysis of HMBC correlations elucidated the sequence of the discrete units. The sequence indicated that the Thr residue next to the acyl chain in **8** was replaced by Ser in **9**.

WS9326I (**10**) was purified as a white powder, having having the molecular formula as $C_{63}H_{84}N_{12}O_{19}$ determined by HR-FAB mass spectroscopy (obsd $[M+Na]^+$ at *m*/*z* 1335.5966, calcd $[M+Na]^+$ 1335.5878), and ^1H and ^{13}C NMR data (Table 4). Careful comparison of NMR spectroscopic data revealed that amino units were identical with those of WS9326A but interestingly, WS9326I (**10**) incorporates an unprecedented 4-amino-2,4-dihydro-3H-pyarzol-3-one and a sugar-derived moiety. It is first WS9326 analogue which has modified starting unit, not amino units. Further analysis of ^{15}NHSQC identified all of nitrogen signals including pyrazole NH_2 protons (δ_H 2.72), indicating δ_H 2.72 was real signal related on pyrazolone moiety. However, there was a problem in constructing the pyrazolne ring by HMBC correlations. None of HMBC signals from pyrazole NH_2, amide nitrogens (δ_H 12.76 and δ_H 8.87) were not correlated with quaternary carbon (δ_C 156.1) in pyrazolone ring. To confirm the planar sturucture of pyrazolone ring, carbon-nitrogen selective hydrogenation using

$NaBH_3CN$ was conducted (Figure 6).[20] The hydrogenation product (**11**) was successfully purified and analyzed by HSQC and HMBC NMR data, establishing 4-amino-1*H*-pyrazol-5-one ring structure.

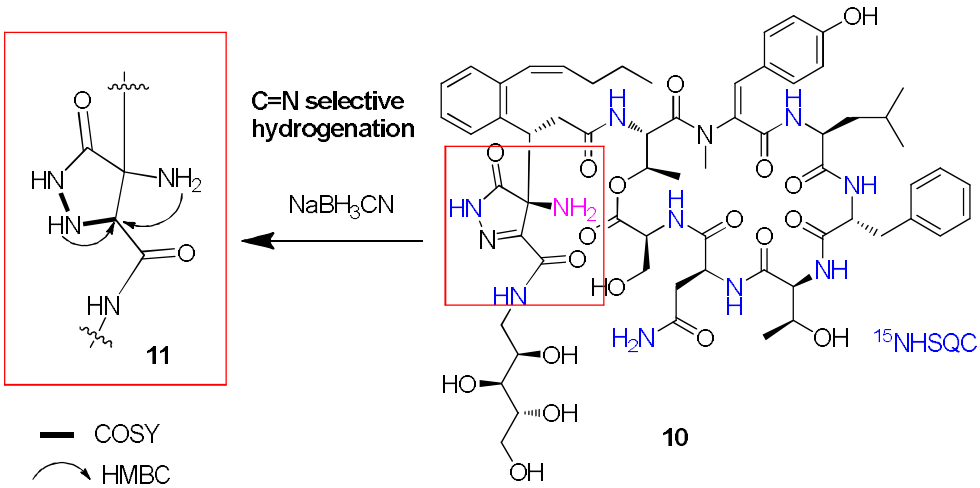

Figure 6. The elucidation of the 4-amino-2,4-dihydro-3H-pyrazol-3-one ring by ^{15}NHSQC and imine-selective reduction followed by COSY and HMBC experiments

The absolute configurations of the amino acid residues in WS9326F (**7**) were established by the advanced Marfey's method.[13] WS9326F (**7**) was hydrolyzed in 6 N HCl at 115 °C for 2 h and the hydrolysate was derivatized with L- and D-FDAA ((1-fluoro-2,4-dinitrophenyl-5)-L-alanine amide). The derivatives were subsequently analyzed by LC/MS, clarifying the L-configurations for Ser-1, N-Me-Tyr, Leu, Thr, Asn, and Ser-2. The Phe residue was assigned to possess D-configuration (Table 4). Because Thr has an additional stereogenic center at the β-position, the retention times of L- and D-FDAA adducts of authentic L-Thr and L-*allo*-Thr were compared in

the LC/MS analysis. But the difference of retention times of products was not clear to determine whether L-Thr or L-*allo*-Thr is. To overcome the problem, I decide to apply O-marfey's method which was reported in mylaboratory previously. O-marfey's method was developed to determine the absolute configurations of α-hydroxy acids attaching L-FDAA to hydroxy groups. Because threonine has β-hydroxy group, not α-position, I planned to attach L-FDAA to both of side including nitrogen at amide bond. Fortunately, I could obtain both of L-FDAA derivatives and L-Thr-L-FDAA-L-FDAA derivatives successfully. Through LC/MS analysis, I found out L-Thr-L-FDAA-L-FDAA product eluted 1.5 min later than L-*allo*-Thr-L-FDAA-L-FDAA product. Based on the retention times, WS9326F (**1**) turned out to bear L-*allo*-Thr, not Thr. The absolute configurations of amino acids in **8**, **9** and **10** were also determined by the same method. As expected by their identical biosynthetic origin with **7**, their amino acids turned out to have L-configuration except Phe. The Thr residue between D-Phe and Asn in **8** was elucidated as L-*allo*-Thr, thus establishing the sequence of PPPA, L-Thr, ΔN-Me-Tyr, L-Leu, D-Phe, L-*allo*-Thr, and L-Asn. Analogously, the complete sequence of **9** was assigned as PPPA, L-Ser, ΔN-Me-Tyr, L-Leu, D-Phe, L-*allo*-Thr, and L-Asn. Following the above derivatives, the complete sequence of **10** was determined as PPPA, L-Thr, ΔN-Me-Tyr, L-Leu, D-Phe, L-*allo*-Thr, L-Asn, and L-Ser.

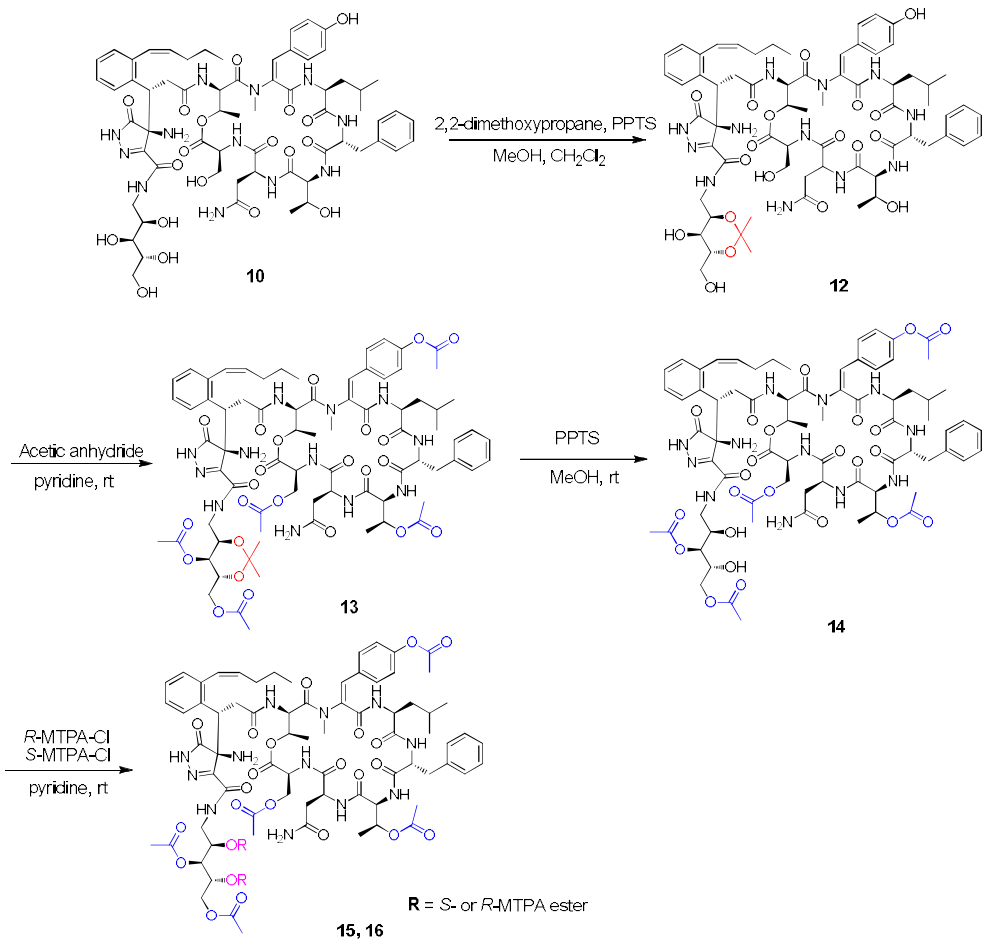

Scheme 2. A four-step derivatization shceme to determine the absolute configuration of aminosugar in 10.

However, determination of absolute configurations of additional chiral centers in modified starting unit of **10** was challenging problem. I decided to determine the absolute configuration of aminosugar moiety initially by four steps of chemical derivatization (Scheme 2). First, WS9326I (**10**) was subjected to acetonide to yield product **12**, which protected 1,3 diols in aminosugar moiety in **10**. Then, ^{1}H and HSQC NMR spectra of the acetonide derivative (**12**) displayed that the ^{1}H and ^{13}C chemical shifts of

two acetonide methyl groups are almost identical (δ_C 25.6−δ_H 1.31; δ_C 25.6−δ_H 1.31), indicating an *anti* relationship of the 1,3-hydroxy groups (Figure 7).[21] The relative configuration of second hydrolxyl group was determined on the basis of the small $^3J_{H20H21}$ value (4.5 Hz) and large $^3J_{H21H22}$ value (9.0 Hz), establishing the relative configurations of hydroxyl groups as *S**, *R**, and *S**. After then, the hydroxyl groups in product **12** was acetylated except protected 1,3 diols. The main product, pentaacetate **13**, was then deprotected by PPTS to restore 1,3 diols for Mosher derivatization. Finally, I derivatized deprotected 1,3 diols in product **14** with methoxy-*α*-trifluoromethylphenylacetyl chloride (MTPA-Cl) to form MTPA diester and analyzed product **15** and **16**, determining the absolute configurations of three hydroxyl groups as *S*, *R*, and *S*.

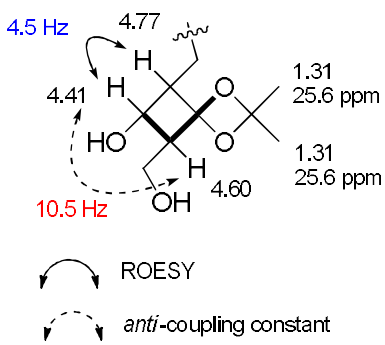

Figure 7. ^{1}H and ^{13}C NMR chemical shifts of acetonide derivative (**12**) indicating *anti* relationship of 1,3-diol with *J* value analysis.

After determination of the absolute configuration of aminosugar in **10**, I had to identify the remained stereogenic centers in pyrazolone ring. Due to quaternary position of C-17, it was hard to find applicapable chemical

derivatization. Consequently, DP4 calculation which was developed by Prof. Goodman group to support the prediction of NMR shielding tensor was conducted.[22] For accuracy of DP4 calculation, the molecular weight of target structure was limited under 500 dalton. Four of target structures were modeled and the conformational search was conducted. Accodingly, DP4 possibility analyses were conducted on 120 possible conformers of four models with experimental and predicted chemical values. Interestingly, the outcome indicated that isomer 4 model with 3*S*, 17*S* was most relavant with a probability of 99.6 % (Figure 8). This result was completely supported by the analysis of ROESY NMR data of **10**, indicating the absolute configuration of five stereogenic centers was 3*S*, 17*S*, 20*S*, 21*R*, and 22*S*.

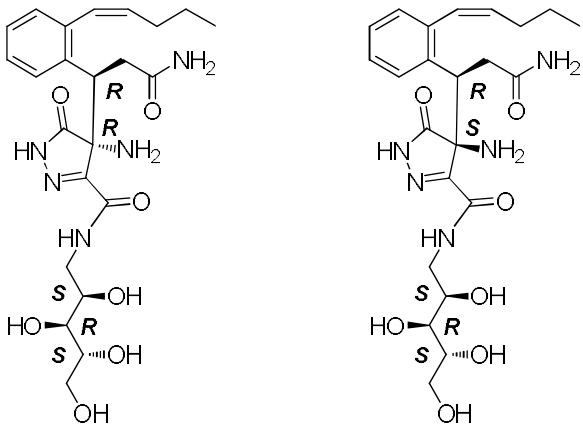

Diastereomer 1 (*RR*)

Diastereomer 2 (*RS*)

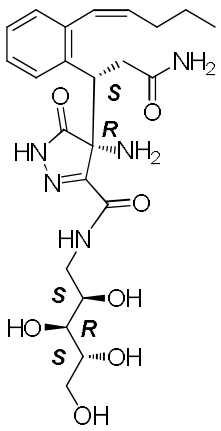

Diastereomer 3 (*SR*)

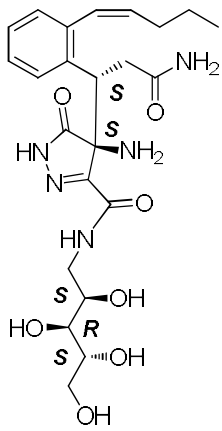

Diastereomer 4 (*SS*)

DP4 Calculation result

both carbon and proton data : Diastereomer 1 (*RR*) - 0.0%
Diastereomer 2 (*RS*) - 0.4%
Diastereomer 3 (*SR*) - 0.0%
Diastereomer 4 (*SS*) - 99.6%

carbon data only : Diastereomer 1 (*RR*) - 0.2%
Diastereomer 2 (*RS*) - 0.0%
Diastereomer 3 (*SR*) - 2.0%
Diastereomer 4 (*SS*) - 97.9%

proton data only : Diastereomer 1 (*RR*) - 0.0%
Diastereomer 2 (*RS*) - 2.1%
Diastereomer 3 (*SR*) - 0.0%
Diastereomer 4 (*SS*) - 97.9%

Figure 8. Four plausible diastereomer of **10** used for the DP4 application.

After determining the absolute configurations of stereogenic centers, I wondered the entire conformations of WS9326G and H (**8** and **9**) would be

folded as structure of WS9326A or linear structures with different conformations because there have been no reports to analyze three-dimensional structures of WS9326s insightfully. For this reason, deep-analysis of ROESY correlations of **8** was conducted initially. Interestingly, I revealed crucial evidences indicating real conformations of **8** might be complicated feature seemed to be like *M*-form, not folded inside like what WS9326s were represented previously (Figure 9). First, the direction of acyl chain group was revised to be vertical on the basis of ROESY correlations between H-1'' (δ_H 6.51), H-2'' (δ_H 5.75), and H-3 (δ_H 7.54), not with H-4 (δ_H 6.90). Additional analysis of ROESY correlations between H-3, 5 (δ_H 6.70) of *N*MeTyr, α-position proton (δ_H 4.63) of Phe, nitrogen proton (δ_H 7.98) of *allo*-Thr, and α-position proton (δ_H 4.19) of Asn revealed that the conformation of *N*MeTyr was converted to inside of structure. Furthermore, methyl group (δ_H 0.70) of Leu exhibited the ROESY correlations with H-3 of acyl chain, and methyl group (δ_H 1.07) of Thr, indicating that conformation of Ser was also converted to inside as *N*MeTyr was. Due to analysis of key ROESY correlations of **8**, entire conformations of **8** was identified as *S*-form not like cyclic form reported previously, and the analysis of ROESY signals of NH of amino acids supported its results. Conformational study of **9** was completed with same procedure, displaying similar feature of **8**. These results might demonstrate how amino acids of WS9326s were built up before conforming their ring formation.

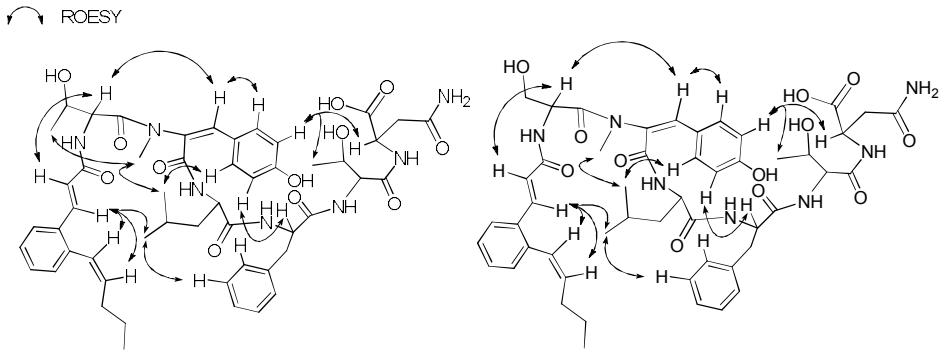

Figure 9. Proposed conformations of WS9326G and H (**8** and **9**) with key ROESY correlations.

The major metabolite, WS9326A was originally reported from *Streptomyces violaceusniger* as a tachykinin antagonist.[23] An additional study about the bioactivities of WS9326 derivatives, WS9326A-E from another *Streptomyces* strain, revealed that WS9326D inhibited *Brugia malayi* asparaginyl-tRNA synthetase and killed the adult *B. malayi* parasite.

For the biological evaluation of the new compounds (**7**-**10**), cytotoxic effects against human carcinoma cell lines such as A549, HCT116, SNU638, K562, SK-HEP1, and MDA-MB231 were tested. However, WS9326F-G (**7**-**10**) did not exhibit significant cytotoxicity against the tested human cancer cells (IC_{50} > 10 μM). In antibacterial and antifungal assays, WS9326F-H (**7**-**10**) did not display any significant inhibitory activity either. Because these compounds were not virtually cytotoxic, I decided to evaluate antiangiogenic activity of **7**-**10** along with the known derivatives. Tumor angiogenesis has been known to play an important role in the growth of

tumor cells and its metastasis because receiving nutrients and oxygen through new vessels can promote the growth of cancer cells.[24] Therefore, inhibition of angiogenesis of tumor has been regarded as a promising strategy for treatment of cancer in a recent.[25] To test the effect of WS9326F-H (**7**-**10**) and WS9326A-E for antiangiogenic activity in endothelial cells, I evaluated the capillary tube formation assay of HUVEC under VEGF induced condition. All of WS9326s showed potent antiangiogenic activity but the suppression ratio of the WS9326F (**7**) at 20 μM exhibited inhibition of endothelial cell network formation, which was similar with VEGF negative condition (Figure 10). In this assay, WS9326F (**7**) was observed to inhibit capillary tube formation of the HUVEC in dose-dependent manner. By contrast, WS9326G, H, and I (**8**,**9**, and **10**) displayed weak or no inhibition activity at the test concentration. These results indicated that cyclic ring formation and chiral center of *N*-methyl tyrosine could be significant factor for antiangiogenesis activity and cytotoxicity of WS9326s.

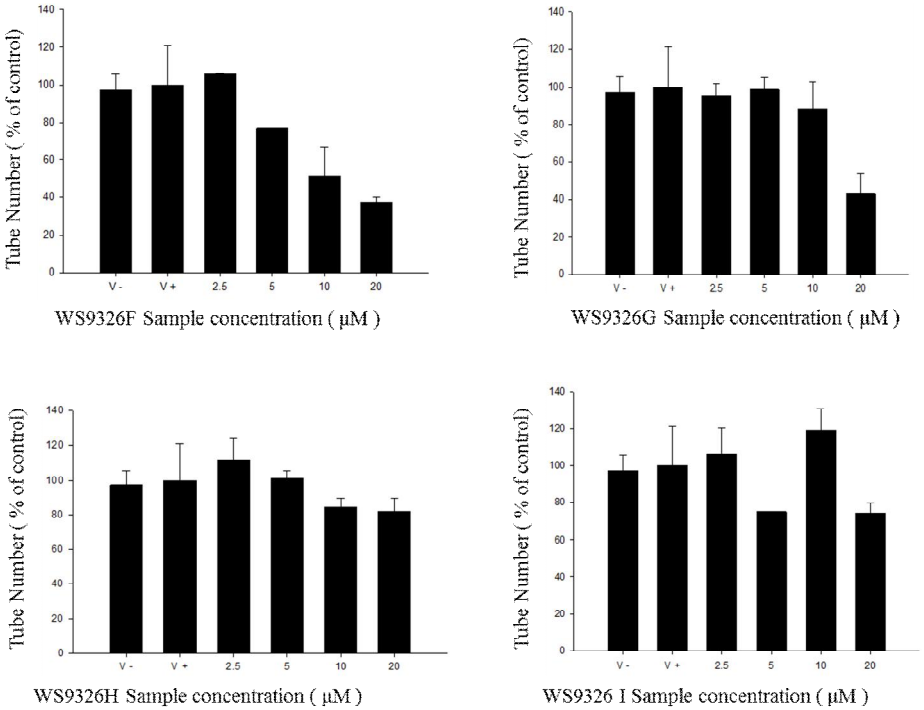

Figure 10. Effect of WS9326F-I on capillary tube formation by endothelial cells. In a 96-well plate coated with matrigel, HUVECs and each concentration of WS9326F-I were added and then incubated for 4-8 h at 37℃. The capillary structures were photographed and quantified.

The depsipeptides synthesized by interaction of PKS and NRPS pathway existed rarely in nature. WS9326F-H, which were isolated from intertidal mudflat-derived *Streptomyces* sp., were consist of 6-7 amino acids with unique acyl chain moiety. To my best knowledge, there were reported the only three classes having this moiety, pepticinamin,[26] skyllamycin,[27] and WS9326s. Aaccording to my paper studies, dehydrotyrosine were discovered in the diketopiperazine compound from a marine sponge, but it

was first class of large peptides which have a dehydrotyrosine in nature. Furthermore, additional modification including an unprecedented 4-amino-2,4-dihydro-3H-pyarzol-3-one of WS9326I was first reported moiety in natural products except synthetic compounds. The structurally novel bioactive peptides discovered from mudflat implicate that searching for unconventional environments of bacteria can be pioneer in discovery of progressive drug candidates.

Table 4. ^{1}H and ^{13}C NMR Data for **7** and **8** in DMSO-d_6[a]

		7		**8**	
position	C/H	δ_H, mult (*J* in Hz)	δ_C	δ_H, mult (*J* in Hz)	δ_C
Acyl	1	–	166.4, s	–	165.6, s
	2	6.44, 1H, d (15.0)	120.0, d	6.90, 1H, d (15.0)	122.8, d
	3	7.77, 1H, d (15.0)	139.8, d	7.54, 1H, d (15.0)	137.5, d
	4	–	132.9, s	–	133.2, s
	5	7.28, 1H, m	126.0, d	7.61, 1H, d (7.0)	126.2, d
	6	7.15, 1H, t (7.5)	127.5, d	7.34, 1H, m	127.7, d
	7	7.09, 1H, t (7.5)	129.5, d	7.36, 1H, m	129.3, d
	8	6.99, 1H, d (7.5)	129.9, d	7.21, 1H, m	130.0, d
	9	–	137.5, s	–	138.1, d
	10	6.31, 1H, d (10.5)	127.0, d	6.51, 1H, d (11.5)	127.1, d
	11	5.63, 1H, m	134.2, d	5.75, 1H, m	134.4, d
	12	2.04, 2H, m	29.7, t	1.97, 2H, m	30.2, t
	13	1.39, 2H, m	22.6, t	1.34, 2H, m	22.2, t
	14	0.83, 3H, t (7.5)	14.0, q	0.79, 3H, t (7.5)	13.7, q
^{1}Ser/^{1}Thr	NH	9.17, 1H, brs		8.30, 1H, brs	
	α	5.33, 1H, t (8.0)	48.1, d	4.93, 1H, m	55.1, d
	β	1.97, 1H, m	63.7, t	4.09, 1H, m	66.6
		3.80, 1H, m			
	γ			1.07, 3H, d (6.0)	20.4, t
	CO	–	170.2, s	–	171.1, s
^{2}*N*MeTyr	NMe	2.62, 3H, s	28.2, q	2.87, 3H, s	33.9, q
/ΔMeTyr	α	5.52, 1H, m	61.6, d	–	131.5, s
	β	2.94, 2H, m	33.4, t	6.56, 1H, s	131.9, d
	1	–	127.2, s	–	123.6, s
	2,6	6.98, 2H, d (8.5)	130.2, d	7.24, 2H, m	131.0, d
	3,5	6.68, 2H, d (8.5)	115.7, d	6.70, 2H, d (8.5)	115.5, d
	4	–	156.4, s	–	159.2, s
	CO	–	166.3, s	–	172.4, s
^{3}Leu	NH	9.18, 1H, brs		8.60, 1H, brs	
	α	4.33, 1H, m	56.0, d	4.42, 1H, m	51.2, d
	β	1.06, 2H, m	39.7, t	0.94, 1H, m	40.6, t
		1.44, 1H, m		1.24, 1H, m	
	γ	1.06, 1H, m	23.9, d	1.22, 1H, m	24.3, d
	δ	0.71, 3H, d (6.5)	22.5, q	0.70, 3H, d (6.5)	21.4, q
		0.71, 3H, d (6.5)	22.5, q	0.70, 3H, d (6.5)	21.4, q
	CO	–	169.4, s	–	172.0, s
^{4}Phe	NH	8.56, 1H, brs		8.42, 1H, brs	
	α	4.81, 1H, m	52.9, d	4.63, 1H, m	54.4, d
	β	2.69, 1H, m	36.4, t	2.70, 1H, m	38.2, t
		3.35, 1H, m		3.12, 1H, m	
	1	–	138.5, s	–	138.2, s
	2,6	7.21, 1H, m	129.2, d	7.28, 1H, d (6.5)	129.6, d
	3,5	7.23, 1H, m	127.7, d	7.21, 1H, m	128.2, d
	4	7.17, 1H, t (7.5)	126.2, d	7.13, 1H, t (6.5)	126.3, d
	CO	–	170.3, s	–	171.5, s
^{5}*allo*Thr	NH	7.28, 1H, brs		7.98, 1H, brs	
	α	4.41, 1H, m	56.9, d	4.11, 1H, m	59.2, d
	β	3.19, 1H, m	69.2, d	3.67, 1H, m	68.0, d
	γ	0.77, 3H, d (6.5)	21.5, q	0.94, 3H, d (6.5)	19.6, q
	CO	–	170.7, s	–	171.4, s
^{6}Asn	NH	8.90, 1H, brs		7.74, 1H, brs	
	α	4.70, 1H, m	51.2, d	4.19, 1H, m	52.5, d
	β	2.50, 1H, m	36.8, t	2.35, 1H, m	38.2, t
		2.63, 1H, m		2.50, 2H, m	
	*γ*CO	–	171.4, s	–	173.3, s
	CO	–	172.2, s	–	173.0, s
^{7}Ser	NH	8.51, 1H, brs –			
	α	4.43, 1H, m	56.0, d		
	β	3.60, 2H, m	60.8, t		
	CO	–	169.7, s		

[a] ^{1}H and ^{13}C data were recorded at 600 and 125 MHz, respectively.

Table 5. ^{1}H and ^{13}C NMR Data for **9** in DMSO-d_6[a]

		9	
position	C/H	δ_H, mult (J in Hz)	δ_C
Acyl	1	–	165.6, s
	2	6.70, 1H, d (15.0)	122.4, d
	3	7.56, 1H, d (15.0)	126.3, d
	4	–	133.2, s
	5	7.58, 1H, d (8.0)	126.3, d
	6	7.33, 1H, t (8.0)	127.7, d
	7	7.37, 1H, t (8.0)	129.4, d
	8	7.20, 1H, m	130.0, d
	9	–	137.4, s
	10	6.53, 1H, d (11.5)	127.2, d
	11	5.78, 1H, m	134.5, d
	12	1.98, 2H, m	30.1, t
	13	1.36, 2H, m	22.4, t
	14	0.82, 3H, t (7.5)	13.8, q
^{1}Ser/^{1}Thr	NH	8.57, 1H, brs	
	α	5.07, 1H, m	55.1, d
	β	3.53, 1H, m	61.2, t
		3.74, 1H, m	
	γ		
	CO	–	172.2, s
^{2}*N*MeTyr	NMe	2.84, 3H, s	33.7, q
/ΔMeTyr	α	–	132.0, s
	β	6.76, 1H, s	131.9, d
	1	–	124.3, s
	2,6	7.28, 2H, m	129.5, d
	3,5	6.65, 2H, d (8.5)	115.2, d
	4	–	158.5, s
	CO	–	172.5, s
^{3}Leu	NH	8.72, 1H, brs	
	α	4.24, 1H, m	52.1, d
	β	1.08, 1H, m	40.0, t
		1.29, 1H, m	
	γ	1.18, 1H, m	24.1, d
	δ	0.72, 3H, d (6.5)	21.7, q
		0.72, 3H, d (6.5)	21.7, q
	CO	–	172.1, s
^{4}Phe	NH	8.43, 1H, brs	
	α	4.62, 1H, m	54.4, d
	β	2.71, 1H, m	38.1, t
		3.12, 1H, m	
	1	–	138.5, s
	2,6	7.26, 1H, m	129.4, d
	3,5	7.23, 1H, m	128.2, d
	4	7.14, 1H, t (6.5)	126.3, d
	CO	–	171.3, s
^{5}*allo*Thr	NH	8.01, 1H, brs	
	α	4.21, 1H, m	58.4, d
	β	3.63, 1H, m	67.2, d
	γ	0.92, 3H, d (6.5)	19.7, q
	CO	–	171.5, s
^{6}Asn	NH	8.10, 1H, brs	
	α	4.52, 1H, m	49.2, d
	β	2.55, 1H, m	36.7
		2.58, 1H, m	
	*γ*CO	–	173.2, s
	CO	–	173.0, s

[a] ^{1}H and ^{13}C data were recorded at 600 and 150 MHz

Table 6. ^{1}H and ^{13}C NMR Data for **10** in pyridine-d_5[a]

		10					
position	C/H	δ_H, mult (*J* in Hz)	δ_C	position	C/H	δ_H, mult (*J* in Hz)	δ_C
Acyl	1	–	170.8, s	[3]Leu	NH	9.81, 1H, brs	
	2	4.57, 1H, dd	39.1, t		α	4.71, 1H, m	56.3, d
		(15.0, 8.5)			*β*	1.71, 1.33, 1H, m	40.5, t
		3.37, 1H, dd			*γ*	1.19, 1H, m	24.6, d
		(15.0, 3.5)			*δ*	0.69, 3H, d (6.5)	22.7, q
	3	4.72, 1H, dd	47.1, d			0.58, 3H, d (6.5)	23.7, q
		(8.5, 3.5)			CO	–	174.3, s
	4	–	136.5, s	[4]Phe	NH	10.0, 1H, brs	
	5	8.76, 1H, d (8.0)	130.0, d		α	5.12, 1H, m	58.7, d
	6	8.30, 1H, t (8.0)	129.0, d		*β*	4.18, 1H, m	37.6, t
	7	7.26, 1H, t (8.0)	127.6, d			4.08, 1H, m	
	8	7.16, 1H, d (8.0)	130.0, d		1	–	130.6, s
	9	–	139.7, s		2,6	7.67, 2H, d (8.0)	130.2, d
	10	6.99, 1H, d (10.5)	130.6, d		3,5	7.30, 2H, t (8.0)	128.6, d
	11	5.59, 1H, m	133.8, d		4	7.24, 1H, t (8.0)	126.5, d
	12	2.16, 2.06, 2H, m	30.7, t		CO	–	173.6
	13	1.30, 1.26, 2H, m	23.3, t	[5]*allo*Thr	NH	9.54, 1H, brs	
	14	0.74, 3H, t (6.5)	14.2, q		α	5.62, 1H, dd	59.9, d
	15	–	176.9, s			(9.0, 9.0)	
	15-NH	12.79, 1H, s			*β*	4.33, 1H, m	70.8, d
	16	–	159.6, s		*γ*	1.73, 3H, d (6.5)	21.9, q
	17	–	62.8, s		CO	–	173.8, s
	17-NH	2.75, 2H, brs		[6]Asn	NH	10.55, 1H, brs	
	18	–	173.4, s		α	6.08, 1H, dd	52.6, d
	18-NH	8.89, 1H, brs				(8.5, 3.5)	
	19	4.98, 1H, m	46.4, t		*β*	3.71, 1H, dd	37.6, t
		4.11, 1H, dd				(15.5, 3.5)	
		(11.0, 3.5)				3.51, 1H, dd	
	20	4.76, 1H, ddd	46.4, s			(15.5, 8.5)	
		(8.0, 4.5, 3.5)			*γ*CO	–	174.5, s
	20-OH	6.5, 1H, brs			CO	–	172.7
	21	4.44, 1H, dd	75.3, d		NH_2	8.72, 2H, brs	
		(10.5, 4.5)		[7]Ser	NH	9.56, 1H, brts	
	21-OH	6.47, 1H, brs			α	5.18, 1H, m	57.7, d
	22	4.59, 1H, m	74.9, d		*β*	4.46, 4.35, 2H, m	63.2, t
	22-OH	6.24, 1H, brs			OH	6.25, 1H, brs	
	23	4.51, 4.35, 2H, m	65.2, t		CO	–	170.7, s
	23-OH	6.19, 1H, brs					
[1]Thr	NH	8.53, 1H, d (9.5)					
	α	5.39, 1H, d (9.5)	53.4, d				
	β	5.82, 1H, q (6.5)	72.7, d				
	γ	0.54, 3H, d (6.5)	15.8, q				
	CO	–	171.4, s				
[2]*N*MeTyr	NMe	3.07, 3H, s	34.8, q				
	α	–	131.6, s				
	β	6.71, 1H, s	130.6, d				
	1	–	131.6, s				
	2,6	7.48, 2H, d (8.0)	131.3, d				
	3,5	7.25, 2H, d (8.0)	116.4, d				
	4	–	159.9, s				
	4-OH	11.70, 1H, brs					
	CO	–	166.8, s				

[a] ^{1}H and ^{13}C data were recorded at 900 and 225 MHz,

III. Hormaomycins B and C: antibiotic cyclic depsipeptides from a marine mudflat-derived *Streptomyces* sp. SNM55

III. I. Results and discussion

Hormaomycin B (**18**) was isolated as a white powder with the molecular formula $C_{54}H_{67}ClN_{10}O_{14}$ on the basis of HRFABMS (obsd $[M+H]^+$ at *m/z* 1115.4611, calcd for 1115.4605) coupled with ^1H and ^{13}C NMR spectroscopy (Table 7). The ^1H spectrum of **18** in $CDCl_3$ presented six amide protons at δ_H 8.98, 8.16, 7.31, 6.85, 6.79, and 6.26, indicating its peptide-derived nature. Consistently, the ^{13}C NMR of **18** also showed seven amide/ester carbons at δ_C 172.2, 171.8, 171.5, 171.1, 169.3, 168.8, and 167.9. The analysis of ^1H, ^{13}C, and HSQC NMR spectra clarified the peptide-derived features of hormaomycin B. As a peptide-derived molecule, hormaomycin B exhibited seven methine signals composing α-positions of amino acids (δ_H/δ_C 5.14/51.2, 3.52/52.2, 4.64/54.5, 4.55/58.4, 4.48/56.4, 4.33/60.8, and 4.26/61.7). Seven amide/ester carbons and seven α-position methines enabled us to deduce that hormaomycin B (**18**) bears seven or more amino acid units. Further analysis of one-bond correlations identified NMR signals that do not belong to ordinary amino acids units. In particular, two olefinic methines (δ_H/δ_C 5.64/128.8 and 5.26/127.8) and two methines (δ_H/δ_C 0.28/20.2 and -0.66/17.7) and one methylene (δ_H/δ_C 0.56 and -0.26/33.4) in the distinctive upfield suggested the existence of unusual units in the molecules. Additionally, two aromatic methines (δ_H/δ_C 6.68/109.8 and 6.08/103.5) with 4.5 Hz ^1H-^1H coupling indicated the existence of a five-membered aromatic ring, which does not correspond to any proteinogenic

amino acid. Based on the overall analysis of the ^{1}H, ^{13}C NMR, and HSQC spectra of **18**, along with the existence of a chlorine atom in the molecular formula, hormaomycin B was expected to be a peptide-derived compound bearing several highly modified amino acid residues.

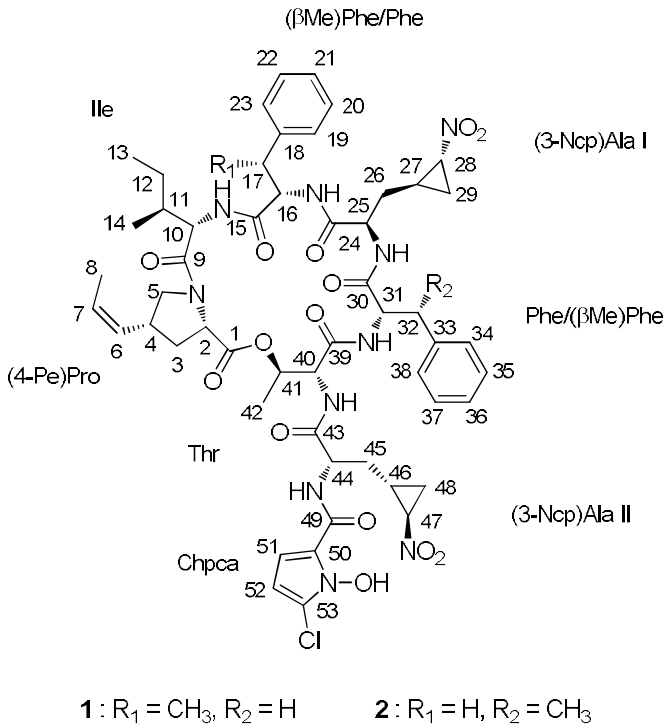

Figure 11. The structures of hormaomycins B and C (**18** and **19**).

Further analysis of HSQC spectral data revealed all of the one-bond ^{1}H-^{13}C correlations in **18**. Subsequent interpretation of the COSY, TOCSY, and HMBC NMR spectra established eight partial structures dissected by amide bonds. These include a *4*-(Z)-propenylproline ((4-Pe)Pro), a β–methylphenylalanine ((β-Me)Phe), two 3-(2-nitrocyclopropyl)alanines ((3-Ncp)Ala), and a 5-chloro-1-hydroxypyrrol-2-carboxylic acid (Chpca), as well as three common amino acids: an isoleucine (Ile), a phenylalanine (Phe), and a threonine (Thr).

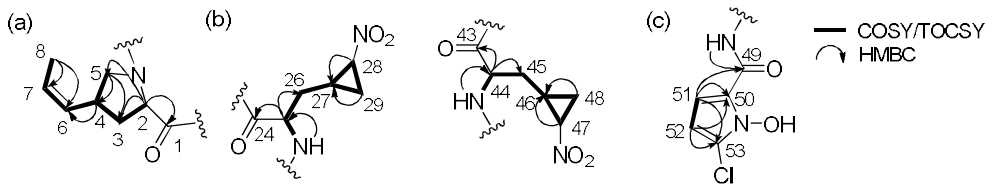

Figure 12. Determination of the unusual partial structures of **18**. (a) 4-*(Z)*-propenylproline, (b) 3-(2-nitrocyclopropyl)alanine I and II, and (c) 5-chloro-1-hydroxypyrrol-2-carboxylic acid.

Specifically, the COSY NMR spectrum exhibited correlations from H_2-3 (δ_H 2.37, 1.80) to H-2 (δ_H 4.26) and H-4 (δ_H 3.27), showing the connectivity from C-2 (δ_C 61.7) to C-4 (δ_C 36.9) through C-3 (δ_C 34.9). Further COSY correlations of H-4 to H_2-5 (δ_H 3.98, 3.31) and H-6 (δ_H 5.26) revealed that C-4 was located immediately adjacent to C-5 (δ_C 53.0) and C-6 (δ_C 127.8). The ^{1}H-^{1}H couplings from H-7 (δ_H 5.64) to H-6 and H-8 (δ_H 1.68) and HMBC correlations from H-8 to two olefinic carbons C-6 and C-7 (δ_C 128.8) established the propenyl substructure connected to C-4. The ^{1}H-^{1}H coupling constant (J = 9.5 Hz) between H-6 and H-7 determined the *Z* configuration of the C-6 double bond. The ^{13}C NMR chemical shift of C-5 (δ_C 53.0) indicated that this carbon is bound to a nitrogen atom. Because there was no detected NH signal in this unit, a proline-type moiety was expected. The HMBC correlation from the α–proton (H-2; δ_H 4.26) to C-5 supported the hypothesis that H-2 and H-5 share one nitrogen to form a pyrrolidine. Furthermore, H-2 displayed a HMBC correlation to the C-1 carbonyl carbon (δ_C 171.8), completing a 4-(*Z*)-propenylproline ((4-Pe)Pro)

unit (Figure 12a). This unit was further confirmed by TOCSY correlations from H-2 to H-8.

The next unusual unit was composed of distinctively shielded protons of H_2-26 (δ_H 0.56, -0.26), H-27 (δ_H 0.28), and H_2-29 (δ_H 1.02, -0.66), along with 25-NH (δ_H 6.26), H-25 (δ_H 3.52), and H-28 (δ_H 2.92), based on COSY and TOCSY NMR spectra. In particular, strong COSY correlations among H-27, H-28, and H_2-29 and their low chemical shifts revealed that this amino unit possesses a cyclopropane. Additionally, the ^{13}C chemical shift (δ_C 58.7) of the C-28 methine in the cyclopropane indicated that this carbon is directly connected to a heteroatom. The IR spectrum exhibited a strong absorption band at 1543 cm^{-1}, which corresponds to a nitro functional group. Therefore, C-28 was determined to bind to a nitro group. These assignments eventually elucidated a 3-(2-nitrocyclopropyl)alanine ((3-Ncp)Ala) unit (Figure 12b). Interestingly, the second (3-Ncp)Ala unit was also identified based on COSY and TOCSY correlations, even though the ^1H chemical shifts of the second unit differ significantly from those of the first (3-Ncp)Ala residue (Figure 12b, Table 7).

Hormaomycin B (**18**) possesses eighteen sp^2 carbons. Twelve of these were assigned in the two benzene rings in a phenylalanine and a β-methylphenylalanine, and two olefinic carbons were used in (4-Pe)Pro. Then, four sp^2 carbons, including two methines, C-51 (δ_C 109.8) and C-52 (δ_C 103.5), and two quaternary carbons, C-50 (δ_C 119.8) and C-53 (δ_C 121.5), remained unassigned. These methine protons, H-51 (δ_H 6.68) and H-

52 (δ_H 6.08), were coupled to each other (4.5 Hz). This coupling constant strongly suggested that these atoms are part of a five-membered aromatic ring. Furthermore, HMBC correlations from H-51 to C-50 and C-53 and from H-52 to C-50 and C-53 established the C-50-C-51-C-52-C-53 connectivity. The last position of the five-membered aromatic ring could be a nitrogen atom rather than an oxygen or sulfur atom based on the ^{13}C chemical shifts of the four sp^2 carbons, indicating a pyrrole ring.[28] This pyrrole ring is connected to C-49 (δ_C 159.7) at C-50 according to the HMBC correlation from H-51 to C-49. This downfield carbon at δ_C 159.7 was assigned as an amide carbonyl carbon based on the heteronuclear coupling from the amide proton 44-NH (δ_H 8.16) to this carbon. The remarkable shielding of C-49 (δ_C 159.7) in the ^{13}C NMR spectrum compared to the chemical shifts of the other seven amide carbons (δ_C 172.2, 171.8, 171.5, 171.1, 169.3, 168.8, and 167.9) might be attributed to the conjugation effect of the pyrrole ring. Detailed examination of the mass and NMR data suggested that the quaternary carbon C-53 and the nitrogen atom in the pyrrole ring should be substituted with heteroatoms. Finally, partial structures dissected by amide bonds were established, and one chlorine atom and one hydroxy group in the molecular formula were not assigned. Considering the chemical shift of C-53 enabled a chlorine atom to be located at C-53. Subsequently, the hydroxy group was assigned to be bound to the nitrogen atom as an oxime functional group. Therefore, 5-chloro-1-hydroxypyrrol-2-carboxylic acid (Chpca) was eventually assembled (Figure

2c).

The sequence of eight partial structures ((4-Pe)Pro, Ile, Phe, (βMe)Phe, (3-Ncp)Ala I and II, Thr, and Chpca) was determined on the basis of HMBC correlations. The long-range ^{1}H-^{13}C coupling from the α–proton of (4-Pe)Pro (H-2; δ_H 4.26) to the carbonyl carbon of Ile (C-9; δ_C 171.5) connected (4-Pe)Pro to Ile. The HMBC correlations from 10-NH (δ_H 7.31) and H-16 (δ_H 4.33) to C-15 (δ_C 167.9) clarified the attachment of (βMe)Phe to Ile. (3-Ncp)Ala I was directly connected to (βMe)Phe based on the HMBC correlations from 16-NH (δ_H 6.85) and H-25 (δ_H 3.52) to C-24 (δ_C 169.3), which belonged to (3-Ncp)Ala I. Phe was positioned next to (3-Ncp)Ala I by ^{1}H-^{13}C long-range coupling from NH-25 (δ_H 6.26) and H-31 (δ_H 4.48) to C-30 (δ_C 168.8). The HMBC correlations from 31-NH (δ_H 6.79) and H-40 (δ_H 4.55) to C-39 (δ_C 171.1) revealed the sequence from Phe to Thr. In addition, the NH proton (δ_H 8.98) of Thr and the α–proton (δ_H 5.14) of (3-Ncp)Ala II displayed HMBC signals linking them to the carbonyl carbon C-43 of (3-Ncp)Ala II, clarifying the connection between Thr and (3-Ncp)Ala II. Chpca was directly connected to (3-Ncp)Ala II on the basis of the HMBC correlations from 44-NH (δ_H 8.16) of (3-Ncp)Ala II (δ_H 8.16) and H-51 (δ_H 6.68) of Chpca to the carbonyl carbon C-49 (δ_C 159.7) belonging to Chpca. Finally the long-range HMBC correlation from H-41 (δ_H 5.40) to the carbonyl carbon at 171.8 ppm (C-1) closed a macrocyclic lactone ring, indicating the planar structure of hormaomycin B (**18**) in a

cyclic depsipeptide (Figure 3).

Hormaomycin C (**19**) was isolated as a white powder, and the molecular formula was deduced as $C_{54}H_{67}ClN_{10}O_{14}$ by analyzing HRFABMS (obsd $[M+Na]^+$ at *m/z* 1137.4432, calcd $[M+Na]^+$ 1137.4424) and ^1H and ^{13}C NMR data (Table 7). The molecular formula of **19** was identical to that of hormaomycin, and it was predicted that hormaomycin C (**19**) would be very similar to **18**. Careful comparison of 1D and 2D NMR data revealed that all eight partial structures identified in hormaomycin B also exist in **19**. However, the extensive analysis of the HMBC NMR spectra showed that the sequence of the units was different. Specifically, the methyl group (17-Me; δ_H 1.29) of (βMe)Phe and the methylene signal (H_2-32; δ_H 2.79, 3.38) of Phe were replaced with a methylene (H_2-17; δ_H 2.91, 2.97) and a methyl group (32-Me; δ_H 1.40) in **19**, indicating the switched positions of (βMe)Phe and Phe between these compounds. The order of the other units was assigned based on further HMBC spectroscopic analysis, completing the planar structure of hormaomycin C (**19**).

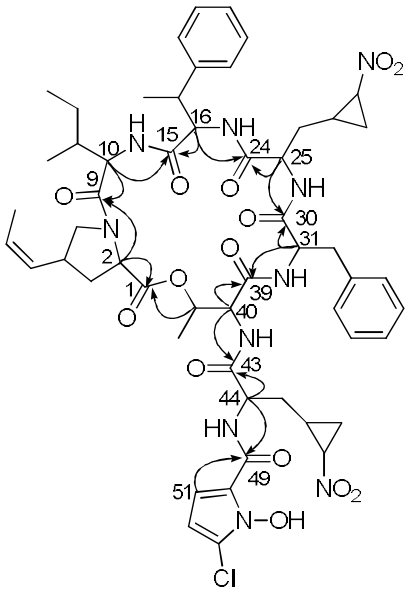

Figure 13. Key HMBC correlations of hormaomycin B (**18**).

During cultivation of the strain SNM55, hormaomycin, which was previously discovered from *Streptomyces griseoflavus*, was identified along with these new compounds. Hormaomycin is a cyclic depsipeptide that bears almost exclusively uncommon amino acids, such as (4-Pe)Pro and (3-Ncp)Ala, as well as Chpca. Because of its structural novelty and remarkable biological activity, chemical synthesis[29] and biosynthetic modifications[30] have been studied in recent decades. However, although artificial analogues have been reported during the total synthesis and biosynthetic engineering of hormaomycin,[29,30] no natural analogues have been discovered. To my best knowledge, hormaomycins B and C are the first natural analogues of hormaomycin that have been obtained without chemical modification or gene cluster manipulation. Hormaomycin possesses two (βMe)Phe units, whereas both hormaomycins B and C bear one (βMe)Phe and one Phe.

Therefore, hormaomycin was utilized to determine the absolute configurations of hormaomycins B and C (**18** and **19**). The ^{1}H and ^{13}C NMR data and CD spectrum of hormaomycin were carefully compared with those of **18** and **19**. Based on the close similarity between the NMR data and CD spectra (Figure 4), as well as their common biosynthetic origin, the absolute configurations of hormaomycins B and C were determined to be identical to that of hormaomycin, which was determined by total synthesis.[29]

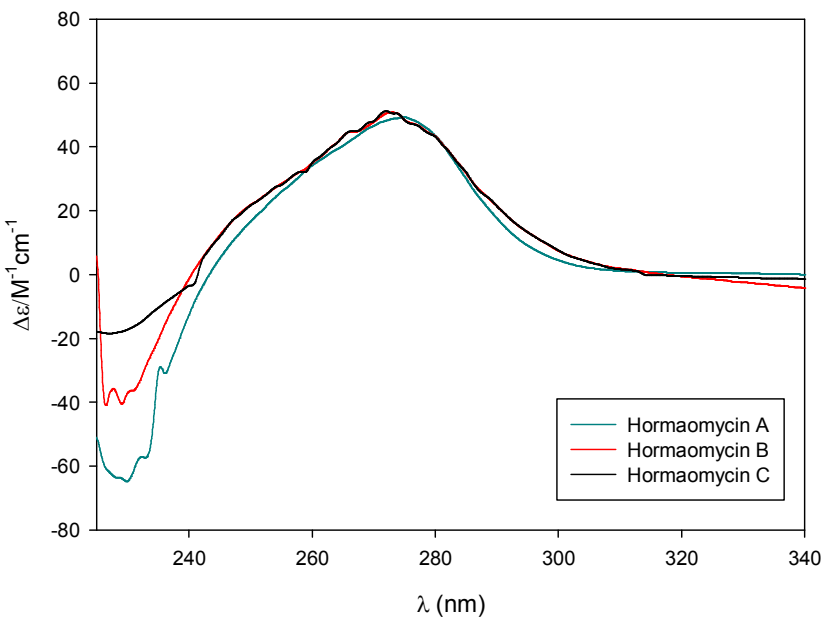

Figure 14. The CD spectra of the hormaomycins in MeOH.

III. II. Bioactivities of hormaomycins

Hormaomycin (**17**) was previously reported to exhibit remarkable antibacterial effects.[31] Therefore, the biological activities of the hormaomycins found here were evaluated with regard to their antimicrobial activities against various pathogenic bacterial strains, including *Staphylococcus aureus* ATCC 25923, *Bacillus subtilis* ATCC 6633, *Kocuria rhizophila* NBRC 12708, *Streptococcus pyogenes* ATCC 19615, *Klebsiella pneumoniae* ATCC10031, *Salmonella enterica* ATCC 14028, *Proteus hauseri* NBRC 3851, and *Escherichia coli* ATCC 25922 (Table 2). Hormaomycin exhibited more potent antibacterial activities against the tested Gram-positive bacteria than against the tested Gram-negative bacteria, particularly against *S. aureus* and *K. rhizophila*, exhibiting MIC values of 0.4 μM and 0.03 μM, respectively. Hormaomycin also exhibited significant antibacterial effects against Gram-negative *P. hauseri*. Hormaomycins B and C (**18** and **19**) displayed potent activity against *K. rhizophila* but showed antibacterial activities against the tested bacteria that were generally 4~32 times weaker than those of hormaomycin. Accordingly, it was hypothesized that the existence of the methyl groups at C-17 and C-32, which form (βMe)Phe, play an important role in the antibacterial potency of the hormaomycins. Further investigations of the antifungal activity were conducted against the pathogenic fungi *Aspergillus fumigatus*, *Trichophyton rubrum*, *T. mentagrophytes*, and *Candida albicans*, but no significant inhibitory activity was observed to result from the hormaomycin treatments.

Table 7. ^{1}H (600 MHz) and ^{13}C NMR (150 MHz) data **18** and **19** in $CDCl_3$

	C/H	**18**			**19**		
		δ_H, mult (*J* in Hz)	δ_C	type	δ_H, mult (*J* in Hz)	δ_C	type
(4–Pe)Pro	1	–	171.8	C	–	171.6	C
	2	4.26, 1H, m	61.7	CH	4.26, 1H, dd (11.0, 6.5)	61.8	CH
	3	2.37, 1H, m	34.9	CH_2	2.36, 1H, m	35.8	CH_2
		1.80, 1H, m			1.81, 1H, m		
	4	3.27, 1H, m	36.9	CH	3.25, 1H, m	37.0	CH
	5	3.98, 1H, m	53.0	CH_2	3.98, 1H, m	53.0	CH_2
		3.31, 1H, m			3.27, 1H, m		
	6	5.26, 1H, dd (9.5, 9.5)	127.8	CH	5.26, 1H, dd (9.0, 9.0)	127.9	CH
	7	5.64, 1H, dq (9.5, 7.0)	128.8	CH	5.63, 1H, dq (9.0, 7.0)	128.8	CH
	8	1.68, 1H, d (7.0)	13.5	CH_3	1.66, 1H, d (7.0)	13.5	CH_3
Ile	9	–	171.5	C	–	171.5	C
	10	4.64, 1H, m	54.5	CH	4.64, 1H, m	54.9	CH
	10–NH	7.31, 1H, brs	–		7.23, 1H, brs	–	
	11	1.88, 1H, m	38.6	CH	1.90, 1H, m	38.2	CH
	12	1.54, 1H, m	25.0	CH_2	1.55, 1H, m	25.0	CH_2
		1.29, 1H, m			1.30, 1H, m		
	13	0.90, 3H, d (7.0)	10.8	CH_3	0.89, 3H, d (7.0)	10.8	CH_3
	14	1.04, 3H, d (7.0)	15.2	CH_3	1.02, 3H, d (7.0)	15.3	CH_3
(βMe)Phe/Phe	15	–	167.9	C	–	171.3	C
	16	4.33, 1H, m	60.8	CH	4.58, 1H, m	55.2	CH
	16–NH	6.85, 1H, brs	–		6.91, 1H, brs	–	
	17	3.02, 1H, m	44.6	CH	2.91, 1H, m	38.0	CH_2
	17-Me	1.29, 3H, d (6.5)	18.0	CH_3	2.97, 1H, m		
	18	–	141.9	C	–	136.5	C
	19	7.11, 1H, d (8.5)	129.0	CH	7.11, 1H, d (8.0)	129.5	CH
	20	7.13, 1H, t (8.5)	127.5	CH	7.15, 1H, t (8.0)	129.0	CH
	21	7.03, 1H, t (8.5)	127.6	CH	7.09, 1H, t (8.0)	127.7	CH
	22	7.13, 1H, t (8.5)	127.5	CH	7.15, 1H, t (8.0)	129.0	CH
	23	7.11, 1H, d (8.5)	129.0	CH	7.11, 1H, d (8.0)	129.5	CH
(3–Ncp)Ala Ⅰ	24	–	169.3	C	–	168.2	C
	25	3.52, 1H, m	52.2	CH	3.55, 1H, m	52.8	CH
	25–NH	6.26, 1H, brs	–		6.37, 1H, brs	–	
	26	0.56, 1H, m	33.4	CH_2	0.78, 1H, m	33.0	CH_2
		-0.26, 1H, m			0.13, 1H, m		
	27	0.28, 1H, m	20.2	CH	0.58, 1H, m	20.4	CH
	28	2.92, 1H, m	58.7	CH	3.04, 1H, m	58.6	CH
	29	-0.66, 1H, m	17.7	CH_2	-0.34, 1H, m	17.4	CH_2
		1.02, 1H, m			1.13, 1H, m		
Phe/(βMe)Phe	30	–	168.8	C	–	168.3	C
	31	4.48, 1H, m	56.4	CH	4.48, 1H, m	60.6	CH
	31–NH	6.79, 1H, brs	–		6.79, 1H, brs	–	
	32	2.79, 1H, m	38.7	CH_2	3.67, 1H, m	37.1	CH
		3.38, 1H, m			1.40, 3H, d (6.5)	13.7	CH_3
	33	–	137.3	C	–	142.6	C
	34	7.22, 1H, m	129.3	CH	7.24, 1H, m	127.9	CH
	35	7.23, 1H, m	127.8	CH	7.25, 1H, m	128.8	CH
	36	7.15, 1H, t (8.5)	127.2	CH	7.17, 1H, t (8.5)	127.3	CH
	37	7.23, 1H, m	127.8	CH	7.25, 1H, m	128.8	CH
	38	7.22, 1H, m	129.3	CH	7.24, 1H, m	127.9	CH
Thr	39	–	171.1	C	–	171.1	C
	40	4.55, 1H, m	58.4	CH	4.52, 1H, m	55.8	CH
	40-NH	8.98, 1H, brs	–		8.95, 1H, brs	–	
	41	5.40, 1H, m	69.4	CH	5.38, 1H, m	69.6	CH
	42	1.52, 3H, m	17.2	CH_3	1.48, 3H, m	17.3	CH_3
(3–Ncp)Ala Ⅱ	43	–	172.2		–	172.1	
	44	5.14, 1H, m	51.2	CH	5.09, 1H, m	51.5	CH
	44-NH	8.16, 1H, brs	–		7.96, 1H, brs	–	
	45	1.80, 1H, m	35.5	CH_2	1.83, 1H, m	35.2	CH_2
		1.60, 1H, m			1.61, 1H, m		
	46	1.93, 1H, m	21.7	CH	1.91, 1H, m	21.7	CH
	47	4.04, 1H, m	59.8	CH	4.05, 1H, m	59.6	CH
	48	1.95, 1H, m	17.8	CH_2	1.95, 1H, m	17.9	CH_2
		1.02, 1H, m			1.01, 1H, m		
Chpca	49	–	159.7	C	–	160.1	C
	50	–	119.8	C	–	119.8	C
	51	6.68, 1H, d (4.5)	109.8	CH	6.81, 1H, d (4.5)	109.8	CH
	52	6.08, 1H, d (4.5)	103.5	CH	6.13, 1H, d (4.5)	104.0	CH
	53	–	121.5	C	–	120.5	C
	NOH	10.8, 1H, brs	–		10.8, 1H, brs	–	

Table 8. Antibacterial activity data of the hormaomycins

compound	MICs (μM)							
	Gram-positive				Gram-negative			
	S. aureus	*B. subtilis*	*K. rhizophila*	*S. pyogenes*	*K. pneumoniae*	*S. enterica*	*P. hauseri*	*E. coli*
Hormaomycin	0.4	1.8	0.03	1.8	>113	>113	0.9	>113
Hormaomycin B	7	14	0.4	14	>115	29	29	>115
Hormaomycin C	7	56	0.23	8	>114	114	14	>114
Ampicillin	<0.17	0.17	<0.17	0.17	45.9	3.7	<0.17	11.5

I. II. Experimental section

General experimental procedures. Optical rotations were measured using a Jasco P–1020 polarimeter (sodium light source, JASCO, Easton, PA, USA) with a 1 cm cell. Infrared (IR) spectra were acquired using a Thermo N1COLET iS10 spectrometer (Thermo, Madison, CT, USA). UV spectra were obtained with a Perkin Elmer Lambda 35 UV/VIS spectrometer (Perkin Elmer, Waltham, MA, USA). Electrospray ionization (ESI) low–resolution LC/MS data were recorded using a matrix-assisted laser desorption/ionization (MALDI) mass spectrometer (AB SCIEX, Framingham, MA, USA) at the National Center for Inter–University Research Facilities (NCIRF) and an Agilent Technologies 6130 Quadrupole mass spectrometer (Agilent Technologies, Santa Clara, CA, USA) coupled with an Agilent Technologies 1200 series high-performance liquid chromatography (HPLC) instrument using a reversed–phase C_{18} column (Phenomenex Luna, 100 × 4.6 mm). High-resolution fast atom bombardment (HR–FAB) mass spectra were recorded using a Jeol JMS–600W high-resolution mass spectrometer (Jeol, München, Germany) at NCIRF. One- and two-dimensional (1D and 2D, respectively) nuclear magnetic resonance (NMR) spectra were obtained using Bruker Avance 500 MHz and Bruker Avance 600 MHz NMR spectrometer (Bruker, Billerica, MA, USA) at NCIRF (National Center for Inter–University Research Facilities) and a Bruker Avance 900 MHz NMR spectrometer (Bruker,

Billerica, MA, USA) at Korea Basic Science Institute (KBSI) at Ochang.

Isolation of the bacterial strain. A sediment sample was collected from a mud flat in Buan, Republic of Korea in a 40 mL sterilized plastic tube. The sample (1 g) was diluted and mixed in 4 mL of sterilized artificial seawater. The mixture was spread on Actinomycete Isolation Agar, A4 medium (1 L seawater, 18 g agar, 100 mg/L cycloheximide), A5 medium (750 mL seawater, 250 mL distilled water, 18 g agar, 100 mg/L cycloheximide), and Chitin–based Agar. The bacterial strain SNM55 was isolated on A5 media as a single strain. The strain was identified as a *Streptomyces* sp. based on the 16S rDNA sequence data (most closely related to *Streptomyces javenis* by 99% identity).

Cultivation and extraction of the bacterial strain. The SNM55 strain was cultivated in 50 mL of yeast extract-malt extract (YEME) medium (4 g yeast extract, 10 g malt extract, and 4 g glucose in 1 L artificial seawater) in a 125 mL Erlenmeyer flask. After cultivation for 3 days on a rotary shaker at 160 rpm at 30 °C, 20 mL of the SNM55 liquid culture was inoculated in a 500 mL Erlenmeyer flask containing 200 mL of YEME medium. After a 2-day incubation, 30 mL of the culture were inoculated in 1 L YEME medium in 2.8 L Fernbach flasks (12 ea × 1 L, total volume 12 L). After 7 days, the entire culture was extracted with 18 L of ethyl acetate. The ethyl acetate layer was separated and removed using anhydrous sodium sulfate. The ethyl acetate extract was concentrated *in vacuo* to yield 4 g of dried material. This procedure was repeated 6 times (72 L culture in total) to

obtain enough mohangamide mass for structural elucidation and for bioassays.

Isolation of mohangamides A and B (1 and 2). The crude extract was adsorbed onto Celite, loaded on a 2 g Sep-Pak C_{18} cartridge, and fractionated with 100 mL each of 20%, 40%, 60%, 80%, and 100% MeOH in water. Mohangamides A and B (**1**–**2**) were detected in the 60% and 80% MeOH/water fractions. To isolate **1** and **2**, the 60% and 80% fractions were subjected to reversed–phase HPLC (Kromasil C_{18} (2): 250 × 10 mm, 5 μm) with a gradient solvent system (65% MeOH/water to 90% MeOH/water over 40 min and 90% MeOH/water from 40 to 50 min, UV 280 nm detection, flow rate: 2 mL/min). Two peaks at retention times of 34.5 and 44.3 min were collected. These compounds were further purified using a C18 HPLC column (Kromasil C_{18} (2): 250 × 10 mm, 5 μm) under isocratic conditions in 55% MeOH/water (UV 280 nm detection, flow rate: 2 mL/min). Finally, mohangamides A (50 mg) and B (29 mg) (**1**-**2**) were isolated at retention times of 20.3 and 26.0 min, respectively. Mohangamides A and B are barely soluble in water. However, they are soluble in DMSO, pyridine, methanol, and ethyl acetate.

Mohangamide A (**1**). $[\alpha]_D$ ¬-82 (c 0.1, MeOH); UV (MeOH) λ_{max} (log ε) 236 (4.93), 280 (4.64) nm; IR (neat) ν_{max} 3292, 1648, 1513, 1249 cm^{-1}; for ^{1}H and ^{13}C NMR data, see Table 1; HRFABMS *m*/*z* 2078.0071 [M]+ (calcd for $C_{107}H_{139}N_{17}O_{26}$ 2078.0077).

Mohangamide B (**2**). $[\alpha]_D$ -54 (c 0.1, MeOH); UV (MeOH) λ_{max} (log ε 236 (4.91), 280 (4.38) nm; IR (neat) ν_{max} 3297, 1648, 1516, 1251 cm^{-1}; for ^1H and ^{13}C NMR data, see Table 2; HRFABMS m/z 2088.9971 [M+Na]+ (calcd for $C_{106}H_{139}N_{17}O_{26}Na$ 2088.9975).

Methanolysis of mohangamide A (3a and **3b).** Mohangamide A (**1**) (20 mg) was dissolved in 2 mL of MeOH, and 28 mg of NaOMe was added to the vial to prepare a 0.5-M NaOMe solution. The reaction mixture was stirred at room temperature for 3 h, and the reaction was quenched with 1 N HCl. The methanolysis product was extracted using water–ethyl acetate partition after evaporating MeOH *in vacuo*. After removing the solvent, the methanolysis products **3a** (7 mg) and **3b** (9 mg) were purified by reversed–phase HPLC (Kromasil C_{18} (2): 250 × 10 mm, 5 μm, UV 280 nm detection, 55%–70% acetonitrile/water gradient solvent system over 40 min, flow rate: 2 mL/min) at retention times of 18 and 23 min, respectively. The structures of **3a** and **3b** were assigned after 1D and 2D NMR and ESI mass spectra (for **3a**, $[M+H]^+$ *m/z* at 1069, molecular formula; $C_{55}H_{72}N_8O_{14}$ / **3b** $[2M+H]^+$ *m/z* at 2147, molecular formula; $C_{54}H_{75}N_9O_{14}$) analyses.

Acetylation of 3b (4). The methanolysis product **3b** was dried *in vacuo* for 24 h. Product **3b** was dissolved in 1 mL of distilled anhydrous pyridine. After flushing with argon gas, 1 mL of acetic anhydride was added and stirred at room temperature for 5 h. The solution was evaporated under high vacuum for 4 h. The product was purely isolated by reversed–phase HPLC (Kromasil C_{18} (2): 250 × 10 mm, 5 μm) with a gradient solvent

system (60% acetonitrile/water to 95% acetonitrile/water over 40 min, UV 280 nm detection, flow rate: 2 mL/min). Tetraacetate **3b** (**4**) (7.5 mg) eluted at 30.8 min, and its structure was determined by ^{1}H NMR spectroscopy and by low-resolution ESI-MS ($[M+H]^+$ *m*/*z* at 1242, molecular formula; $C_{62}H_{83}N_9O_{18}$).

Tetraacetate (4) : ^{1}H NMR (600 MHz, DMSO–d_6) δ 8.39–8.27 (m, 4H), 8.13 (brs, 1H), 8.08 (brs, 1H), 7.37–7.15 (m, 7H), 7.01 (d, *J*=8.5, 2H), 6.92 (brs, 1H), 6.60 (s, 1H), 6.53 (d, *J* =14.5, 1H), 5.63 (brs, 1H), 5.21–5.18 (m, 2H), 5.10–5.05 (m, 3H), 4.99 (m, 1H), 4.76–4.70 (m, 2H), 4.67 (m, 1H), 4.59 (m, 1H), 4.28–4.22 (m, 2H), 3.64 (s, 3H), 3.10–3.07 (m, 2H), 2.92 (s, 3H), 2.90–2.85 (m, 4H), 2.73 (brs, 1H), 2.54 (m, 1H), 2.46 (m, 1H), 2.28 (s, 3H), 2.00 (s, 3H), 1.92 (s, 3H), 1.87 (m, 2H), 1.77 (s, 3H), 1.30–1.20 (m, 4H), 1.13 (m, 1H), 1.07 (m, 3H), 1.05 (m, 3H), 0.80 (t, *J* =7.5, 3H), 0.69 (d, *J* =7.5, 3H), 0.69 (d, *J* =7.5, 3H).

OsO_4 oxidation of 4 (5). Tetraacetate (**4**) (7.5 mg) was dissolved in 2 mL acetone in a 40-mL vial, and 5 mg of NMO (4–methylmorpholine *N*–oxide) and 20 μL of OsO_4 in H_2O solution were added to the vial. The reaction was conducted at 40 °C for 3 h. The mixture was dried under low pressure and purified by HPLC using a gradient solvent system (65% MeOH/water to 90% MeOH/water over 40 min, C_{18} reversed–phase column 250 × 10 mm, 5 μm, UV 280 nm detection, flow rate: 2 mL/min). The OsO_4 oxidation product **5** (4 mg) was isolated at a retention time of 41.5 min. The planar structure of **5** was confirmed by 1D and 2D NMR and ESI mass

spectral ($[M+H]^+$ *m/z* at 1276, molecular formula; $C_{62}H_{85}N_9O_{20}$. Compound **5** was stable during further acylation and subsequent CD spectroscopic measurement.

Esterification of 5 (6). A 4 mg quantity of OsO_4 oxidation product (**5**) was completely dried in vacuo for 24 h and dissolved in 1 mL of distilled anhydrous pyridine. A catalytic amount of DMAP (dimethylaminopyridine) and 20 μL of DMAB-Cl (4–(dimethylamino) benzoyl chloride) were added to the solution under argon gas. The reaction mixture was stirred at 40 °C for 5 h. The mixture was then dried and redissolved in MeOH. The dissolved material was injected on reversed–phase HPLC (Kromasil C18 (2): 250 × 10 mm, 5 μm, UV 280 nm detection, 40%–90% acetonitrile/water gradient system, flow rate: 2 mL/min). The bis-benzoyl ester product (**6**) was purified at 37 min. The structure of **6** was confirmed by ^{1}H NMR and ESI mass spectral ([M+H]+ m/z at 1570, molecular formula; $C_{80}H_{103}N_{11}O_{22}$) analyses.

Bis–benzoyl ester (**6**) : 1H NMR (500 MHz, DMSO– d_6) δ 8.43–8.32 (m, 6H), 8.03 (d, *J*=8.5, 2H), 7.94 (d, *J* =8.5, 2H), 7.36–7.20 (m, 5H), 6.93 (brs, 2H), 6.83 (d, *J* =8.5, 2H), 6.79(d, *J* =8.5, 2H), 6.62 (brs, 2H), 6.26 (s, 1H), 5.85 (brs, 1H), 5.48 (brs, 1H), 5.30 (d, *J*=6.0, 1H), 5.15–5.00 (m, 4H), 4.76–4.54 (m, 5H), 4.28–4.24 (m, 3H), 3.62 (s, 3H), 3.09 (s, 3H), 3.09 (s, 3H), 3.08–3.04 (m, 2H), 3.02 (s, 3H), 3.02 (s, 3H), 2.89 (s, 3H), 2.88–2.83 (m, 4H), 2.73 (brs, 1H), 2.54 (m, 1H), 2.46 (m, 1H), 1.99 (s, 3H), 1.98 (s, 3H), 1.90 (s, 3H), 1.85 (m, 2H), 1.78 (s, 3H), 1.31–1.23 (m, 5H), 1.04 (m,

3H), 1.02 (m, 3H), 0.83 (t, *J*=7.5, 3H), 0.69 (m, 3H), 0.69 (m, 3H).

Advanced Marfey's method. Mohangamide A (**1**) (3 mg) was hydrolyzed in 0.5 mL of 6 N HCl at 115 °C. After 2 h, the reaction vial was cooled down in ice water for 3 min. Then the HCl was removed *in vacuo* and the dry material was resuspended in 0.5 mL of H_2O, and dried three times to remove residual HCl completely. After the hydrolysate was lyophilized for 24 h, it was divided into two portions each in an 8 mL vial, and was dissolved in 100 μL of 1 N $NaHCO_3$, followed by the addition of 50 μL of either 10 mg/mL L-FDAA (1-fluoro-2,4-dinitrophenyl-5-L-alanine amide) or D-FDAA (1-fluoro-2,4-dinitrophenyl-5-D-alanine amide) in acetone, respectively. The reaction mixtures were incubated in a water bath at 80 °C for 3 min. Then 50 μL of 2 N HCl was added to quench the reaction by neutralization. Additionally, 300 μL of aqueous 50% CH_3CN was added to the solution to dissolve the mixture. A 10 μL aliquot of each reaction mixture was analyzed by LC/MS with a gradient solvent system (20% to 60% CH_3CN with 0.1% formic acid over 40 min, C_{18} reversed-phase column 100 × 4.6 mm, UV detection at 340 nm). The elution sequences of the FDAA derivatives in the LC/MS analysis established that phenylalanine possessed a D-configuration, whereas the other residues (Thr, Leu, Asn, and Ser) corresponded to L-amino acids (Table S4). For the absolute configurations of mohangamide B (**2**), the same procedures above were performed. The absolute configurations of the amino acid units commonly existing in **1** and **2** were identical. Different units, such as ^{8}Ser

and ^{9}*N*-MeTyr, were determined to be the L-form.

GITC derivatization. The hydrolysate of mohangamide A (**1**) was dissolved in H_2O (1 mg/mL) in an 8 mL vial. Then 100 μL of 1% GITC (2,3,4,6-tetra-*O*-acetyl-β-d-glucopyranosyl isothiocyanate) in acetone and 100 μL of 6% triethylamine were added to the vial. The reaction mixture was stirred for 15 min at room temperature. After stirring, 100 μL of 5% acetic acid was added to dilute the reaction mixture. The reaction mixture was analyzed by LC/MS with a gradient solvent system (10% to 100% CH_3CN with 0.1% formic acid over 20 min, C_{18} reversed-phase column 100 × 4.6 mm, UV detection at 254 nm). The authentic standards of L-Thr and *allo*-L-Thr were also derivatized by using the identical method. The GITC derivatives of the hydrolysate were injected simultaneously with those of the standard L-Thr and *allo*-L-Thr. The GITC derivatives of authentic L-Thr and *allo*-L-Thr eluted at 10.6 min and 10.3 min, respectively. The GITC derivatives of the hydrolysate of **1** displayed two retention times identical to those of L-Thr and *allo*-L-Thr (10.6 and 10.3 min), indicating mohangamide A (**1**) possesses both of them in its amino acid residues.

Isocitrate Lyase (ICL) activity assay. The 1-mL reaction volume consisted of 20 mM sodium phosphate buffer (pH 7.0), 1.27 mM threo-DL-(+)-isocitrate, 3.75 mM $MgCl_2$, 4.1 mM phenylhydrazine, and 2.5 μg/mL of recombinant ICL. The reaction was immediately initiated following the addition of substrate with or without a prescribed concentration of the inhibitor dissolved in DMSO (final concentration, 0.5%). Glyoxylate

phenylhydrazone formation was spectrophotometrically assessed at 324 nm after incubation at 37 °C for 30 min. Protein concentrations were measured using the Bradford method with the Bio-Rad protein assay kit (Bio-Rad) and bovine serum albumin as the standard. An inhibitor-free control was also prepared, and the percent inhibition of ICL enzyme activity for each compound was calculated relative to the inhibitor-free control. 3-Nitropropionic acid was used as a positive control.

Antibacterial activity Assay. Gram-positive bacteria (*Staphylococcus aureus* ATCC 25923, *Bacillus subtilis* ATCC 6633, and *Kocuria rhizophila* NBRC 12708) and gram-negative bacteria (*Salmonella enteric* ATCC 14028, *Proteus hauseri* NBRC 3851, and *Escherichia coli* ATCC 25922) were used for the antimicrobial activity tests.[22] The bacteria were incubated overnight in Luria Bertani (LB) broth at 37 °C, harvested by centrifugation, and washed twice with sterile distilled water. The compound solutions were prepared in DMSO. Each solution was diluted with Plate Count Broth (Difco) to generate serial 2-fold dilutions in the range of 50 to 0.8 μg/mL. Aliquots (10 μL) of the broth containing the test bacteria were added to each 96-well microtiter plate at a final concentration of 5×10^5 colony-forming units (cfu)/mL. The plates were incubated for 12 h at 37 °C. The MIC values were determined as the lowest concentration at which there is no visible growth. Ampicillin was used as a reference compound.

Cytotoxicity assay. The cytotoxicity for cultured cancer cells of compounds **1** and **2** was evaluated with a sulforhodamine B (SRB) assay.

Six human cancer cell lines (HCT116, MDA-MB231, SNU638, A549, K562, and SK-HEP1) were seeded into 96-well plates at 3×10^4 cells/mL and incubated with various concentrations of each compound at 37 °C in a humidified atmosphere with 5% CO_2. After 72 h, the cells were fixed with a 10% TCA solution for 1 h, and the cellular proteins were stained with 0.4% SRB in 1% acetic acid. The stained cells were dissolved in 10 mM Tris buffer (pH 10.0). The effects of **1** and **2** on cell cytotoxicity were calculated as a percentage relative to the solvent-treated control. The IC_{50} values were determined by non-linear regression analysis (percent survival *versus* concentration). Etoposide was used as positive control.

Plate assay. *C. albicans* strains were grown in a 6.7% yeast nitrogen base (YNB) containing 2% glucose at 28 °C for 24 h, harvested by centrifugation, and washed twice with sterile distilled water. Mohangamide A was dissolved in DMSO and added to YNB agar plates containing 2% glucose or 2% potassium acetate with serial two-fold dilutions in the range 8 × IC_{50}-1 × IC_{50}. Five microliters of the broth containing each strain was added to each plate (final concentration, 1×10^4 cells/mL), and the culture plates were incubated for 60 h at 28 °C.

II. II. Experimental section

Isolation of WS9326F-I (7–10). The crude extract was concentrated with celite and loaded on a 2 g Sep-Pak C_{18} cartridge. The yellow powder was fractionated with 100 mL each of 20%, 40%, 60%, 80%, and 100% MeOH in water. WS9326F–H (**1**–**3**) were obtained in the 60%–80% MeOH/H_2O fractions. The 60% and 80% fractions were separated by semi-preparative reversed–phase HPLC (Kromasil C_{18} (2): 250 × 10 mm, 5 μm) using a gradient solvent system (65% MeOH/water to 90% MeOH/water over 40 min and 90% MeOH/water from 40 to 50 min, UV 280 nm detection, flow rate: 2 mL/min) to yield **7** (8 mg, t_R 37.2 min), **8** (6.5 mg, t_R 35.5 min), **9** (7 mg, t_R 35.2 min), and **10** (5.5 mg, t_R 17.5 min),. Each of compounds were further purified with a C_{18} HPLC column (Kromasil C_{18} (2): 250 × 10 mm, 5 μm) using isocratic conditions in 50% ACN/water (UV 280 nm detection, flow rate: 2 mL/min). WS9326F–I (**7**–**10**) were collected as pure compounds at retention times of 34.3min, 29.5, 26.2, and 15.7 min, respectively.

WS9326F (7): White powder; $[\alpha]^{25}_D$ +56 (*c* 0.5, MeOH); UV (MeOH) λ_{max} (log ε) 285 (4.46) nm; IR (neat) ν_{max} 3286, 2956, 1653, 1547, 1252 cm^{-1}; ^1H and ^{13}C NMR data, see Table 4; HRFABMS *m*/*z* 1025.4983 $[M + H]^+$ (calcd for $C_{53}H_{68}N_8O_{13}$, 1025.4984).

*WS9326G (**8**)*: White powder; $[\alpha]^{25}_D$ +32 (*c* 0.5, MeOH); UV (MeOH) λ_{max} (log ε) 285 (4.28) nm; IR (neat) ν_{max} 3297, 2958, 1650, 1546, 1395 cm^{-1}; ^1H and ^{13}C NMR data, see Table 4; HRFABMS *m*/*z* 990.4598 $[M + Na]^+$ (calcd

for $C_{51}H_{65}N_7O_{12}Na$, 990.4589).

*WS9326H (**9**)*: White powder; $[\alpha]^{25}_D$ +48 (*c* 0.5, MeOH); UV (MeOH) λ_{max} (log ε) 285 (4.5) nm; IR (neat) ν_{max} 3284, 2957, 1655, 1548, 1278 cm^{-1}; ^1H and ^{13}C NMR data, see Table 5; HRFABMS *m/z* 976.4438 $[M + Na]^+$ (calcd for $C_{50}H_{63}N_7O_{12}Na$, 976.4432).

*WS9326I (**10**)*: White powder; $[\alpha]^{25}_D$ +37 (*c* 0.5, MeOH); UV (MeOH) λ_{max} (log ε) 285 (4.12) nm; IR (neat) ν_{max} 3275, 2954, 1650, 1544, 1264 cm^{-1}; ^1H and ^{13}C NMR data, see Table 6; HRFABMS *m/z* 1335.5966 $[M + Na]^+$ (calcd for $C_{63}H_{84}N_{12}O_{19}Na$, 1335.5878).

Preparation of hydrogenated derivative of 10 (11). WS9326I (**10**) (1.5 mg) was prepared in a 40 mL vial and dried under high vacuum for 24 h. Then, compound **10** was dissolved in 2:1 mixture of acetic acid and methanol (1 mL) with sodium cyanoborohydride (3 mg). The solution was stirred at rt under argon for 4 h. To quench the reaction, 10 % HCl aqueous solution was added. The reaction mixture was fractionated by flash column reversed-phase chromatography using a gradient solvent system of MeOH/H_2O (20%, 40%, 60%, 80%, and 100%). The product **11** was purified by re by reversed-phase HPLC (Phenomenex Luna 5 μm C_{18} (2) 250 × 10.0 mm, flow rate 2 mL/min, UV 254 nm detection) with a gradient solvent system (15% to 85% ACN/H_2O) for 40 min. The acetonide product (**12**) eluted at a retention time of 20.6 min (1 mg, 67 %) under the HPLC conditions. The molecular formula of **11** was confirmed as $C_{63}H_{86}N_{12}O_{19}$ by ESIMS analysis ($[M + H]^+$ *m/z* at 1314).

Hydrogenated product (**11**). ^{1}H NMR (600 MHz, pyridine-d_5)) δ_H 12.15 (s, 1H), 11.82 (br, 1H), 10.42-10.40 (br, 2H), 9.49-9.46 (m, 2H), 8.76-74 (br, 2H), 8.31 (br, 1H), 8.07 (br, 1H), 7.96 (br, 1H), 8.32 (br, 1H), 8.16 (b r, 1H), 7.64-7.60 (m, 3H), 7.37-7.34 (m, 4H), 7.27-7.25 (m, 4H), 7.11-7.07 (m, 3H), 6.85 (d, J = 10.5, 1H), 6.03 (m, 1H), 5.71 (m, 2H), 5.48 (m, 1 H), 5.40 (d, J = 10.5 Hz, 1H), 5.27 (m, 1H), 5.12 (m, 1H), 4.76 (m, 1H), 4.6 0 (m, 1H), 4.50-4.46 (m, 3H), 4.42-4.41 (m, 2H), 4.37-4.34 (m, 3H), 4.46-4.44 (m, 2H), 4.31-4.28 (m, 2H), 4.26-4.21 (m, 2H), 3.91 (m, 1H), 3.77 (m, 1H), 3.60 (m, 2H), 3.55 (m, 1H), 3.50 (m, 1H), 3.39-3.35 (m, 2H), 2.98 (s, 3H), 2.81 (m, 1H), 2.45 (br, 2H), 2.06-2.04 (m, 2H), 1.52 (d, J = 6.5 Hz, 3H), 1.41 (m, 1H), 1.33 (s, 1H), 1.20-1.15 (m, 2H), 0.62 (d, J = 6.5 Hz, 6H), 0.55 (d, J = 6.5 Hz, 3H), 0.48 (d, J = 6.5 Hz, 3H).

Advanced Marfey's method. Each of 2 mg of WS9326F, G, H, and I (**7**, **8**, **9**, and **10**) were hydrolyzed in 0.5 mL of 6 N HCl at 115 °C. After stirring mixtures for 2 h, the reaction vial were cool down rapidly in the ice box for 3min and concentrated in *vacuo*. For removing residual HCl entirely, 0.5 mL of H_2O was added to each of vials and removed the solvent three times. The hydrolysates were lyophilized for 24 h. After lyophilization, each of hydrolysates were separated into two 8 mL vials, and were soluble in 100 μL of 1 N $NaHCO_3$. And then, 50 μL of either 10mg/mL L-FDAA (1-fluoro-2,4-dinitrophenyl-5-L-alanine amide) or D-FDAA (1-fluoro-2,4-

dinitrophenyl-5-D-alanine amide) in acetone was added to each of vials. The vials were placed in 80 °C water bath for 3 min. Then, 50 μL of 2 N HCl was added to neutralize the solvent and 300 μL of aqueous 50% CH_3CN was added. A 10 μL aliquot of each reaction mixture was injected to LC-MS and analyzed with a gradient solvent system (20% to 60% ACN with 0.1% formic acid over 40 min, C_{18} reversed-phase column 100 × 4.6mm, UV at 340 nm). The absolute configuration of all of the amino acid residues in **7-10** were confirmed as L, except phenylalanine (as D) as same as WS9326A.

Preparation of acetonide derivative of 10 (12). WS9326I (**10**) (5 mg) was prepared in a 40 mL vial and dried under high vacuum for 24 h. After adding pyridinium *p*-toluenesulfonate (1 mg), the mixture was dissolved in anhydrous MeOH (200 μL) and anhydrous CH_2Cl_2 (2 mL) at rt. Then, 2,2-dimethoxypropane (4 mL) was added to the reaction vial. The solution was stirred at rt under argon for 48 h. To quench the reaction, a saturated $NaHCO_3$ aqueous solution was added. The reaction mixture was fractionated by flash column reversed-phase chromatography using a gradient solvent system of MeOH/H_2O (20%, 40%, 60%, 80%, and 100%). The acetonide derivative (**12**) was eluted in the 80% and 100% MeOH/H_2O fractions. The final product (**12**) was purified by reversed-phase HPLC (Phenomenex Luna 5 μm C_{18} (2) 250 × 10.0 mm, flow rate 2 mL/min, UV 254 nm detection) with a gradient solvent system (25% to 65% ACN/H_2O) for 40 min. The acetonide product (**12**) eluted at a retention time of 29.3 min (3.5 mg, 83%) under the HPLC conditions. The molecular formula of **12**

was confirmed as $C_{66}H_{88}N_{12}O_{19}$ by ESIMS analysis ($[M + H]^+$ *m/z* at 1353). Acetonide product (**12**). ^{1}H NMR (600 MHz, pyridine-d_5)) δ_H 12.84 (s, 1H), 11.73 (s, 1H), 10.55 (br, 1H), 10.02 (br, 1H), 9.88 (br, 1H), 9.58-9.56 (br, 2H), 9.52 (br, 1H), 8.56 (br, 1H), 8.32 (br, 1H), 8.16 (br, 1H), 7.75-7.67 (m, 3H), 7.48-7.46 (m, 2H), 7.32-7.26 (m, 7H), 7.02-7.00 (m, 2H), 6.72 (d, *J* = 10.5, 1H), 6.11 (m, 1H), 5.84 (m, 2H), 5.61-5.58 (m, 3H), 5.40 (d, *J* = 10.5 Hz, 1H), 4.78-4.72 (m, 5H), 4.61-4.53 (m, 3H), 4.46-4.44 (m, 2H), 4.37-4.32 (m, 5H), 4.20-4.04 (m, 3H), 3.71 (m, 1H), 3.62 (m, 1H), 3.52 (m, 1H), 3.38 (m, 1H), 3.08 (s, 3H), 2.17 (m, 2H), 2.06-2.04 (m, 2H), 1.73 (d, *J* = 6.5 Hz, 3H), 1.41 (s, 3H), 1.31 (s, 3H), 1.28-1.25 (m, 5H), 0.74 (t, *J* = 6.5 Hz, 3H), 0.69 (d, *J* = 6.5 Hz, 3H), 0.58 (m, 6H).

Acetylation of 12 (13). The acetonide product **12** was dried *in vacuo* for 24 h. Product **12** was dissolved in 1 mL of distilled anhydrous pyridine. After flushing with argon gas, 1 mL of acetic anhydride was added and stirred at room temperature for 5 h. The solution was evaporated under high vacuum for 4 h. The product was purely isolated by reversed–phase HPLC (Kromasil C_{18} (2): 250 × 10 mm, 5 μm) with a gradient solvent system (45 % acetonitrile/water to 95 % ACN/H_2O over 40 min, UV 280 nm detection, flow rate: 2 mL/min). Pentaacetate **12** (**13**) (3 mg) eluted at 32.8 min, and its structure was determined by ^{1}H NMR spectroscopy and by low-resolution ESI-MS ([M+H]+ m/z at 1562, molecular formula; $C_{76}H_{98}N_{12}O_{24}$).

Pentaacetate (**13**). ^{1}H NMR (600 MHz, pyridine-d_5)) δ_H 13.14 (s, 1H), 10.33 (s, 1H), 10.05 (d, J = 6.5 Hz, 1H), 10.02 (br, 1H), 9.52 (d, J = 7.5 Hz, 1H), 9.34 (d, J = 9.0 Hz, 1H) 8.95 (br, 1H), 8.74-8.72 (br, 2H), 8.36 (d, J = 8.5 Hz, 1H), 8.06 (d, J = 7.5 Hz, 1H) 7.84 (d, J = 8.0 Hz, 2H), 7.62 (br, 1H), 7.39 (d, J = 8.0 Hz, 2H), 7.34 (d, J = 7.5 Hz, 2H), 7.31 (m, 1H), 7.24 (m, 1H), 7.16-7.14 (m, 2H), 7.13 (d, J = 7.5 Hz, 1H), 6.97 (d, J = 10.0 Hz, 1H), 6.76 (s, 1H), 5.96-5.93 (m, 3H), 5.81 (m, 1H), 5.77 (m, 1H), 5.66 (m, 1H), 5.52-5.49 (m, 2H), 5.37 (d, J = 10.0 Hz, 1H), 5.07 (m, 2H), 4.70-4.67 (m, 3H), 4.62-4.56 (m, 2H), 4.28-4.24 (m, 3H), 4.14-4.09 (m, 4H), 3.59-3.51 (m, 3H), 3.26 (m, 1H), 3.13 (s, 3H), 2.71 (br, 2H), 2.22 (s, 3H), 2.18 (m, 2H), 2.12-2.10 (m, 2H), 2.00 (s, 3H), 1.83 (s, 3H), 1.70 (d, J = 6.5 Hz, 3H), 1.69 (s, 3H), 1.42 (s, 3H), 1.32-1.30 (m, 2H), 1.28 (s, 3H), 1.24-1.22 (m, 2H), 0.85 (d, J = 6.5 Hz, 3H), 0.76 (t, J = 6.5 Hz, 3H), 0.60 (d, J = 6.5 Hz, 3H), 0.49 (d, J = 6.5 Hz, 3H).

Preparation of Acetonide deprotection product of 13 (14). Product **13** (3 mg) was prepared in a 40 mL vial and dried under high vacuum for 24 h. After adding pyridinium *p*-toluenesulfonate (1 mg), the mixture was dissolved in anhydrous MeOH (1 mL) at rt. The solution was stirred at rt under argon for 4 h. To quench the reaction, a saturated $NaHCO_3$ aqueous solution was added. The reaction mixture was fractionated by flash column reversed-phase chromatography using a gradient solvent system of MeOH/H_2O (20%, 40%, 60%, 80%, and 100%). The final product (**14**) was eluted in the 80% and 100% MeOH/H_2O fractions. The product **14** was

isolated by reversed-phase HPLC (Phenomenex Luna 5 μm C_{18} (2) 250 × 10.0 mm, flow rate 2 mL/min, UV 254 nm detection) with a gradient solvent system (45% to 95% ACN/H_2O) for 40 min. The product **14** eluted at a retention time of 26.5 min (1.5 mg, 50 %) under the HPLC conditions. The molecular formula of **14** was confirmed as $C_{73}H_{94}N_{12}O_{24}$ by ESIMS analysis ($[M + H]^+$ *m*/*z* at 1522).

Acetonide deprotected product (**14**). ^1H NMR (600 MHz, pyridine-d_5)) δ_H 13.15 (s, 1H), 11.64 (s, 1H), 10.44 (br, 1H), 9.93 (br, 1H), 9.84 (br, 1H), 9.52 (br, 1H), 9.25 (br, 1H), 8.93 (br, 1H), 8.76 (br, 1H), 8.40 (br, 1H), 8.32 (br, 1H), 8.24 (br, 1H), 7.81 (d, *J* = 8.0, 2H), 7.55-7.53 (m, 2H), 7.48-7.46 (m, 2H), 7.39-7.36 (m, 2H), 7.33 (t, *J* = 8.0, 1H), 7.21 (m, 1H), 7.00 (*J* = 8.0, 2H), 6.80 (d, *J* = 10.5 Hz, 1H), 6.72 (s, 1H), 6.27 (m, 1H), 5.88 (m, 2H), 5.77-5.67 (m, 3H), 5.50 (t, *J* = 6.5 Hz, 1H), 5.34 (d, *J* = 10.5 Hz, 1H), 5.17 (m, 1H), 5.06 (m, 1H), 4.63 (m, 1H), 4.57-4.53 (m, 3H), 4.36-4.29 (m, 2H), 4.23-4.21 (m, 3H), 4.16 (m, 1H), 4.09-4.01 (m, 3H), 3.55 (m, 1H), 3.49 (m, 1H), 3.39 (m, 1H), 3.30 (m, 1H), 3.00 (s, 3H), 2.29 (m, 2H), 2.14 (s, 3H), 2.06-2.04 (m, 2H), 1.98 (s, 3H), 1.69 (s, 3H), 1.64 (d, *J* = 6.5 Hz, 3H), 1.41 (s, 3H), 1.33-1.28 (m, 2H), 1.23 (s, 3H), 1.16-1.14 (m, 2H), 0.76 (t, *J* = 6.5 Hz, 3H), 0.64 (d, *J* = 6.5 Hz, 3H), 0.50 (m, 6H).

MTPA esterification of 14 (15, 16). The acetonide deprotected pr oduct **14** were prepared individually in 40-mL vials (two 1-mg sample s for each compound) and dried completely under high vacuum overni ght. After adding catalytic amounts of crystalline dimethylaminopyridin

e (DMAP) to each reaction vial, freshly distilled anhydrous pyridine (1 mL) was added under argon gas. The reaction mixtures were stirre d at room temperature for 5 min. After 5 min, *R*- and *S*-α-methoxy t rifluoromethyl-phenylacetic acid (MTPA) chloride (20 μL) were added, respectively. The reactions were carried out for 3 h at room temperat ure with stirring. The reactions were quenched by adding 50 μL of MeOH. The reaction products were purified by HPLC using gradient elution conditions of 40% to 100% aqueous acetonitrile over 20 min with a reversed-phase C_{18} column (Kromasil C_{18} (2): 250 × 10 mm, 5 μm; flow rate: 2 mL/min; UV detection at 280 nm). The di-*S*- and di-*R*-MTPA esters (**15** and **16**) of **14** eluted at 30.3 and 32.2 min, res pectively. The $\Delta\delta_{S-R}$ values around the stereogenic centers of the MTP A esters were assigned based on the analysis of ^{1}H and ^{1}H-^{1}H COSY NMR spectra.

The molecular formula of **15** and **16** was confirmed as $C_{93}H_{109}F_6N_{12}O_{28}$ by ESIMS analysis ($[M + H]^+$ *m*/*z* at 1955).

S-MPTA ester of **14** (**15**). ^{1}H NMR (600 MHz, pyridine-d_5)) δ_H 13.25 (s, 1H), 11.54 (s, 1H), 10.63 (br, 1H), 10.31 (br, 1H), 10.26 (br, 1H), 9.69 (br, 1H), 9.13 (br, 1H), 8.93 (br, 1H), 8.63 (br, 1H), 8.59 (br, 1H), 8.22 (br, 1H), 7.87 (d, *J* = 8.0, 2H), 7.54-7.48 (m, 8H), 7.42-7.38 (m, 8H), 7.33-7.27 (m, 3H), 7.05 (*J* = 10.5, 1H), 6.88 (s, 1H), 6.01-5.99 (m, 2H), 5.90 (m, 1H), 5.85 (m, 1H), 5.77-5.67 (m, 4H), 5.58-5.55 (m, 2H), 5.50 (m, 1H), 5.44 (m, 1H), 5.34 (m, 1H), 5.25 (m, 1H), 5.17 (m, 1H), 4.79 (m, 1H), 4.71 (m, 1H), 4.63

(m, 1H), 4.39 (m, 1H), 4.34 (m, 1H), 4.25 (m, 1H), 4.15 (m, 1H), 4.08 (m, 1H), 3.53 (s, 3H), 3.51 (s, 3H), 3.41 (m, 1H), 3.32-3.31 (m, 2H), 3.13 (s, 3H), 2.35 (m, 2H), 2.19 (s, 3H), 2.15 (s, 3H), 2.03 (s, 3H), 1.77 (s, 3H), 1.64 (d, J = 6.5 Hz, 3H), 1.47 (s, 3H), 1.34-1.32 (m, 2H), 1.31 (s, 3H), 1.22-1.20 (m, 2H), 0.82 (t, J = 6.5 Hz, 3H), 0.72 (d, J = 6.5 Hz, 3H), 0.58 (d, J = 6.5 Hz, 3H), 0.52 (d, J = 6.5 Hz, 3H).

R-MPTA ester of **14** (**16**). ^{1}H NMR (600 MHz, pyridine-d_5)) δ_H 13.26 (s, 1H), 11.47 (s, 1H), 10.28 (br, 1H), 9.73 (br, 1H), 9.64 (br, 1H), 9.15 (br, 1H), 8.96-8.85 (m, 2H), 8.50 (br, 1H), 8.39 (br, 1H), 8.06 (br, 1H), 7.78-7.76 (m, 4H), 7.60-7.56 (m, 4H), 7.50-7.36 (m, 6H), 7.42-7.38 (m, 5H), 7.33-7.27 (m, 2H), 7.01 (J = 8.0, 1H), 6.94 (s, 1H), 5.94-5.89 (m, 2H), 5.69-5.64 (m, 5H), 5.55-5.52 (m, 4H), 5.12-5.10 (m, 4H), 4.85 (m, 1H), 4.81 (m, 1H), 4.64-4.62 (m, 2H), 4.57-4.55 (m, 2H), 4.24 (br, 2H), 4.10 (m, 1H), 3.82 (m, 1H), 3.72 (m, 1H), 3.62 (s, 3H), 3.56 (s, 3H), 3.13 (s, 3H), 2.32 (m, 2H), 2.23 (s, 3H), 2.06 (s, 3H), 1.94 (s, 3H), 1.71 (s, 3H), 1.65 (d, J = 6.5 Hz, 3H), 1.52 (s, 3H), 1.40-1.38 (m, 2H), 1.34 (s, 3H), 1.29-1.27 (m, 2H), 0.82 (t, J = 6.5 Hz, 3H), 0.60 (m, 6H), 0.54 (d, J = 6.5 Hz, 3H).

DP4 analysis. For the DP4 application, conformers of diastereomers of four models within 10 kJ/mol found in the MMFF force field were regarded and the geometry of the conformers was optimized at the B3LYP/6-31G++ level in the gas phase. The shielding tensor values of the optimized conformers were computed at the B3LYP/6-31++ level. These values were averaged based on the Boltzmann population in the associated Gibbs free

energy and utilized for DP4 analysis facilitated by an Excel sheet provided by the original authors.

Antifungal activity assay. *Candida albicans* ATCC 10231 was cultivated with YPD medium (1% yeast extract, 2% peptone, and 2% dextrose). After incubation for 48 h at 28 °C, the cells were harvested by centrifugation and washed twice with sterile distilled water. *Aspergillus fumigatus* HIC 6094, *Trichophyton rubrum* NBRC 9185, and *T. mentagrophytes* IFM 40996 were plated onto potato dextrose agar plates and incubated for 2 weeks at 28 °C. Spores were harvested and washed twice with sterile water, and then the spores were resuspended in water to an initial inoculum concentration of 5×10^5 spores/mL. In each well of a 96-well plate, 10 μL of the cell suspension was mixed with 90 μL of potato dextrose broth (Difco) (5×10^4 cells/mL) containing the test compound in DMSO solutions (final concentration, 0.5%).[22] A culture containing DMSO (0.5%) and a culture supplemented with amphotericin B were used as a solvent control and as a positive control, respectively.

***In vitro* capillary tube formation assay.** Matrigel (70 μl/well) was coated on 96-well plate and polymerized for 30 min at 37 ℃. HUVECs (1.5×10^4 cells/well) and WS9326A-E, WS9326F-I (**7-10**) (0-20μM) were seeded onto each well of the Matrigel-coated 96-well plate with EBM-2 medium . Then, cells were incubated for 8hrs. The formation of endothelial cell tubular structure was visualized under an inverted microscope and photographed. Furthermore, tube formation was quantified by calculating

the tube number and was expressed as a percentage by normalization with untreated control cells.

III. III. Experimental section

Isolation of the hormaomycins. The extract of SNM55 (one sixth of the 4 g of dry material collected) was absorbed on Celite and loaded on a 2 g Sep-Pak C_{18} cartridge. Then, the extract was fractionated with 20 mL each of 20%, 40%, 60%, 80%, and 100% MeOH in water and 1:1 MeOH/dichloromethane. The hormaomycins were detected in the 80% and 100% MeOH/water fractions by LC/MS. The 80% and 100% fractions were combined into one vial and subjected to semi-preparative reversed–phase HPLC (Kromasil C_{18} (2): 250 × 10 mm, 5 μm) using a gradient solvent system (65% MeOH/H_2O to 90% MeOH/H_2O over 40 min and 100% MeOH from 40 min to 50 min, UV 280 nm detection, flow rate: 2 mL/min). Three fractions containing the hormaomycins were collected at retention times of 43 min, 45 min, and 52 min. Each of the hormaomycins was purified by an isocratic solvent system (75% acetonitrile/H_2O, UV 280 nm detection, flow rate: 2 mL/min) using a reversed–phase C_{18} column (Kromasil C_{18} (2): 250 × 10 mm, 5 μm). Hormaomycins B (**18**) (4 mg), hormaomycin C (**19**) (3 mg), and hormaomycin (6 mg) eluted as pure compounds at retention times of 14.5 min, 15.2 min, and 18.4 min, respectively, under the final purification conditions.

Hormaomycin B (**18**): $[\alpha]_D$ 21.9, (c 0.025, MeOH); UV (MeOH) λ_{max} (log ε) 208 (4.57), 271 (4.08) nm; IR (neat) ν_{max} 3309, 2958, 1626, 1543, 1369 cm^{-1}; for ^1H and ^{13}C NMR data, see Table 1; HRFABMS *m*/*z* 1115.4611 $[M+H]^+$ (calcd for $C_{54}H_{68}ClN_{10}O_{14}$ 1115.4605).

Hormaomycin C (**19**): $[\alpha]_D$ 29.9, (c 0.025, MeOH); UV (MeOH) λ_{max} (log ε) 208 (4.57), 271 (4.09) nm; IR (neat) ν_{max} 3343, 2931, 1627, 1554, 1362 cm^{-1}; for ^1H and ^{13}C NMR data, see Table 1; HRFABMS *m*/*z* 1137.4432 $[M+Na]^+$ (calcd for $C_{54}H_{67}ClN_{10}O_{14}Na$ 1137.4424).

Conclusions. As one approach to maximize microbial chemical diversity, altering the culture conditions of a chemically prolific marine actinomycete strain (SNM55) led us to discover hormaomycins B and C (**18** and **19**). These hormaomycins are structurally unique cyclic depsipeptides that incorporate various unusual units, such as 4-(*Z*)-propenylproline, 3-(2-nitrocyclopropyl)alanine, β-methylphenylalanine and 5-chloro-1-hydroxypyrrol-2-carboxylic acid. The hormaomycins inhibited various pathogenic Gram-positive and Gram-negative bacteria. To the best of my knowledge, hormaomycins B and C are the first natural analogues of hormaomycin. The discovery of these new members of the hormaomycin family provides additional evidence that marine actinomycetes possess the potential to produce still-untapped bioactive secondary metabolites, which can be synthesized through diverse biosynthetic pathways under appropriate culture conditions.

Part B

Polyketides from marine *Streptomyces* spp.

I. Mohangic acids A-E, *p*-aminoacetophenonic acids from a marine mudflat-derived *Streptomyces* sp. SNM31

I. I. Results and discussion

Mohangic acid A (**20**) was isolated as a yellow gum with a molecular formula of $C_{26}H_{37}NO_6$ according to ^{1}H and ^{13}C NMR and high-resolution FAB mass spectroscopy. The ^{1}H NMR (in CD_3OD) spectrum of **20** showed each of two overlapped aromatic protons at δ_H 7.77 and 6.64, six olefinic protons from 6.26 to 5.69 ppm, three carbinol protons at 4.48, 4.03, and 3.12 ppm, nine aliphatic protons between 2.97 and 1.22 ppm, and three methyl groups at 1.02, 0.90, and 0.87 ppm in the shielded region. The ^{13}C NMR and HSQC spectra of **20** displayed one ketone carbonyl at 200.3 ppm, one carboxylic acid carbon at 177.8 ppm, 12 sp^2 carbons between 155.5 and 114.6 ppm, three oxygenated sp^3 carbons at 80.8, 74.3, and 70.5 ppm, six aliphatic sp^3 carbons between 44.5 and 34.5 ppm, and three methyl carbons at δ_C 18.4, 15.5, and 14.2. Because 12 olefinic carbon signals (six double bonds) and two carbonyl carbons accounted for eight of the nine degrees of unsaturation deduced from the molecular formula of **20**, mohangic acid A (**20**) must contain a ring structure.

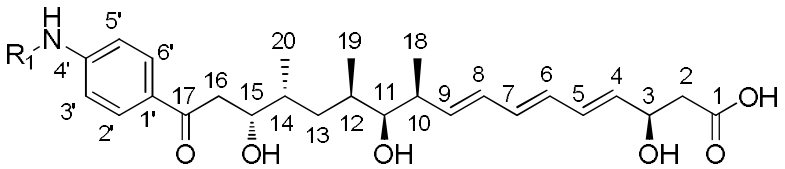

20 R_1 = H **21** R_1 = $^{7'}CH_3$ **22** R_1 = $^{7'}CO^{8'}CH_3$

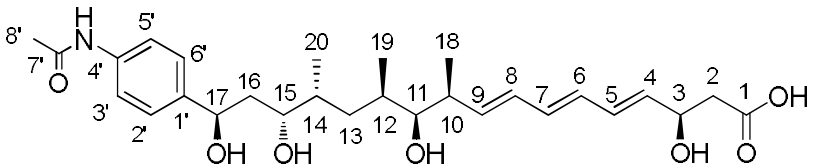

23

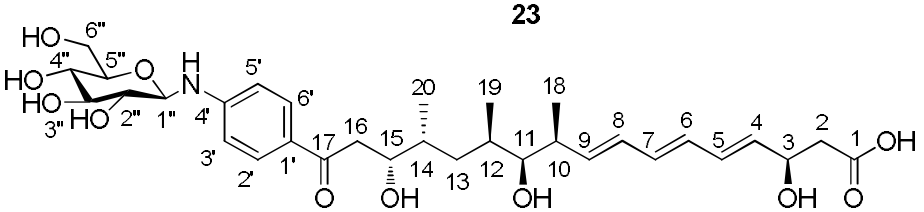

24

All $^1J_{CH}$ correlations were fully assigned by analysis of HSQC spectroscopic data (Table 9). Interpretation of the COSY and HMBC spectra elucidated two partial structures (Figure 15). First, the COSY correlations from H_2-2 (δ_H 2.41) to H-3 (δ_H 4.48) showed connectivity from C-2 (δ_C 44.5) to C-3 (δ_C 70.5). The oxygenated carbon C-3 was deduced to be directly connected to sp^2 carbon C-4 (δ_C 135.7) on the basis of the COSY correlation between H-3 and H-4 (δ_H 5.69). Further analysis of the COSY correlations of the six olefinic protons resulted in the construction of a triene moiety running from C-4 to C-9 (δ_C 138.4). The geometries of the double bonds in the triene structure were determined to be 4*E*, 6*E*, and 8*E* on the basis of the *trans* ^1H–^1H coupling constants (J = 15.0 Hz) observed in the olefinic proton peaks. The COSY correlation between H-9 (δ_H 5.72) and H-

10 (δ_H 2.42) revealed that the triene moiety was connected to the C-10 aliphatic carbon (δ_C 41.6). In addition, COSY correlations from H-10 to H_2-16 (δ_H 2.97, 2.95) expanded the chain from C-10 to C-16 (δ_C 42.4). Three doublet methyl groups (C-18, C-19, and C-20; δ_C 18.4, 14.2, and 15.5) were located at C-10, C-12 (δ_C 34.5), and C-14 (δ_C 37.4), respectively, according to the H_3-18 (δ_H 1.02)/H-10, H_3-19 (δ_H 0.87)/H-12, and H_3-20 (δ_H 0.90)/H-14 (δ_H 1.71) homonuclear correlations. The $^2J_{CH}$ couplings from H_2-2 to C-1 (δ_C 177.8) and from H_2-16 to C-17 (δ_C 200.3) established the first partial structure, a chain composed of 20 carbons bearing three branch methyl groups.

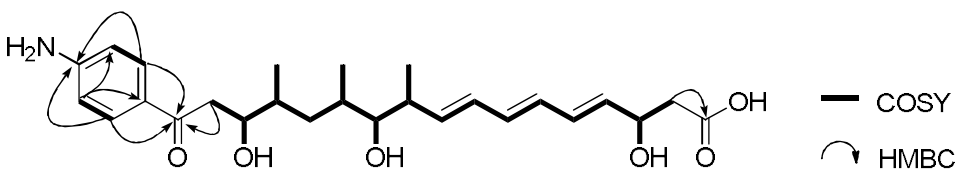

Figure 15. Key COSY and HMBC correlations of mohangic acid A (**20**).

The ^{1}H NMR spectroscopic data of **20** displayed a typical feature of *para*-substituted aromatic ring protons, H-2'/H-6' (δ_H 7.77/δ_H 7.77) and H-3'/H-5' (δ_H 6.64/δ_H 6.64). Strong COSY correlations between H-2'/H-6' and H-3'/H-5' and HMBC correlations from these protons indicated an aromatic ring. HMBC correlations from H-2'/H-6' to C-17 indicated connectivity between the chain and the aromatic ring via the carbonyl carbon C-17. A primary amine group deduced from the molecular formula was assigned at C-4' (δ_C 155.5), which was the last open position requiring a functional

group based on the chemical shift of C-4', thus completing the planar structure of **20**. The assigned structure was further confirmed by the analysis of 1D and 2D NMR data of **20** acquired in pyridine–d_5 (Table10).

Mohangic acid B (**21**) was obtained as a yellow gum, and its molecular formula was deduced to be $C_{27}H_{39}NO_6$ on the basis of HRFABMS data combined with ^{1}H and ^{13}C NMR spectroscopic data (Table 9). Careful comparison of NMR spectroscopic data revealed that the ^{1}H NMR spectrum of **21** in CD_3OD was very similar to that of **20**. Careful analysis of the 1D and 2D NMR spectroscopic data of **21** revealed that mohangic acid B (**21**) differs from **20** by one *N*-methyl group (δ_H 2.83; δ_C 30.4). A $^3J_{CH}$ correlation from the *N*-methyl protons (δ_H 2.83) to C-4' (δ_C 155.0) assigned the methyl group C-7" to the amine at C-4' in the *para*-substituted aromatic ring. Thus, the structure of mohangic acid B (**21**) was determined as an *N*-methyl analogue of **20**.

Mohangic acid C (**22**) was purified as a yellow gum determined to possess a molecular formula of $C_{28}H_{39}NO_7$ on the basis of HRFABMS data in combination with ^{1}H and ^{13}C NMR data (Table 9). The 1D and 2D NMR spectroscopic data of **22** displayed features analogous to those of **21** except for the absence of an *N*-methyl group (δ_H 2.83; δ_C 30.4) in **21** and the presence of a singlet methyl group (δ_H 2.13; δ_C 22.5) and an additional carbonyl carbon (δ_C 171.0) in **22**. Further analysis of 2D NMR spectra indicated the presence of an *N*-acetyl group, thus elucidating the structure of **22** as the *N*-acetylated congener of **20**.

Mohangic acid D (**23**) was isolated as a yellow gum. The molecular formula was assigned as $C_{28}H_{41}NO_7$ on the basis of HRFABMS and ^1H and ^{13}C spectroscopic data (Table 9). Although the NMR spectra of **23** were similar to those of **22**, an additional signal of a carbinol proton (δ_H 4.85) directly bound to an oxygenated carbon (δ_C 71.5) and the lack of the ketone carbonyl signal (δ_C 200.0) previously observed in the ^{13}C spectrum of **22** indicated distinct a difference between **22** and **23**. Analysis of 2D NMR spectra indicated that the C-17 ketone carbonyl in **22** was reduced to a hydroxy group in **23**, subsequently establishing the planar structure of **23**.

Mohangic acid E (**24**) was obtained as a yellow gum with a molecular formula of $C_{32}H_{47}NO_{11}$ on the basis of the HRFABMS and ^1H and ^{13}C spectroscopic data (Table 1). In contrast to the mohangic acids B–D (**21**–**23**), the molecular weight of **24** is 162 Da larger than that of **20**. In addition, mohangic acid E (**24**) is much more hydrophilic than the other congeners based on reversed-phase HPLC analysis. These observations led us to speculate that mohangic acid E (**24**) should be a glycosylated version of **20**. Careful analysis of the 1D and 2D NMR spectra revealed that mohangic acid E possesses one hexose. This hexose was determined to be a β–glucose by analysis of the coupling constants $^3J_{HH}$ and $^1J_{CH}$ (154 Hz)[32] and on the basis of ROESY NMR correlations among the axially oriented sugar protons. Further analysis of HMBC correlation from δ_H 4.63, δ_H 7.84 to δ_C 153.6 and ROESY correlation between δ_H 4.63 and δ_H 6.82 revealed that the β–glucose is located on the aromatic nitrogen. To determinate the absolute

configuration of the glucose moiety in **24**, it was subjected to acid hydrolysis. The hydrolysate and authentic L- and D-glucose samples were respectively derivatized with hexamethyldisilazane (HMDS) and TMS-Cl.[33] GC/MS analysis of the derivatives clarified that the glucose in mohangic acid E (**24**) has a D-configuration because the derivative of the glucose in **24** exhibited a retention time consistent with that of authentic D-glucose derivative.

Mohangic acids A-E (**20**–**24**) have several stereogenic centers in their chains. To determine their configurations, I performed comprehensive spectroscopic analyses and various chemical derivatizations. I first conducted homo-decoupling spectroscopic experiments of mohangic acid A (**20**) to extract exact $^{3}J_{HH}$ values for H-10/H-11, H-11/H-12, H-12/H_2-13, H_2-13/H-14, and H-14/H-15 couplings; the ^{1}H–^{1}H coupling constants for these protons were not measurable in the ordinary ^{1}H NMR spectra because of their complicated multiplicities. After ^{1}H-^{1}H coupling constants were clearly measured, long-range heteronuclear coupling constants were acquired by a HETLOC (hetero half-filtered TOCSY) NMR experiment.[34] *J*–based configuration analysis was performed using the obtained $^{3}J_{HH,}$ $^{3}J_{CH}$, and $^{2}J_{CH}$ values and ROESY NMR correlations (Figure 16).[15] On the basis of the *J*–based configuration analysis, the most appropriate rotamers from C-10 to C-15 were selected.

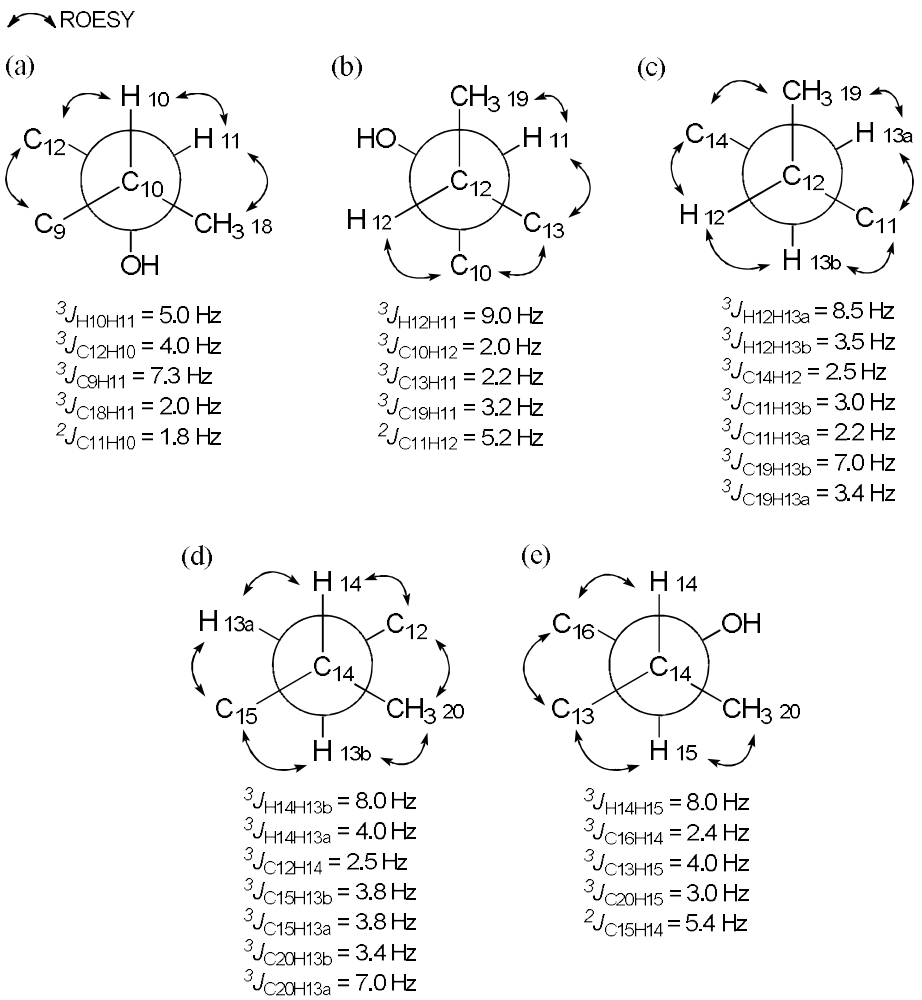

Figure 16. *J*–based configuration analysis of mohangic acid A (**20**) at (a) C-10 and C-11, (b) C-11 and C-12, (c) C-12 and C-13, (d) C-13 and C-14, and (e) C-14 and C-15.

The relationship between C-9 and H-11 was deduced as *anti* because of the large corresponding $^{3}J_{C9H11}$ value (7.3 Hz). The $^{3}J_{H10H11}$ (5.0 Hz), $^{3}J_{C12H10}$ (4.0 Hz), and $^{3}J_{C18H11}$ (2.0 Hz) values indicated *gauche* relationships between H-10/H-11, C-12/H-10, and C-18/H-11. The $^{2}J_{C11H10}$ value (1.8 Hz) indicated an *anti* relationship between the hydroxy group at C-11 and H-10,

and ROESY correlations between the H-10/H-11, H-10/H-12, and H-11/H_3-18 supported the rotamer depicted in Figure 16a. An *anti* relationship between H-11 and H-12 was established on the basis of the large $^3J_{H11H12}$ value (9.0 Hz). The $^3J_{C10H12}$ (2.0 Hz), $^3J_{C13H11}$ (2.2 Hz), and $^3J_{C19H11}$ (3.2 Hz) completely assigned the relationships of C-10/H-12, C-13/H-11, and C-19/H-11 as *gauche*. Moreover, the large $^2J_{C11H12}$ (5.2 Hz) value and observed ROESY correlations supported the rotamer shown in Figure 16b. The methylene group at C-13 is not a stereogenic center. However, the two protons bound to this carbon are distinguishable in the ^{1}H NMR spectrum, thus allowing for consecutive *J*–based analysis to relate configurations from C-12 to C-14 through C-13. The $^3J_{H12H13a}$ (8.5 Hz) and $^3J_{C19H13b}$ (7.0 Hz) values implied *anti* relationships of H-12/H-13a and C-19/H-13b. *Gauche* relationships of C-14/H-12, C-11/H-13b, C-11/H-13a, and C19/H-13a were deduced on the basis of the small $^3J_{CH}$ values (2.2–3.4 Hz). A strong ROESY correlation between H_3-19 and H-13a supported a *gauche* relationship between C-19 and H-13a, clarifying the proper rotamer depicted in Figure 16c. This rotamer was consistent with the observed ROESY correlations around C-12 and C-13. The $^3J_{H13bH14}$ (8.0 Hz) and $^3J_{C20H13a}$ (7.0 Hz) values indicated *anti* relationships of H-13b/H-14 and C-20/H-13a. The other coupling constants supported the rotamer depicted in Figure 16d. The H_3-20/H-13b ROESY correlation, along with the other observed ROESY correlations, further supported this rotamer structure. An *anti* relationship between H-14 and H-15 was indicated by the $^3J_{H14H15}$ (8.0 Hz) value. The C-

16/H-14, C-13/H-15, and C-20/H-15 relationships were deduced as *gauche* on the basis of the $^{3}J_{C16H14}$ (2.4 Hz), $^{3}J_{C13H15}$ (4.0 Hz), and $^{3}J_{C20H15}$ (3.0 Hz) values. The large $^{2}J_{C15H14}$ value (5.4 Hz) and the ROESY NMR signals between H-13 and H-16 indicated that the rotamer in Figure 2e was the most appropriate structure. Overall, detailed *J*–based configuration analysis revealed that the relative configurations of the stereogenic centers in the chain moiety are 10*S**, 11*S**, 12*R**, 14*R**, and 15*S**.

Because mohangic acid D (**23**) bears an additional stereogenic center at C-17, further chemical derivatization and NMR spectroscopic analysis were required to establish its configuration. I first hydrogenated mohangic acid D (**23**) with 10% Pd/C under 1 atm of H_2 at room temperature to increase its stability for further derivatization. The hydrogenated product (**25**) was then derivatized with 2,2-dimethoxy propane to furnish an acetonide derivative (**26**) for the 1,3-diol moiety at C-15 and C-17. The ^{1}H and HSQC NMR spectra of the acetonide derivative (**26**) showed that the ^{1}H and ^{13}C chemical shifts of two acetonide methyl groups are almost identical (δ_C 24.6−δ_H 1.39; δ_C 24.6−δ_H 1.39), indicating an *anti* relationship of the 1,3-hydroxy groups (Figure 17).[21]

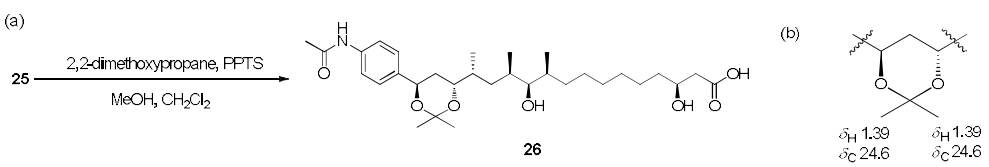

Figure 17. (a) Acetonide formation of hydrogenation product (**25**) of mohangic acid D (**23**) (b) ^{1}H and ^{13}C NMR chemical shifts of acetonide derivative (**26**) indicating *anti* relationship of 1,3-diol.

For the assignment of the absolute configurations of the asymmetric carbons at C-3, C-10, C-11, C-14, and C-15 in **20**, I initially attempted MTPA derivatization on the secondary alcohol groups in mohangic acid A to apply the modified Mosher's method. However, mohangic acid A (**20**) was degraded as soon as *S*- or *R*-MTPA-Cl reagent was added to **20**. We therefore attempted to stabilize **20** by hydrogenation of the triene; however, the hydrogenated product was also degraded during MTPA derivatization. Therefore, I used an alternative method developed by Kishi and co-workers that involves bidentate chiral NMR solvents, (*R*,*R*)- and (*S*,*S*)-bis-α-methylbenzylamine-*p*-Me (BMBA).[35] The NH groups in the bidentate chiral NMR solvents build N··H–O hydrogen bonds through interactions with isolated alcohols, resulting in the discrimination of the chemical shifts of the carbons adjacent to the secondary hydroxy groups. The analysis of these ^{13}C chemical shift behaviors in (*R*,*R*)- and (*S*,*S*)-bidentate chiral NMR solvents by calculation of $\Delta\delta_{(R,R)\text{-}(S,S)}$ values can establish the relative and absolute configurations of secondary alcohols.[36] Because the bidentate chiral solvents were not commercially available, I synthesized the solvents (*R*,*R*)- and (*S*,*S*)-bis-α-methylbenzylamine-*p*-Me (BMBA).[36] The ^{13}C NMR spectra of 15 mg of mohangic acid A (**1**) in a 5:2 mixture of (*R*,*R*)-BMBA and pyridine–d_5 and in a 5:2 mixture of (*S*,*S*)-BMBA and pyridine–d_5 were recorded. Careful comparison of the ^{13}C NMR spectra in the bidentate solvents enabled clear detection of shifts of the ^{13}C signals associated with

the carbons flanking C-3, C-11, and C-15 each with a secondary hydroxy group (Figures 18). By calculating $\Delta\delta_{(R,R)\text{-}(S,S)}$ values at C-4/C-2, C-12/C-10, and C-14/C-16, I determined the absolute configurations of the stereogenic centers of C-3, C-11, and C-15 as 3*R*, 11*S*, and 15*S*. Subsequently, I assigned the absolute configurations of the other stereogenic centers in mohangic acid (**20**) as 10*S*, 12*R*, and 14*R* on the basis of the relative configuration determined *vide supra*.

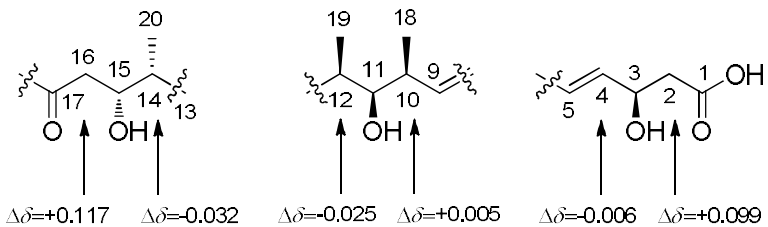

Figure 18. Chemical shift differences [$\Delta\delta = \delta(R,R) - \delta(S,S)$] observed for the indicated carbons in a 5:2 mixture of (*R*,*R*)- and (*S*,*S*)-BMBA and pyridine–d_5.

Mohangic acids B-E (**21**–**24**) were proposed to possess configurations identical to those of **20** at the common stereogenic centers because of the strong similarity among the NMR data for their chains and because of their common biosynthetic origin. In addition, circular dichroism (ECD) spectra of mohangic acids A-E displayed almost identical features, with a strong Cotton effect at 220 nm, clearly supporting their identical absolute configurations of 3*R*, 10*S*, 11*S*, 14*R*, and 15*S* (Figure 19). The additional stereogenic center at C-17 of mohangic acid D was also deduced as 17*R* on

the basis of the relative configuration established by acetonide derivatization, as previously mentioned.

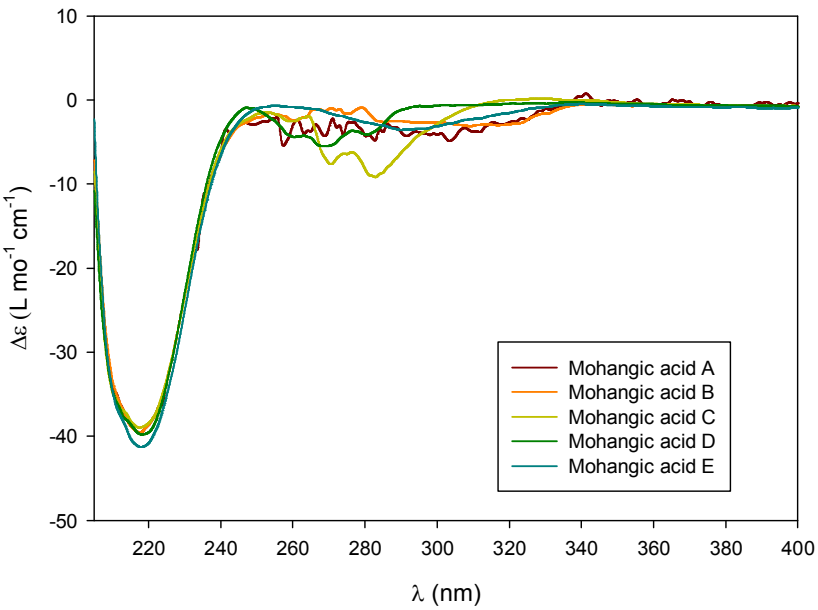

Figure 19. ECD spectra of mohangic acids A–E (**20**–**24**).

The biological activities of mohangic acids A-E (**20**–**24**) were evaluated in several ways. In a cytotoxicity assay against human cancer cell lines such as A549 (lung cancer), HCT116 (colon cancer), SNU638 (gastric cancer), K562 (leukemia), SK-HEP1 (liver cancer), and MDA-MB231 (breast cancer), mohangic acids A-E did not display significant cytotoxic activities (IC_{50} > 10 μM). The mohangic acids (**20**–**24**) were also evaluated for growth inhibition activity against pathogenic bacteria (*Staphylococcus aureus*, *Bacillus subtilis*, *Kocuria rhizophila*, *Salmonella enterica*, *Proteus hauseri*, and *Escherichia coli*) and fungi (*Candida albicans* and *Aspergillus fumigatus*). However, no antimicrobial effects were observed (MIC > 128

μM).

Because the mohangic acids exhibited no cytotoxicity, their biological activities were tested with respect to cancer chemoprevention. Cancer chemoprevention is considered to play an important role in decreasing the risk of cancer development, involving prevention, delay or reversal of the process of carcinogenesis.[37] In particular, one important cancer prevention strategy is to enhance the deactivation of radicals and electrophiles via phase II enzymes.[38] Quinone reductase (QR), one of the representative phase II detoxification enzymes, is known to function as a cancer chemopreventative.[39] A QR induction assay was conducted for evaluating the bioactivities of **20**–**24** in the cultured Hepa-1c1c7 murine hepatoma cell line. In this assay, 0.1% dimethyl sulfoxide (DMSO) was used as a control and *β*-naphthoflavone (2 μM) was used as a positive control. As shown in Figure 6, mohangic acid E (**24**) at a concentration of 20 μM displayed a significant 2.1-fold increase in QR induction activity compared with control. However, mohangic acids A-D (**20**–**23**) exhibited no remarkable activities. Mohangic acid E (**24**) induced QR activity in a concentration-dependent manner without cytotoxicity and with QR activity enhancements of 1.3-, 1.5-, 1.8-, 2.1-, and 2.2-fold at 2, 5, 10, 20, and 30 μM of **24**, respectively (Figure 20, 21). These results suggest that the glucose moiety in **24** is particularly important for the QR activity in this class of the compounds.

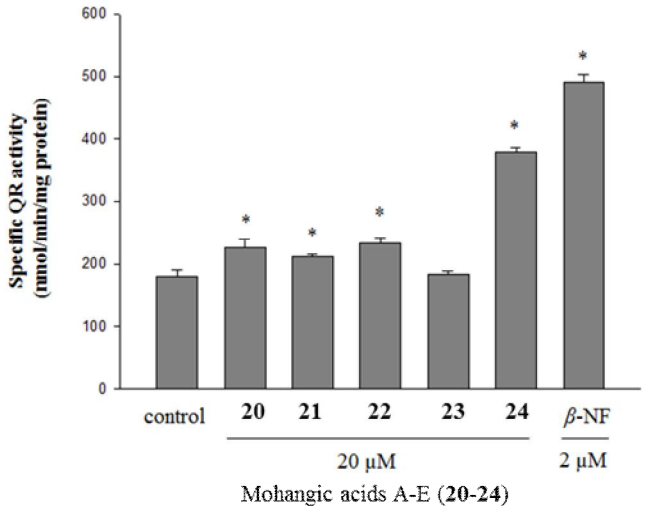

Figure 20. Effect of **20**–**24** on the induction of quinone reductase in murine Hepa1c1c7 cells. Cells were grown for 24 h, and then exposed to **20**–**24** for 24 h. Quinone reductase activities were measured in cell lysates by reduction of a tetrazolium dye and expressed as nmol/min/mg protein. Values represent the mean ±SD of four determinations. *$P < 0.001$ indicates statistically significant differences from the control group.

Mohangic acids A-E commonly bear a *para*-substituted aromatic ring with an amine and an alkyl chain. The structural feature of the mohangic acids is related to (2*E*)-11-(4'-aminophenyl)-5,9-dihydroxy-4,6,8-trimethyl-11-oxo-undec-2-enoic acid[16] and (5*E*)-7-(4'-aminophenyl)-2,4-dimethyl-7-oxo-hept-5-enoic acid,[17] both of which were independently isolated from mangrove-derived *Streptomyces griseus* strains. However, these known compounds have different chain lengths and do not incorporate the triene moiety in the mohangic acids. In addition, modification at the amine group

of **21**–**24** by substitution with a methyl, acetyl, or glycosyl group has not previously been reported in this class.

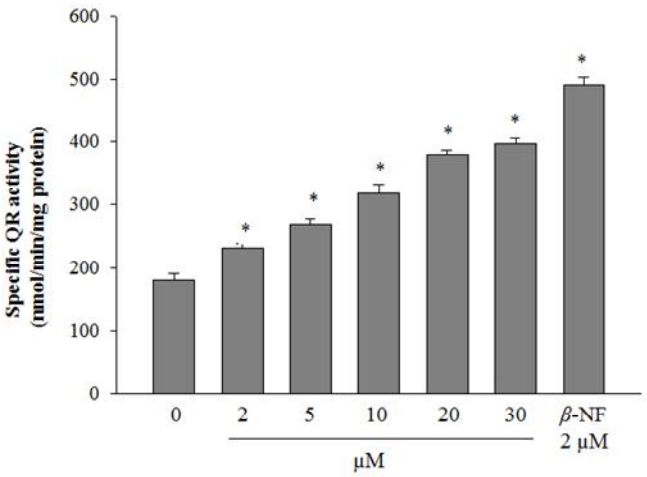

Figure 21. Effect of **24** on the induction of quinone reductase in murine Hepa1c1c7 cells. Cells were grown for 24 h, and then exposed to **24** for 24 h. Quinone reductase activities were measured in cell lysates by reduction of a tetrazolium dye and expressed as nmol/min/mg protein. Values represent the mean ±SD of four determinations. *$P < 0.001$ indicates statistically significant differences from the control group.

The absolute configurations of the natural products belonging to this class have not been determined,[38,39] possibly as a consequence of the structural instability of the aminoacetophenonic group during chemical derivatizations. my extensive spectroscopic analysis using bidentate chiral NMR solvents enabled us to determine the absolute configurations of the mohangic acids by avoiding chemical derivatizations. To my best knowledge, candicidins

D,[40] which has been reported as an antifungal antibiotics in a recent, has an identical *p*-aminoacetophenonic moiety at the terminal position of macrolide ring structure but its relative and absolute configurations were dissimilar from that of mohangic acids A-E (**20**-**24**). The biological activities of the compounds belonging to the *p*-aminoacetophenonic acids have not been reported previously.[40,41] My report of QR activity induced by treatment of mohangic acid E (**24**), which is a glycosylated version of *p*-aminoacetophenonic acid, represents the first biological evaluation of this class of the compounds and reveals the biological importance of glycosylation at the amino group in **24**. The discovery of the mohangic acids, along with the results of my previous studies,[42] highlights that microorganisms inhabiting relatively uninvestigated marine environments, such as an intertidal mudflat, could be a promising source of structurally and biologically active new secondary metabolites.

Table 10. ^{1}H and ^{13}C NMR Data of **20-24** in CD_3OD[a].

positon	Mohangic acid A (1)		Mohangic acid B (2)		Mohangic acid C (3)		Mohangic acid D (4)		Mohangic acid E (5)	
	δ_C, type	δ_H, mult (*J* in Hz)	δ_C, type	δ_H, mult (*J* in Hz)	δ_C, type	δ_H, mult (*J* in Hz)	δ_C, type	δ_H, mult (*J* in Hz)	δ_C, type	δ_H, mult (*J* in Hz)
1	177.8, C	–	178.0, C	–	176.5, C	–	179.0, C	–	178.5, C	–
2	44.5, CH_2	2.41, d (6.5)	45.0, CH_2	2.41, d (6.5)	43.0, CH_2	2.40, d (6.5)	45.0, CH_2	2.37, d (6.5)	45.0, CH_2	2.40, d (6.5)
3	70.5, CH	4.48, dd (6.5, 6.5)	70.5, CH	4.49, dd (6.5, 6.5)	68.5, CH	4.47, dd (6.5, 6.5)	71.0, CH	4.46, dd (6.5, 6.5)	70.5, CH	4.47, dd (6.5, 6.5)
4	135.7,CH	5.69, dd (15.0, 6.5)	136.0, CH	5.69, dd (15.0, 6.5)	133.5, CH	5.67, dd (15.0, 6.5)	136.0, CH	5.66, dd (15.0, 6.5)	135.5, CH	5.71, dd (15.0, 6.5)
5	131.8, CH	6.26, dd (15.0, 10.5)	132.0, CH	6.27, dd (15.0, 10.5)	132.1, CH	6.25, dd (15.0, 10.5)	131.5, CH	6.26, dd (15.0, 10.5)	131.5, CH	6.27, dd (15.0, 10.5)
6	132.0, CH	6.12, m	131.5, CH	6.12, dd (15.0, 10.5)	129.5, CH	6.11, dd (15.0, 10.5)	132.5, CH	6.11, dd (15.0, 10.5)	132.0, CH	6.09, dd (15.0, 10.5)
7	134.7, CH	6.19, dd (15.0, 10.0)	135.0, CH	6.19, dd (15.0, 10.5)	133.0, CH	6.20, dd (15.0, 10.5)	134.5, CH	6.19, dd (15.0, 10.5)	134.5, CH	6.18, dd (15.0, 10.5)
8	132.2, CH	6.09, dd (15.0, 10.0)	132.5, CH	6.09, dd (15.0, 10.5)	130.0, CH	6.08, dd (15.0, 10.5)	132.0, CH	6.09, dd (15.0, 10.5)	131.8, CH	6.11, dd (15.0, 10.5)
9	138.4, CH	5.72, dd (15.0, 8.5)	138.5, CH	5.71, dd (15.0, 8.5)	137.0, CH	5.70, dd (15.0, 8.5)	138.5, CH	5.70, dd (15.0, 8.5)	138.0, CH	5.73, dd (15.0, 8.5)
10	41.6, CH	2.42, ddd (8.5, 6.5, 5.0)	41.5, CH	2.43, ddd (8.5, 6.5, 5.0)	39.5, CH	2.43, ddd (8.5, 6.5, 5.0)	42.0, CH	2.44, ddd (8.5, 6.5, 5.0)	41.5, CH	2.43, ddd (8.5, 6.5, 5.0)
11	80.8, CH	3.12, dd (9.0, 5.0)	79.8, CH	3.12, dd (9.0, 5.0)	79.0, CH	3.11, dd (9.0, 5.0)	81.0, CH	3.09, dd (9.0, 5.0)	80.5, CH	3.12, dd (9.0, 5.0)
12	34.5, CH	1.63, dddd (9.0, 8.5, 6.5, 3.5)	35.0, CH	1.62, dddd (9.0, 8.5, 6.5, 3.5)	34.5, CH	1.61, dddd (9.0, 8.5, 6.5, 3.5)	34.5, CH	1.58, dddd (9.0, 8.5, 6.5, 3.5)	34.5, CH	1.61, dddd (9.0, 8.5, 6.5, 3.5)
13a	37.0, CH_2	1.31, ddd (12.5, 8.5, 4.0)	37.0, CH_2	1.31, ddd (12.5, 8.5, 4.0)	36.9, CH_2	1.31, ddd (12.5, 8.5, 4.0)	37.0, CH_2	1.24, ddd (12.5, 8.5, 4.0)	37.5, CH_2	1.31, ddd (12.5, 8.5, 4.0)
13b		1.22, ddd (12.5, 8.5, 3.5)		1.21, ddd (12.5, 8.5, 3.5)		1.21, ddd (12.5, 8.5, 3.5)		1.21, ddd (12.5, 8.5, 3.5)		1.23, ddd (12.5, 8.5, 3.5)
14	37.4, CH	1.71, dddd (8.5, 8.0, 6.5, 4.0)	37.5, CH	1.71, dddd (8.5, 8.0, 6.5, 4.0)	37.5, CH	1.70, dddd (8.5, 8.0, 6.5, 4.0)	38.0, CH	1.63, dddd (8.5, 8.0, 6.5, 4.0)	37.5, CH	1.73, dddd (8.5, 8.0, 6.5, 4.0)
15	74.3, CH	4.03, ddd (9.0, 8.0, 4.0)	74.5, CH	4.04, ddd (8.5, 8.0, 4.0)	73.8, CH	4.05, ddd (9.0, 8.0, 4.0)	72.0, CH	3.75, ddd (9.0, 8.0, 3.0)	74.0, CH	4.05, ddd (9.0, 8.0, 4.0)
16a	42.4, CH_2	2.97, dd (15.5, 9.0)	42.5, CH_2	2.98, dd (15.5, 8.5)	43.2, CH_2	3.10, dd (15.5, 9.0)	43.2, CH_2	1.73, dd (12.0, 9.0, 3.0)	42.5, CH_2	3.03, dd (15.0, 9.0)
16b		2.95, dd (15.5, 4.0)		2.94, dd (15.5, 4.0)		2.96, dd (15.5, 4.0)		1.62, m		2.95, dd (15.0, 4.0)
17	200.3, C	–	200.5, C	–	200.0, C	–	71.5, CH	4.85, m	200.5, C	–
18	18.4, CH_3	1.02, d (6.5)	18.7, CH_3	1.01, d (6.5)	17.0, CH_3	1.01, d (6.5)	19.0, CH_3	1.01, d (6.5)	18.5, CH_3	1.01, d (6.5)
19	14.2, CH_3	0.87, d (6.5)	14.4, CH_3	0.87, d (6.5)	13.0, CH_3	0.85, d (6.5)	14.5, CH_3	0.86, d (6.5)	14.5, CH_3	0.87, d (6.5)
20	15.5, CH_3	0.90, d (6.5)	15.5, CH_3	0.89, d (6.5)	14.0, CH_3	0.89, d (6.5)	15.4, CH_3	0.81, d (6.5)	15.5, CH_3	0.89, d (6.5)
1'	127.8, C	–	126.8, C	–	134.1, C	–	139.1, C	–	139.1, C	–
2'	132.3, CH	7.77, d (8.0)	132.0, CH	7.80, d (8.0)	129.2, CH	7.94, d (8.0)	127.5, CH	7.28, d (8.0)	131.5, CH	7.84, d (8.0)
3'	114.6, CH	6.64, d (8.0)	112.2, CH	6.58, d (8.0)	118.5, CH	7.68, d (8.0)	121.5, CH	7.51, d (8.0)	114.0, CH	6.82, d (8.0)
4'	155.5, CH	–	155.0, C	–	144.8, C	–	143.5, C	–	153.6, C	–
5'	114.6, CH	6.64, d (8.0)	112.2, CH	6.58, d (8.0)	118.5, CH	7.68, d (8.0)	121.5, CH	7.51, d (8.0)	114.0, CH	6.82, d (8.0)
6'	132.3, CH	7.77, d (8.0)	132.0, CH	7.80, d (8.0)	129.2, CH	7.94, d (8.0)	127.5, CH	7.28, d (8.0)	131.5, CH	7.84, d (8.0)
7'			30.4, CH_3	2.83, s	171.0, C	–	172.0, C	–		
8'					22.5, CH_3	2.13, s	24.0, CH_3	2.11, s		
1''									86.0, CH	4.63, d (9.0)
2''									71.5, CH	3.37, m
3''									79.4, CH	3.47, dd (9.0, 8.5)
4''									74.5, CH	3.35, m
5''									78.5, CH	3.41, ddd (9.0, 5.5, 2.5)
6''									63.0, CH_2	3.64, dd (12.0, 5.5)
										3.86, dd (12.0, 2.5)

[a] ^{1}H and ^{13}C NMR were recorded at 600 and 150 MHz, respectively.

II. QM-HiFSA-aided structure determination of succinilenes A-D, triene polyols from a marine-derived *Streptomyces* sp. SAK1

II. I. Results and discussion

Succinilene A (**27**) was isolated as a yellow gum, and its molecular formula was deduced as $C_{24}H_{38}O_7$ based on HR-FAB mass spectrometry (obsd $[M-H]^-$ at *m/z* 437.2550, calcd $[M-H]^-$ 437.2539) in combination with ^1H and ^{13}C NMR data (Table 11). The ^1H NMR spectrum of **27** in pyridine-d_5 exhibited typical signatures of polyenes and polyols, with seven olefinic protons (δ_H 6.3664, 6.3158, 6.2929, 6.2885, 6.1280, 5.9506, and 5.5426) and four protons attached to oxygen-bearing carbons (δ_H 5.0898, 4.3745, 3.9176, and 3.7579). Further analysis of the ^1H NMR spectrum of **27** revealed the existence of eleven aliphatic protons between δ_H 2.9046 and δ_H 1.8105, a singlet methyl group bound to an olefinic carbon (δ_H 1.8616), two doublet methyl groups (δ_H 1.1907 and 0.9973), and a triplet methyl group (δ_H 1.1619) bound to an sp^3 aliphatic carbon. The ^{13}C and gHSQC NMR spectra displayed two carbonyl carbons (δ_C 175.7 and 172.7), seven olefinic sp^2 carbons (δ_C 132.8, 132.6, 132.5, 132.0, 131.7, 131.6, and 127.2), one quaternary olefinic carbon (δ_C 140.1), four oxygen-bound methine carbons (δ_C 76.8, 75.5, 74.2, and 74.1), six aliphatic carbons (δ_C 39.8, 38.0, 37.1, 30.4, 30.3, and 27.5), and four methyl group carbons (δ_C 17.2, 16.6, 12.2, and 10.9). Based on the UV absorption maximum at 270 nm and the eight olefinic carbon signals, succinilene A (**27**) was expected to bear three conjugated double bonds and an isolated double bond. These four double bonds along with two carbonyl functional groups accounted for all of the six

double bond equivalents inherently calculated from the molecular formula, thus indicating that succinilene A (**27**) is a linear compound.

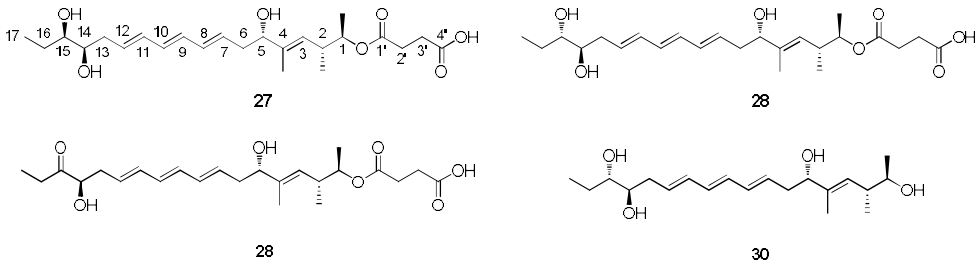

Figure 22. Structures of succinilenes A-D (**27**–**30**).

Given this information, all ^{13}C-^{1}H one-bond correlations were assigned by analysis of the gHSQC NMR spectrum (Table 1). Interpretation of COSY and HMBC NMR spectroscopic data readily led to the elucidation of the gross structure of succinilene A (**27**). First, the COSY signals from a terminal triplet methyl group (H_3-17 at δ_H 1.1619) to aliphatic methylene protons (H_2-16 at δ_H 1.8578 and δ_H 1.8105) connected C-17 (δ_C 10.9) to C-16 (δ_C 27.5). The aliphatic carbon C-16 was elucidated to be directly connected to the oxygenated carbon C-15 (δ_C 75.5) based on the COSY correlations between H-15 (δ_H 3.7579) and H-16. The homonuclear correlation between H-15 and H-14 (δ_H 3.9176) revealed that an oxygen-bound methine carbon (C-14 at δ_C 74.2) was connected to C-15, indicating the existence of a diol moiety. Further COSY analysis verified the connectivity between H-14 and H_2-13 (δ_H 2.7253 and 2.6745), identifying the C-14–C-13 bond. The aliphatic carbon C-13 was connected to the sp^2 carbon C-12 (δ_C 132.8) based on a 3-bond ^{1}H-^{1}H coupling signal between

H-12 (δ_H 6.1280) and H-13. Additional COSY correlations among the six olefinic protons from H-12 to H-7 (δ_H 5.9506) indicated the construction of a triene moiety from C-12 to C-7 (δ_C 132.8 to δ_C 132.0), which is consistent with the UV absorption maximum at 270 nm. The triene moiety was located next to C-6 based on the $^3J_{HH}$ couplings between H_2-6 (δ_H 2.6519 and 2.5631) and H-7. The homonuclear correlations of H_2-6 with the oxygenated proton (H-5 at δ_H 4.3745) showed C-6-C-5 (δ_C 76.8) connectivity. The HMBC correlations from a singlet methyl proton (H_3-4-Me; δ_H 1.8616) to C-5, C-4 (δ_C 140.1), and C-3 (δ_C 127.2) indicated expansion of the chain from C-5 to C-3 through C-4. The olefinic methine C-3 was assigned next to C-2 (δ_C 37.1), with a branched methyl group (H_3-2-Me; δ_H 0.9973/δ_C 16.6) attached to C-2. The COSY correlation from H-1 (δ_H 5.0898) to H-2 and H_3-1-Me identified the connectivity of C-1 (δ_C 74.1) and C-2, establishing the first partial structure from C-17 to C-1, a chain composed of 20 carbons bearing three hydroxyl groups and a treiene moiety. Based on additional 2D NMR analysis, the aliphatic H_2-2' (δ_H 2.8516 and δ_H 2.8436) displayed $^3J_{HH}$ and $^3J_{CH}$ correlations to adjacent aliphatic H_2-3' peaks (δ_H 2.9015, and δ_H 2.8990) and two carbonyl carbons C-1' and C-4' (δ_C 172.7 and 175.7), completing the second partial structure as a succinic acid. These two partial structures were connected based on a key HMBC correlation from H-1, of which deshielded chemical shift (δ_H 5.0898) is indicative for the existence of an ester linkage, to C-1', resulting in the gross structure of **27** (Figure 23a).

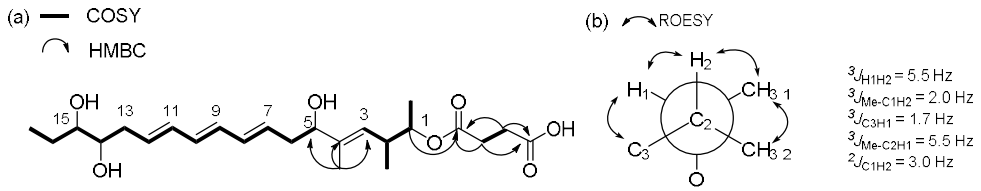

Figure 23. (a) Determination of the planar structure of succinilene A based on the analysis of key COSY and HMBC correlations. (b) *J*-based configuration analysis of succinilene A (**27**) at C-1 and C-2.

Succinilene B (**28**) was obtained as a yellow gum. The molecular formula was determined as $C_{24}H_{38}O_7$ on the basis of HR-FABMS data (obsd $[M-H]^-$ at *m*/*z* 437.2550, calcd $[M-H]^-$ 437.2539) along with ^1H and ^{13}C NMR spectroscopic data (Table 11). The molecular formula and the UV spectrum of **2** were identical to those of **27**, indicating that succinilene B (**28**) is structurally analogous to succinilene A (**27**). The 1D and 2D NMR data of **28** also displayed very similar patterns to those of **27**, as expected. Further analysis of NMR spectroscopic data resulted in the construction of the gross structure of **28**, which was identical to that of **27**. Actually, most of the ^{13}C chemical shifts of **28** were very similar to those of **27**, within 0.2 ppm. However, the ^{13}C peaks of C-13 to C-16 around the oxymethine group located adjacent to the terminal ethyl group differed by 0.5~1 ppm compared to the same peaks in **27**, indicating that succinilene B (**28**) is a diastereomer of **27** that possesses different stereochemistry at C-13 or/and C-14.

Succinilene C (**29**) was purified as a yellow gum and determined to possess a molecular formula of $C_{24}H_{36}O_7$ on the basis of HR-FABMS data (obsd $[M+H]^+$ at *m/z* 437.2562, calcd $[M+H]^+$ 437.2545) combined with ^1H and ^{13}C NMR spectral data (Table 12). Based on the molecular weight and UV spectrum of **29**, it was expected that one of the hydroxyl groups in succinilene C (**29**) had been oxidized to a ketone group. According to the comparison of the 1D and 2D NMR spectroscopic data of **29** with those of **27**, the oxygen-bound proton (H-15, δ_H 3.7579) in **27** was absent in **29**, and a ketone carbon signal (δ_C 214.0) was detected instead, clarifying that the hydroxyl group at the C-15 position in **27** had been oxidized to the ketone group in **29**. This assignment was also supported by the 3-bond HMBC correlations from H_3-17 (δ_H 1.0890) and H_2-13 (δ_H 2.7803 and 2.6591) to C-15 and H_3-17/H-16 and H_2-13/H-14 COSY correlations.

Succinilene D (**30**) was isolated as a yellow gum, and its molecular formula was deduced to be $C_{20}H_{34}O_4$ based on the corresponding HR-FABMS data (obsd $[M+Na]^+$ at *m/z* 361.2347, calcd $[M+Na]^+$ 361.2355) and ^1H and ^{13}C NMR spectroscopic data (Table 12). The molecular weight of **30** was 100 Da lower than those of **27** and **28**, possibly indicating that the terminal succinic acid moiety in **27** and **28** might have been cleaved. Through the careful analysis of the 1D and 2D NMR spectral data, the gross structure of succinilene D (**30**) was elucidated to be the left part of **27** or **28**, which is the methanolysis product of **27** or **28** that lacks the succinic acid moiety.

The relative configurations of **27** were established by analyzing the ^{1}H–^{1}H coupling constants and hetero half-filtered TOCSY (HETLOC) NMR data.[34] To determine the relationship between C-1 and C-2, *J*-based configuration analysis was performed with $^{3}J_{HH}$, $^{3}J_{CH}$, and $^{2}J_{CH}$ values and ROESY NMR data,[15] selecting the most suitable rotamer between C-1 and C-2 (Figure 23b). The relationship between H-1 and 2-Me was elucidated as *anti* based on the high $^{3}J_{CH}$ value (5.5 Hz). The $^{3}J_{H1H2}$ (5.5 Hz), $^{3}J_{C1\text{-}MeH2}$ (2.0 Hz), and $^{3}J_{C3H1}$ (1.7 Hz) values indicated *gauche* relationships for H-1/H-2, 1-Me/H-2, and C-3/H-1. Moreover, the small $^{2}J_{C1H2}$ (3.0 Hz) value and the ROESY NMR signals between the H-1/H-2, H-1/H-3, H-2/1-Me, and 1-Me/2-Me led to elucidation of the rotamer depicted in Figure 2b. ROESY correlations also supported the rotamer, thus proposing 1*R** and 2*R** configuration (Figure 23b).

To determine the absolute configurations of the stereogenic centers at C-1, C-2, C-5, C-14, and C-15 in succinilene A (**27**), the modified Mosher's method was applied. Methanolysis was performed to detach the succinic acid moiety, which enabled derivatization of the hydroxyl group at C-1 with MTPA-Cl (α-methoxy-(trifluoromethyl) phenyl acetyl chloride). After purifying the methanolysis product (**31**) of succinilene A, the secondary alcohols in **31** were derivatized using *R*- and *S*-MTPA-Cl. Analysis of the ^{1}H and COSY NMR spectroscopic data for these *S*- and *R*-MTPA esters (**34** and **35**) led to the assignment of the $\Delta\delta_{S\text{-}R}$ values, establishing 1*R*, 5*S*, 14*R*, and 15*R* configurations (Figure 24a). Based on the established relative

configuration, the absolute configuration of C-2 was determined to be 2*R*. The relative configurations and absolute configurations of succinilene B (**28**) were determined to be 1*R*, 2*R*, 5*S*, 14*R*, and 15*S* using the same procedure applied for **27** (Figure 3b). The relative and absolute configurations of succinilene C (**29**) were analogously established as 1*R*, 2*R*, 5*S*, and 15*R* through application of the modified Mosher's method to the methanolysis product (**33**) of **29** (Figure 24c). Because the gross structure of succinilene D (**30**) was identical to the methanolysis products (**31** and **32**) of **27** and **28**, the ^{1}H NMR and CD spectra of **30** were compared with those of **31** and 3**2**. The ^{1}H NMR data for **32** was identical to those of **30** but was different from the ^{1}H NMR spectrum of **31**, indicating that the relative configuration of **30** is identical to that of **32**. In addition, the CD spectra of **30** and **32** were identical, thus leading to the assignment of 1*R*, 2*R*, 5*S*, 14*R*, and 15*S* configurations for **30** (Figure 25).

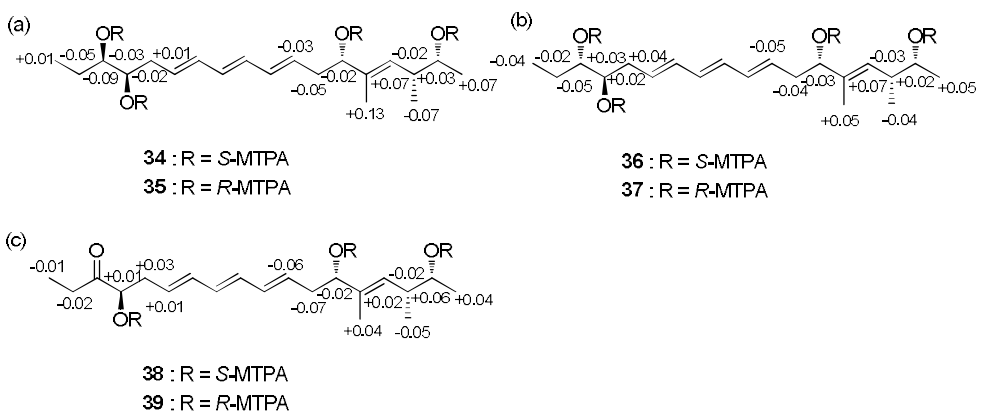

Figure 24. (a) $\Delta\delta_{S-R}$ values of the MTPA esters (**34** and **35**) in pyridine-d_5.

(b) $\Delta\delta_{S-R}$ values of the MTPA esters (**36** and **37**) in pyridine-d_5. (c) $\Delta\delta_{S-R}$ values of the MTPA esters (**38** and **39**) in pyridine-d_5.

Even though the absolute configurations of the stereogenic centers in **27-30** were completely assigned, the full assignments of the double bond geometries were not straightforward. The geometries of the double bonds of C-7/C-8 and C-11/C-12 in the succinilenes (**27-30**) were determined as 7*E* and 11*E* based on the H-7/H-8 and H-11/H-12 *trans*-coupling constant values (14.5 Hz). However, it was virtually impossible to clarify the double bond geometry of C-9/C-10 in **27-30** because the H-9 and H-10 olefinic protons greatly overlap, displaying second-order peaks in the ^{1}H NMR spectra and thus hampering the accurate deconvolution of the ^{1}H-^{1}H coupling constants between H-9 and H-10, even at higher magnetic field (900 MHz).

Therefore, a recently developed computational analysis system, QM-HiFSA, was utilized to extract the H-9/H-10 coupling constants of the succinilenes using PERCH software.[45] After geometry optimization and dynamic simulation of molecules using the MMS module, the basic ^{1}H NMR parameters were predicted based on the 3D structural information. Then, the obtained initial parameters were optimized by iterative quantum mechanical simulation against experimental spectra. The iteration was repeated until both the simulated and experimental spectra were in excellent agreement with each other, with root mean square (RMS) values below 0.1

(RMS = 0.075 for **27**; RMS = 0.066 for **28**; RMS = 0.093 for **29**; RMS = 0.091 for **30**). Thus, the precise ^{1}H NMR parameters were determined with high precision (chemical shifts: δ_H, 0.1 ppb; coupling constants: *J*, 10 mHz) (Tables 11 and 12).[46] The *J* couplings of the highly overlapped olefinic proton signals (H-9 and H-10) of **27**-**30** were calculated to be 14.03 Hz, 14.79 Hz, 15.05 Hz, and 14.86 Hz (*cis J* couplings ca. 10-12 Hz; *trans J* couplings ca. 14-18 Hz),[47, 48] respectively. These results confirmed the geometry of the *trans*-olefinic protons (H-9 and H-10) in **27**-**30** (Figure 25).

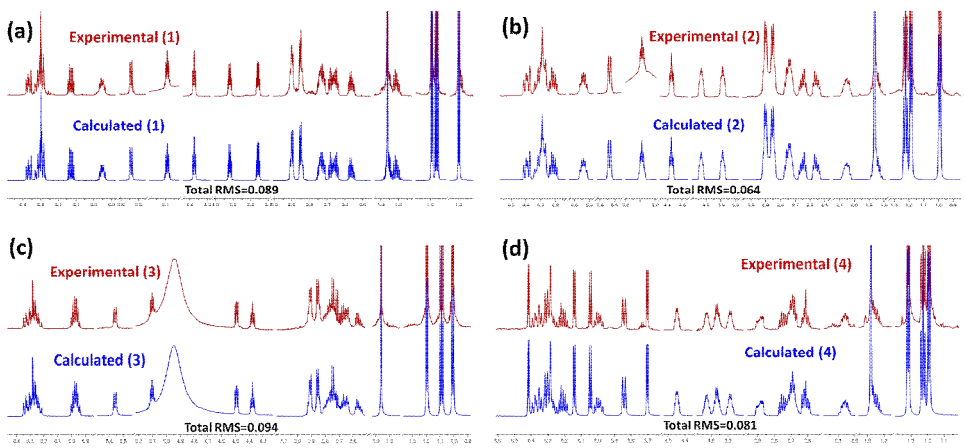

Figure 25. ^{1}H NMR fingerprints of compounds **27** (a) - **30** (d) generated by HiFSA. Comparison of the observed (red, obtained in pyridine-d_5) and calculated (blue) ^{1}H spectra.

II. II. Bioactivities of succinilenes

Bioactivities of succinilenes A-D. The biological activities of the succinilenes (**27-30**) were primarily evaluated for cytotoxicity against human cancer cells. In this assay, succinilene A showed moderate cytotoxicity against the gastric carcinoma cell line SNU638, with an IC_{50} value of 12.1 μg/mL (27.6 μM), whereas succinilenes B–D did not display significant inhibitory activities against the tested cancer cell lines. As part of the efforts to search for biological activities, a nitrate assay was performed for **27**–**30**. Overproduction of nitric oxide (NO) is highly associated with inflammation, and the pathway that regulates NO production is considered a useful target for anti-inflammatory agents.[49] RAW 264.7 cells were treated with LPS (1 μg/mL), which induces inflammatory responses.[50,51] When the cells were pretreated with various concentrations of the succinilenes (0, 20, or 40 μM) 30 min prior to LPS stimulation, NO production was gradually inhibited in a concentration-dependent manner, except for treatment with succinilene D (**30**). No significant effect on cell viability, as determined by the MTT assay (> 90% cell survival), was observed at the tested concentrations, indicating that the inhibition of NO production by the tested compounds was not mediated by a cytotoxic effect. As a result, among the four compounds, succinilene C (**29**) exhibited the most remarkable inhibitory activity against NO production. By contrast, succinilene D, without succinic acid connected through an ester linkage, resulted in the overproduction of NO (Figure 26).

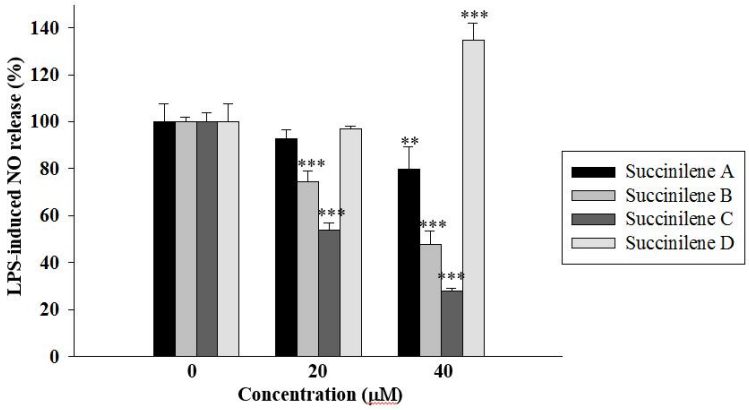

Figure 26. Inhibitory effects of succinilenes A-D (**27-30**) on LPS-induced NO production. RAW 264.7 cells (3×10^5 cells/mL) were stimulated with LPS (1 μg/mL) in the presence or absence of **27-30**. After 20 h, the cultured media were collected, and the nitrite concentrations were measured using the Griess reaction. * $P < 0.05$, ** $P < 0.01$, *** $P < 0.001$ are considered statistically significant compared to the control group.

Table 11. . ^{1}H and ^{13}C NMR Data of **27** and **28** in pyridine-d_5[a]

	27			**28**		
C/H	δ_H [a]	mult (*J* in Hz)	δ_C [b]	δ_H [c]	mult (*J* in Hz)	δ_C [d]
1	5.0898	dq (6.35, 5.50)	74.1, d	5.0882	dq (6.35, 5.75)	74.1, d
1-Me	1.1907	d (6.35)	17.2, q	1.1862	d (6.35)	17.2, q
2	2.7397	ddq (9.74, 6.82, 5.50)	37.1, d	2.7356	ddq (9.60, 6.76, 5.75)	37.2, d
2-Me	0.9973	d (6.82)	16.6, q	0.9916	d (6.76)	16.7, q
3	5.5426	d (9.74)	127.2, d	5.5359	d (9.60)	127.2, d
4	–	–	140.1, s	–	–	140.1, s
4-Me	1.8616	s	12.2, q	1.8618	s	12.1, q
5	4.3745	dd (7.04, 6.04)	76.8, d	4.3721	dd (6.69, 6.34)	76.9, d
6	2.6519	ddd (-14.00, 7.30, 7.04)	39.8, t	2.6498	ddd (-14.11, 7.47, 6.69)	39.8, t
	2.5631	ddd (-14.00, 7.50, 6.04)		2.5587	ddd (-14.11, 7.10, 6.34)	
7	5.9506	ddd (14.65, 7.50, 7.30)	132.0, d	5.9395	ddd (14.81, 7.47, 7.10)	131.9, d
8	6.2885	dd (14.65, 10.77)	132.5, d	6.2814	dd (14.81, 10.73)	132.6, d
9	6.2929	dd (14.03, 10.77)	131.6, d	6.2773	dd (14.79, 10.73)	131.6, d
10	6.3158	dd (14.03, 10.49)	131.7, d	6.3179	dd (14.79, 10.53)	131.7, d
11	6.3664	dd (15.19, 10.49)	132.6, d	6.3913	dd (15.19, 10.53)	132.7, d
12	6.1280	ddd (15.19, 7.50, 7.12)	132.8, d	6.2145	ddd (15.19, 7.45, 7.24)	133.0, d
13	2.7253	ddd (-14.36, 7.50, 4.66)	38.0, t	2.8829	ddd (-14.13, 7.24, 3.36)	37.5, t
	2.6745	ddd (-14.36, 8.02, 7.12)		2.7481	ddd (-14.13, 8.12, 7.45)	
14	3.9176	ddd (8.02, 4.66, 4.33)	74.2, d	4.0324	ddd (8.12, 5.84, 3.36)	74.9, d
15	3.7579	ddd (8.68, 4.33, 3.88)	75.5, d	3.8871	ddd (8.72, 5.84, 2.69)	76.1, d
16	1.8578	ddq (-13.87, 7.38, 3.88)	27.5, t	2.0541	ddq (-13.61, 7.36, 2.69)	26.5, t
	1.8105	ddq (-13.87, 8.68, 7.49)		1.8504	ddq (-13.61, 8.72, 7.42)	
17	1.1619	dd (7.49, 7.38)	10.9, q	1.2234	dd (7.42, 7.36)	10.9, q
1'	–	–	172.7, s	–	–	173.0, s
2'	2.8516	ddd (-11.48, 7.29, 6.04)	30.3, t	2.8496	ddd (-18.10, 7.13, 6.33)	30.6, t
	2.8436	ddd (-11.48, 7.54, 5.82)		2.8496	ddd (-18.10, 8.56, 4.83)	
3'	2.9046	ddd (-16.39, 7.29, 5.82)	30.4, t	2.9078	ddd (-15.38, 8.56, 7.13)	30.8, t
	2.8954	ddd (-16.39, 7.54, 6.04)		2.9022	ddd (-15.38, 6.33, 4.83)	
4'	–	–	175.7, s	–	–	176.2, s

[a] ^{1}H and ^{13}C NMR were recorded at 900 and 225 MHz, respectively.

Table 12. . ^{1}H and ^{13}C NMR Data of **29** and **30** in pyridine-d_5[a]

	29			**30**		
C/H	δ_H [a]	mult (*J* in Hz)	δ_C [b]	δ_H [a]	mult (*J* in Hz)	δ_C [b]
1	5.1041	dq (6.33, 5.27)	74.2, d	3.9666	ddq (6.23, 5.00, 4.60)	70.8, d
1-Me	1.1944	d (6.33)	17.3, q	1.3158	d (6.23)	21.0, q
2	2.7403	ddq (9.97, 6.86, 5.27)	37.2, d	2.6988	ddq (9.62, 6.85, 5.00)	39.6, d
2-Me	1.0069	d (6.86)	16.6, q	1.1905	d (6.85)	17.0, q
3	5.5580	d (9.97)	127.4, d	5.8422	d (9.62)	128.6, d
4	–	–	140.3, s	–	–	138.8, s
4-Me	1.8616	s	12.4, q	1.8782	s	12.1, q
5	4.3767	dd (7.10, 6.06)	76.9, d	4.4482	ddd (7.07, 5.51, 3.83)	77.2, d
6	2.6443	ddd (-13.79, 6.93, 6.06)	39.8, t	2.6890	ddd (-13.68, 7.07, 7.00)	39.9, t
	2.5606	ddd (-13.79, 7.12, 7.10)		2.6130	ddd (-13.68, 7.99, 5.51)	
7	5.9652	ddd (14.66, 7.12, 6.93)	132.6, d	5.9948	ddd (14.80, 7.99, 7.00)	132.1, d
8	6.2708	dd (14.66, 10.63)	132.5, d	6.2974	dd (14.80, 10.62)	132.7, d
9	6.2902	dd (15.05, 10.63)	132.4, d	6.2738	dd (14.86, 10.62)	131.8, d
10	6.2414	dd (15.05, 10.72)	131.2, d	6.3186	dd (14.86, 10.55)	132.1, d
11	6.3255	dd (15.14, 10.72)	133.7, d	6.3706	dd (15.21, 10.55)	133.0, d
12	5.9778	ddd (15.14, 7.41, 7.00)	129.8, d	6.2091	ddd (15.21, 7.38, 7.16)	133.2, d
13	2.7803	ddd (-13.49, 7.27, 7.00)	38.2, t	2.8870	ddd (-14.32, 7.38, 3.45)	37.6, t
	2.6591	ddd (-13.49, 7.41, 4.88)		2.7460	ddd (-14.32, 8.46, 7.16)	
14	4.4922	dd (7.27, 4.88)	77.2, d	4.0282	dddd (8.46, 5.85, 5.74, 3.45)	75.0, d
15	–	–	214.0, s	3.8872	dddd (8.87, 5.85, 5.90, 3.10)	76.2, d
16	2.7549	dq (-14.89, 7.05)	31.7, t	2.0620	ddq (-13.56, 7.35, 3.10)	26.5, t
	2.7206	dq (-14.89, 7.45)		1.8533	ddq (-13.56, 8.87, 7.37)	
17	1.0890	dd (7.45, 7.05)	7.8, q	1.2266	dd (7.37, 7.35)	10.8, q
1'	–	–	172.7, s			
2'	2.8525	ddd (-16.88, 7.01, 6.26)	30.3, t			
	2.8525	ddd (-16.88, 8.79, 4.47)				
3'	2.9172	ddd (-16.89, 8.79, 7.01)	30.0, t			
	2.9060	ddd (-16.89, 6.26, 4.47)				
4'	–	–	175.3, s			
OH-1				5.7021	d (4.60)	
OH-5				6.4159	d (3.83)	
OH-14				6.1408	d (5.74)	
OH-15				6.0448	d (5.90)	

[a] ^{1}H and ^{13}C NMR were recorded at 600 and 150 MHz, respectively.

III. Ullengacenes A and B, dimeric benz[*a*]anthracenes linked by a mono-sulfide bond derived from volcanic island *Streptomyces* sp. SUD119

III. I. Result and discussion

Ullengacene A (**40**) was isolated as a yellow gum, and its molecular formula was determined as $C_{42}H_{42}O_{10}S$ on the basis of HRFABMS data (obsd. $[M+Na]^+$ at *m/z* 761.2394, calcd. $[M+Na]^+$ at *m/z* 761.2396) in combination with ^1H and ^{13}C NMR spectroscopic data (Table 13). Interpretation of ^1H, ^{13}C and HSQC NMR data of 4**0** in DMSO-d_6 identified four aromatic protons and carbons (δ_H 7.59, δ_C 130.6; δ_H 7.40, δ_C 130.0; δ_H 7.11, δ_C 121.9, δ_H 7.05, δ_C 110.3) and eight quaternary carbons (δ_C 157.2, 148.9, 141.7, 141.5, 141.4, 136.8, 128.5, and 122.4), indicating the existence of aromatic ring. Further analysis of 1D and HSQC NMR data revealed that the existence of one carbonyl signal at δ_C 199.8, three protons bound to oxygen-bearing carbons (δ_H 6.44, δ_C 64.1; δ_H 6.32, δ_C 67.2; δ_H 4.19, δ_C 72.2), two exchangeable protons attached to oxygen (δ_H 5.69 and δ_H 4.99), two methoxy groups (δ_H 3.81, δ_C 55.6; δ_H 2.98, δ_C 53.7), three aliphatic protons and carbons (δ_H 2.71, δ_H 2.55, δ_C 67.2; δ_H 2.08, δ_C 37.3), and one methyl group (δ_H 1.02, δ_C 18.0).Interestingly, the sum of proton and carbon signals showed half amount of its molecular weight, indicating that the structure of **40** should be assembled as dimer feature. Despite is dimeric feature, the number of ^1H and ^{13}C signals were still not enough to meet its molecular weight, dedicating the existence of other elements except proton, carbon, and oxygen. For identification of exact component of **40**, energy

dispersive X-ray (EDX) was performed. This experiment relies on an interaction of X-ray excitation with the target compound. This is characterized due to the fundamental principle that each element has a unique atomic structure permitting a unique set of peaks on its electromagnetic emission spectrum. Based on the EDX experiment connected with field emission scanning electron microscope (FE-SEM) which enable to probe surface of target compound, elements consist of ullengacene A (**40**) was completely identified to have one sulfur including protons, carbons, and oxygens.

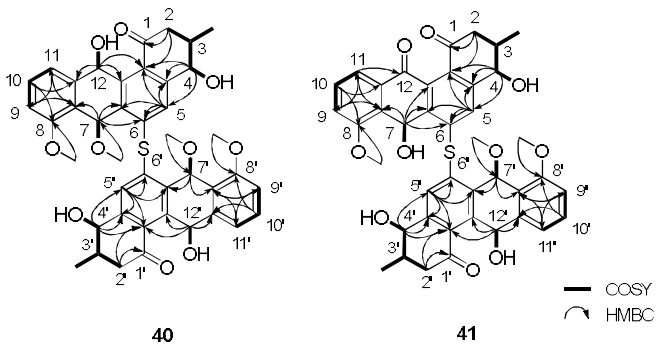

Figure 26. Key COSY and HMBC correlations of ullengacenes A and B (**40** and **41**).

Given these information, interpretation of COSY and HMBC NMR spectroscopic data led us to elucidate the gross structure of ullengacene A (**40**). First, the COSY signals from a aliphatic methylene protons (H_2-2 at δ_H 2.71 and 2.55) to aliphatic methine proton (H-3 at δ_H 2.08) connected C-2 (δ_C 46.1) to C-3 (δ_C 37.3). The homonuclear correlation between doublet methyl group (H_3-3-Me at δ_H 1.02) and H-3 revealed connectivity of methyl

carbon (C-3-Me at δ_C 18.0) and C-3. The aliphatic carbon C-3 was verified to be directly connected to the oxygen-bound carbon C-4 (δ_C 72.2) based on the COSY signals between H-3 and H-4 (δ_H 4.19).Further COSY analysis identified the connectivity between H-4 and H-4-OH (δ_H 5.69), indicating oxygenated carbon C-4 did not expand to other ester bond. The HMBC correlations from H_2-2 to ketone carbon (C-1 at δ_C 199.8) and quaternary carbon (C-12b at δ_C 128.5), and from H-4 to C-4a (δ_C 148.9) and C-12b clarified that carbon frame from C-1 to C-12b formed a six-membered ring for first partial structure. Additional HMBC correlations from H-4 to C-5 (δ_C 130.6) and from H-5 (δ_H 7.59) to four quaternary carbon including C-4a, C-6 (δ_C 136.8), C-6a (δ_C 141.4), and C-12b exhibited connectivity of six-membered ring to uncovered aromatic ring. The hetero nuclear correlation from H-7 (δ_H 6.32) to C-6a and C-12a (δ_C 141.5), and from H-12 (δ_H 6.44) to C-12a and C-12b led to construction of six-membered aromatic ring structure connected adjacent to first partial structure.

Additional aromatic ring was established easily by ^{1}H-^{1}H homonuclear correlations of aromatic protons from H-10 (δ_H 7.40) to H-9 and H-11 (δ_H 7.05 and δ_H 7.11), connecting the aromatic carbons C-9, C-10, and C-11 (δ_C 110.3, 130.0, and 121.9). In this spin system, the vicinal coupling constants were measured as 7.5 Hz, supporting these protons are originated from a 6-membermed aromatic ring. This spin system was completely identified based on the HMBC correlations from H-9 to C-7a (δ_C 122.4) and

C-11, from H-10 to C-8 (δ_C 157.2) and C-11a (δ_C 141.7), and from H-11 to C-9 and C-7a. In the HMBC spectrum, the methoxy group (H_3-8-OMe at δ_H 3.81) also displayed connectivity of aromatic quaternary carbon at C-8 constructing anisole moiety. The $^3J_{CH}$ correlations from H-7 to C-6a and C-7a, and from H-12 to C-11a, C-12a, and C-12b established complete benz[*a*]anthracene moiety, connecting four six-membered ring systems. Further COSY correlation between H-12 and H-12-OH (δ_H 4.99) and HMBC correlation from H3-7-OMe resulted in construction of monomer structure of **40**. Because of dimer feature of ullengacene A (**40**) including one sulfur based on the molecular weight and EDX experiments, the full structure of **40** was dedicated to dimer linked by sulfur bridge. In a comprehensive assignments of NMR spectroscopic data, we found out that the quaternary carbon C-6 was not occupied due to lack of signal, indicating the position C-6 have to be connected to a sulfur bridge. Consequently, these benz[*a*]anthracene monomers were linked by the one sulfur bond bridge attached adjacent to each of C-6 sites. Therefore, the planar structure of ullengacene A (**40**) was established as a structurally new dimer feature of benz[*a*]anthracene satisfying the 22 degree of unsaturation (Figure 26).

Ullengacene B (**41**) was obtained as a yellow gum with molecular formula as $C_{41}H_{38}O_{10}S$ based on the HRFABMS data (obsd. $[M+H]^+$ at *m*/*z* 723.2275, calcd. $[M+H]^+$ at *m*/*z* 723.2264), ^1H, and ^{13}C NMR spectroscopic data (Table 13). The molecular formula and the UV spectrum of **41** were similar to those of **40**, indicating the ullengacene B (**41**) is structurally

analogous to ullengacene A (**40**). Further EDX experiment for **41** was performed and I found out the elements spectrum of **41** displayed similar pattern of **1**, including protons, carbons, oxygens, and one sulfur. However, careful comparison of the ^{1}H and ^{13}C NMR data of **41** noticed that the number of protons and carbons of **41** exhibited almost double amount of those of **40**. Given these information, ullengacene B (**41**) was speculated as derivative of **40** with feature of pseudo-dimer, not dimer. The comprehensive 1D and 2D NMR analysis revealed that methoxy group signal of **40** at δ_H 2.98 (H_3-7-OMe) was replaced by proton signal of **41** at δ_H 5.96 (H-7-OH). Additional difference of **40** and **41** was due to the absence of carbinol signal (H-12 at δ_H 6.44; C-12 at δ_C 64.1) and the presence of ketone signal (C-12 at δ_C 196.8), establishing pseudo-dimer feature of **41** with shifting of chemical signals from those of **40**. The pseudo-dimer structure of **41** was completely confirmed by the analysis of ROESY signals between H-4 (δ_H 4.32)/H-4'-OH (δ_H 5.71), H-4-OH (δ_H 5.51)/H-4' (δ_H 4.30), H-5 (δ_H 7.57)/H-5' (δ_H 7.81), and H-7 (δ_H 6.35)/H-7' (δ_H 6.18).

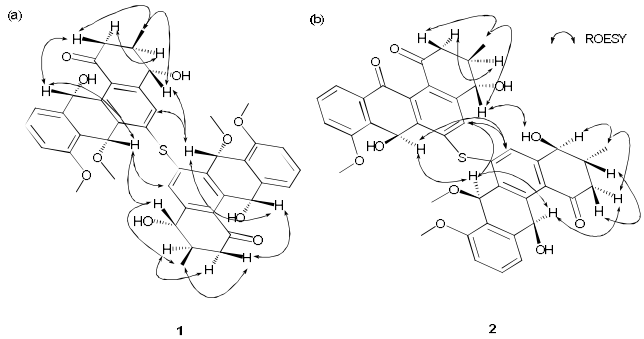

Figure 27. (a) Key ROESY correlations of ullengacene A (**40**). (b) Key ROESY correlations of ullengacene B (**41**).

The scheme for determination of the absolute configuration of benz[*a*]anthraquinones and benz[*a*]anthacenes were previously reported using crystallography and ECD calculation. The chemical reactions for stereogenic centers has not been described because the steric hindrance of the structure disrupted chemical derivatization to act on. Therefore, ECD calculation was performed to determine the absolute configuration of **40**. First, the relative configuration of **40** was established by the analysis of $^{3}J_{HH}$ values and ROESY NMR spectroscopic data (Figure 27a). The relationship between H-3 and H-4 was deduced as *anti* due to the large corresponding $^{3}J_{H3H4}$ value (8.5 Hz). The ROESY correlation between H-2b, H-3-Me, H-4, H-7, H-7', and H-12 were observed. For identification of clear the long-range ROESY signals, I performed 1D ROESY NMR experiment. As a result, 1D ROESY NMR experiment on H-4 exhibited exact peaks of H-2b, H-3-Me and H-7', establishing the relative configuration of **40** as 3*R**, 3'*R**, 4*S**, 4'*S**, 7*R**, 7'*R**, 12*S**, and 12'*S**. Furthermore, additional

computational analysis for prediction of NMR shielding tensor was applied to support the relative configuration of **40** using DP4 analysis. However, it was difficult to apply DP4 analysis onto the full structure of **40** for accuracy of DP4 modeling calculation (<500 dalton). Accordingly, DP4 possibility analysis was conducted on monomer feature of **40** with experimental and predicted CS values of the two diastereomer A and B. The outcome indicated that diastereomer A with 7*R*, 12*S* was the most relevant with a probability of 91.6 %, as I expected. This result shows application of DP4 possibility analysis can be powerful tools for determination of relative configuration between chiral centers with long distance.

The relative configuration of **41** was also established by careful analysis of ^{1}H-^{1}H coupling constants and ROESY data. The relationship between H-3 and H-4 was revealed as *anti* with the large corresponding $^{3}J_{H3H4}$ value (8.0 Hz). Also, the relationship between H-3' and H-4' was elucidated as *anti* based on the high $^{3}J_{H3'H4'}$ value (8.0 Hz). However, the ROESY signals of **41** displayed slightly different patterns from those of **40**. First, the ROESY correlations between H-2b (δ_H 2.58), H-3-Me (δ_H 1.02), and H-4 (δ_H 2.03) displayed identical signals with those of **40**. Further ROESY analysis with 1D ROESY experiments on H-7' (δ_H 6.18) revealed that H-7, H-7', H-12' (δ_H 6.43), H-2'b (δ_H 2.54), H-3'-Me (δ_H 1.04), and H-4' (δ_H 4.30) were located in the same direction, establishing the relative configuration of **2** as 3*R**, 3'*R**, 4*S**, 4'*S**, 7*S**, 7'*R**, 12'*S** (Figure 27b).

Interestingly, careful ROESY analysis discovered the key correlation from H-4 to H-4'-OH which was not detected in that of **40** indicating the relative configuration of **41** was identical that of **40** except C-7 but the arrangement of two of ring structures was reversed in three dimensional space.

For determination of the absolute configuration of **40**, an energy-minimized structure of each conformer was calculated on the basis of the relative configuration of **40**. Then, ECD (electronic circular dichroism) calculations for the conformers of the two enantiomers of **40** were conducted by time-dependent density-functional theory (TD-DFT) at the B3LYP/def2-TZVPP//B3LYP/def-SVP level for all atoms. The experimental ECD spectrum of **40** showed a diagnostic positive Cotton effect at 324 nm and a negative Cotton effects at 292 nm and 350 nm, respectively. As depicted in Figure 3, the calculated ECD spectrum of the enantiomer with the 3*R*, 3'*R*, 4*S*, 4'*S*, 7*R*, 7'*R*, 12*S*, and 12'*S* configuration corresponded with the experimental ECD spectrum (Figure 28), whereas the other enantiomer with 3*S*, 3'*S*, 4*R*, 4'*R*, 7*S*, 7'*S*, 12*R*, and 12'*R* configuration displayed the opposite ECD spectrum, determining the absolute configuration of **40** as 3*R*, 3'*R*, 4*S*, 4'*S*, 7*R*, 7'*R*, 12*S*, and 12'*S*. The absolute configuration of **41** was also determined as 3*R*, 3'*R*, 4*S*, 4'*S*, 7*S*, 7'*R*, 12'*S* by the comparison of the experimental ECD spectrum and the calculated ECD spectra of **41** using same procedure. However, I had to confirm the possibility for conversion of the absolute configuration of **40** at C-3', 4', 7' and 12' position because NMR chemical shifts of **40** will be identical even those of stereogenic center

were reversed. For determination of the exact absolute configuration, the modified Mosher's method was applied to obtain enantiomer or diastereomer of **40**. Due to its steric hinderence reported previously, *S*-MTPA-Cl was used for derivatization with overdose of dimethylaminopyridine (DMAP). Fortunately, reaction was successfully act on successfully and ^{1}H NMR spectrum of *R*-MTPA ester of **40** displayed feature of enantiomer, indicating the absolute configuration of **40** at C-3', 4', 7' and 12' position are identical with that of C-3, 4, 7, and 12. Further derivatization of *S*-MTPA ester was also performed well and analysis of the ^{1}H and COSY NMR spectroscopic data for these *S*- and *R*-MTPA esters led to the assignment of the Δ_{S-R} values, identifying 3*S*, 3'*S* configuration. Based on the relative configuration, the absolute configuration of C-4, 4', 7, 7', 12 and 12' were confirmed to be 3*R*, 3'*R*, 4*S*, 4'*S*, 7*R*, 7'*R*, 12*S*, and 12'*S,* as I expected with ECD calculations.

(a)

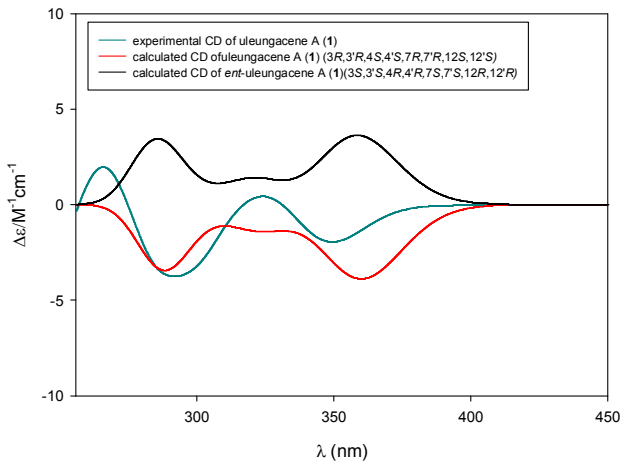

(b)

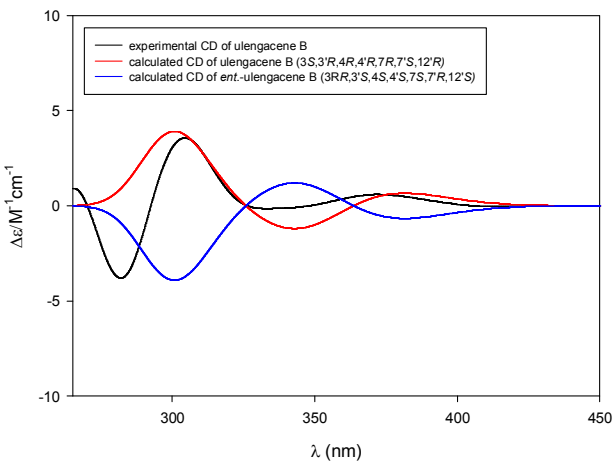

Figure 28. ECD spectra of ullengacene A and B (**40** and **41**).

In search of monomer derivatives of **40** to compare the biological activities, ullengacene C (**42**) was finally obtained as a pure compound. U llengacene C (**42**) was isolated as a yellow gum having molecular formula

as $C_{20}H_{20}O_5$ on the basis of the HRFABMS data (obsd. $[M+H]^+$ at *m*/*z* 340.1324, calcd. $[M+H]^+$ at *m*/*z* 340.1316), ^1H, and ^{13}C NMR spectroscopic data (Table S1). Careful comparison of 1D and 2D NMR data with **40** indicated the planar structure of **42** was almost identical with that of **40** except methoxy group signal of **40** at δ_H 2.98 (H_3-7-OMe) which was disappeared in **42**. Further analysis of *J*-based configuration and ROESY NMR data of **40** revealed that the relative configuration of **42** was completely identical with that of **40**. The absolute configuration of **42** was determined by ECD calculation as 3*R*, 4*S*, 7*R*, and 12*S*, notifying compound **42** should be a precursor of **40** in biosynthetic pathway. Furthermore, two kinds of known compounds belonging to benz[a]anthraquinone class, rubiginoneA_2 and fujianmycin A were also prepared for the comparison of bioactivities with **40**-**42**.

The biological activities of benz[*a*]anthracene class compounds were reported to display moderate antibiotic activity previously. Therefore, I first evaluated ullengacene s A-C for antibacterial and antifungal activities. Unfortunately, ullengacene s A-C (**40**-**42**) did not display any significant inhibitory activity either. Additional bioassay for cytotoxicity effects against human carcinoma cell lines A549, HCT116, SNU638, K562, SK-HEP1, and MDA-MB231 were tested, however ullengacenes A-C (**40**-**42**) did not showed remarkable cytotoxicity against the human cancer cells (IC_{50} > 10 μM). Because these compounds displayed no cytotoxicity, ullengacenes A-B (**40**-**42**) were evaluated with respect to cancer chemoprevention. Cancer

chemoprevention has been regarded as prolific approach for decreasing the risk of cancer development, involving prevention, delay, or reversal of the process of carcinogenesis. We focused two strategies for cancer chemoprevention including enhancement of the deactivation of radicals and electrophiles via phase II enzymes, and inhibiting angiogenesis in growth of tumor cells.

First, a QR induction assay was performed to evaluate the bioactivities of **40-42** in the cultured Hepa-1c1c7 murine hepatoma cell line using 0.1 % dimethyl sulfoxide (DMSO) as a control and *β*-naphthoflavone (2 μM) as a positive control. As shown in Figure 29a, ullengacene A **(40**) at a concentration of 20 μM exhibited a remarkable 2.4-fold increase in QR induction activity against the control. However, ullengacene B (**41**) displayed relatively weak activity compared with **40**. Interestingly, further biological evaluation for antiangiogeneic activity showed opposite results. In this assay, I evaluated the capillary tube formation assay of HUVEC under VEGF induced condition using endothelial cells. The suppression ratio of the ullengacene B (**41**) at 40 μM displayed inhibition of endothelia cell network formation, which was similar with VEGF negative condition (Figure 4b) with no cytotoxicity. Ullengacene B (**41**) was observed to inhibit capillary tube formation of the HUVEC in dose dependent manner. On the other hand, ullengacene A (**40**) exhibited no inhibition activity with same concentration. These results indicated that variation of chiral centers and existence of methoxy groups resulting in arrangement of ring formation

could be significant factor for cancer chemoprevention. Furthermore, monomer compounds were evaluated for QR induction and anti-angiogenesis activities with same procedures but none of them displayed remarkable activity, supporting that the dimer feature of benz[*a*]anthracene can be a key scaffolds to exhibit biological activities.

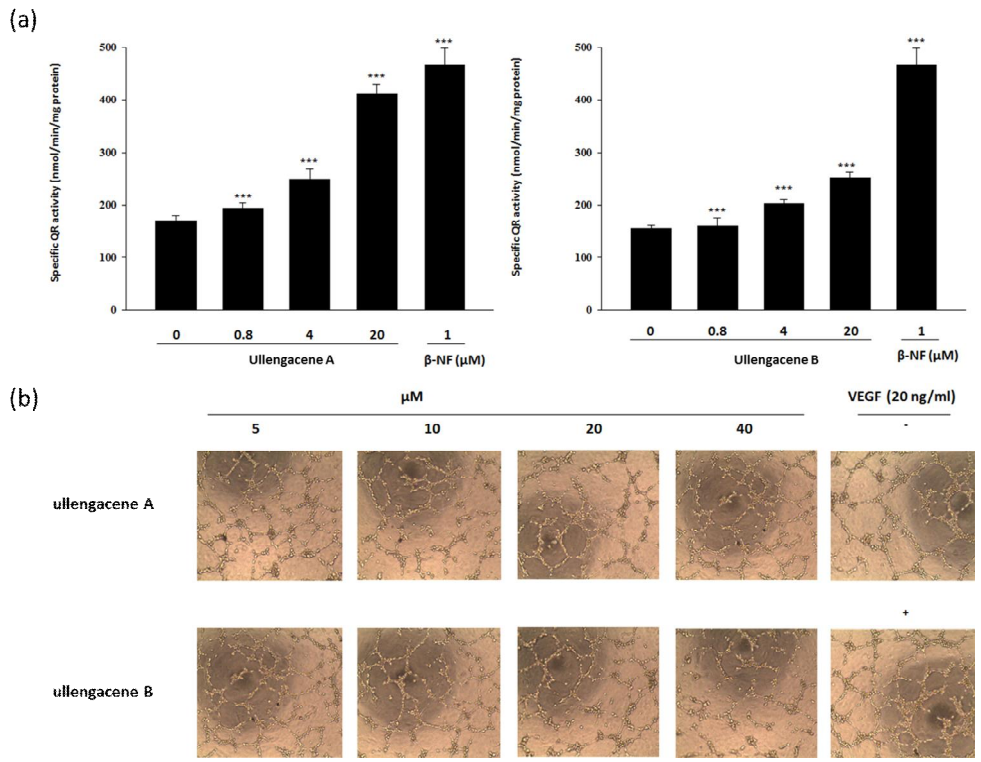

Figure 29. (a) Effect of **40** and **41** on the induction of quinone reductase in murine Hepa1c1c7 cells. Cells were grown for 24 h, and then exposed to **40** - **41** for 24 h. Quinone reductase activities were measured in cell lysates by reduction of a tetrazolium dye and expressed as nmol/min/mg protein. Values represent the mean ± SD of four determinations. ***P <0.001 indicates statistically significant differences from the control group. (b) Effect of **40** and **41** on capillary tube formation by endothelial cells. In 96-

well plate coated with matrigel, HUVECs and each concentration of **40** and **41** were added and then incubation for 4-8 h at 37℃. The capillary structures were photographed and quantified.

In summary, new benz[*a*]anthracene class compounds, ullengacenes A, B and C (**40**, **41** and **42**), were isolated from the *Streptomyces* sp. collected in sediment of volcanic island, Uleung-do. In natural products derived from bacteria, several dimeric compounds were reported very seldom with a sulfide bond bridge. Especially, dimeric compounds possessing a mono-sulfide bond bridge were extremely rare. To my best knowledge, ullengacenes A and B (**40** and **41**) are first dimeric benz[*a*]anthracene class compounds linked by a mono-sulfide bond bridge derived from *Streptomyces* sp. Moreover, the biological activities of the compounds belonging to benz[*a*]anthracene class have been reported to display antibiotic activity. my report of QR induction activity and antiangiogenic activity evaluated by ullengacenes A and B (**40** and **41**), which are dimer version of benz[*a*]anthracene class, propose the first biological evaluation of this class of compounds and the biological importance of structural arrangement of ring formation and dimeric composition. Regarding the structural novelty and biological activity of the ullengacenes, my discovery provides the evidence that marine microorganisms derived from relatively uncommon environments could be a prolific source for inspiring structurally new scaffolds with novel biological activities.

Table 13. . ^{1}H and ^{13}C NMR Data of **40** and **41** in DMSO-d_6

	40		**41**	
no.	δ_H, mult (*J* in Hz)	δ_C	δ_H, mult (*J* in Hz)	δ_C
1	–	199.8, s	–	198.2, s
2	2.71, 1H, d (15.0, 4.5)	46.1, t	2.75, 1H, d (14.0, 4.5)	45.9, t
	2.55, 1H, d (15.0, 9.5)		2.58, 1H, d (14.0, 8.0)	
3	2.08, 1H, dddd (9.5, 8.5, 6.5, 4.5)	37.3, d	2.03, 1H, dddd (8.5, 8.0, 6.5, 4.5)	39.8, d
3-Me	1.02, 3H, d (6.5)	18.0, q	1.02, 3H, d (6.5)	19.6, q
4	4.19, 1H, dd (8.5, 4.0)	72.2, d	4.32, 1H, d (8.0)	72.4, d
4a	–	148.9, s	–	145.2, s
4-OH	5.69, 1H, d (4.0)		5.51, 1H, br	
5	7.59, 1H, s	130.6, d	7.57, 1H, s	130.2, d
6	–	136.8, s	–	138.6, s
6a	–	141.4, s	–	141.3, s
7	6.32, 1H, s	67.2, d	6.35, 1H, s	59.1, d
7a	–	122.4, s	–	130.4, s
7-OMe/	2.98, 3H, s	53.7, q		
7-OH			5.96, 1H, br	
8	–	157.2, s	–	157.1, s
8-OMe	3.81, 3H, s	55.6, q	3.87, 3H, s	56.1, q
9	7.05, 1H, d (8.0)	110.3, d	7.38, 1H, d (8.0)	115.9, d
10	7.40, 1H, t (8.0)	130.0, d	7.56, 1H, t (8.0)	133.6, d
11	7.11, 1H, d (8.0)	121.9, d	7.42, 1H, d (8.0)	117.8, d
11a	–	141.7, s	–	141.5, s
12	6.44, 1H, d (6.0)	64.1, d	–	196.8, s
12-OH	4.99, 1H, d (6.0)			
12a	–	141.5, s	–	140.6, s
12b	–	128.5, s	–	129.8, s
1’	–	199.8, s	–	199.9, s
2’	2.71, 1H, d (15.0, 4.5)	46.1, t	2.77, 1H, d (14.0, 8.0)	46.1, t
	2.55, 1H, d (15.0, 4.5)		2.54, 1H, d (14.0, 4.5)	
3’	2.08, 1H, dddd (8.5, 6.5, 4.5, 4.5)	37.3, d	2.15, 1H, dddd (8.5, 8.0, 6.5, 4.5)	37.4, d
3’-Me	1.02, 3H, d (6.5)	18.0, q	1.04, 3H, d (6.5)	18.3, q
4’	4.19, 1H, dd (8.5, 4.0)	72.2, d	4.30, 1H, d (8.0)	72.6, d
4’a	–	148.9, s	–	144.7, s
4’-OH	5.69, 1H, d (4.0)		5.71, 1H, br	
5’	7.59, 1H, s	130.6, d	7.81, 1H, s	132.2, d
6’	–	136.8, s	–	155.7, s
6’a	–	141.4, s	–	138.9, s
7’	6.32, 1H, s	67.2, d	6.18, 1H, s	68.0, d
7’a	–	122.4, s	–	123.1, s
7’-OMe	2.98, 3H, s	53.7, q	3.21, 3H, s	55.3, q
8’	–	157.2, s	–	157.4, s
8’-OMe	3.81, 3H, s	55.6, q	3.51, 3H, s	55.6, q
9’	7.05, 1H, d (8.0)	110.3, d	6.90, 1H, d (8.0)	110.6, d
10’	7.40, 1H, t (8.0)	130.0, d	7.32, 1H, t (8.0)	130.2, d
11’	7.11, 1H, d (8.0)	121.9, d	7.06, 1H, d (8.0)	122.3, d
11’a	–	141.7, s	–	142.2, s
12’	6.44, 1H, d (6.0)	64.1, d	6.43, 1H, s	65.1, d
12’-OH	4.99, 1H, d (6.0)		4.74, 1H, br	
12’a	–	141.5, s	–	135.5, s
12’b	–	128.5, s	–	133.3, s

[a] ^{1}H and ^{13}C NMR were recorded at 600 and 150 MHz, respectively.

I. II. Experimental section

General experimental procedures. Optical rotations were recorded using a JASCO P-200 polarimeter with a 1 cm cell. UV spectra were obtained on a Perkin Elmer Lambda 35 UV/Vis spectrophotometer. ECD spectra were acquired on an Applied Photopysics Chirascan-plus circular dichroism spectrometer. IR spectra were obtained using a Thermo Nicolet iS10 detector. ^{1}H, ^{13}C and 2D NMR spectra were recorded on Bruker Avance 600 MHz spectrometers at the National Center for Inter-University Research Facilities (NCIRF) at Seoul National University and on a Bruker Avance II 900-MHz NMR spectrometer at the Korea Basic Science Institute (KBSI) at Ochang. Chemical shifts of all NMR spectra were referenced to residual protonated solvent peaks for CD_3OD (δ_H/δ_C, 3.33/49.2) or pyridine–d_5 (δ_H/δ_C, 8.74, 7.58, 7.21/150.4, 135.9, 123.9). Electrospray ionization (ESI) low–resolution LC/MS data were acquired on an Agilent Technologies 6130 quadrupole mass spectrometer coupled with an Agilent Technologies 1200–series HPLC. High-resolution fast atom bombardment (HR–FAB) mass spectra were obtained using a Jeol JMS–600W high–resolution mass spectrometer at NCIRF. GC analysis was performed on an Agilent 6850–series gas chromatograph using an HP-5 column (cross-linked 5% PHM/Siloxan, Macherey und Nagel) and a flame ionization detector. Instant Ocean sea-salt mix was used to prepare seawater-based media.

Bacterial isolation. A mud sample was collected from the Mohang mudflat in Buan, Republic of Korea. The sample was dried at room temperature for (rt) 3 h, and the dry sediment (1 g) was diluted in 4 mL of st erilized artificial seawater. The mixture was spread onto actinomycete isolation agar, A4 medium (1 L seawater, 18 g agar, 100 mg/L cycloheximide), A5 medium (750 mL seawater, 250 mL distilled water, 18 g agar, 100 mg/L cycloheximide), and chitin-based agar (1 L seawater, 18 g agar, 5 g chitin powder, 100 mg/L cycloheximide) by stamping, spreading, or both. The single-strain SNM31 was isolated on A5 medium. The strain SNM31 (GenBank accession #KT921418) was phylogenetically identified as a *Streptomyces* sp. on the basis of the 16S rDNA sequence analysis (most closely related to *Streptomyces griseus*, 99% identity).

Cultivation and extraction of the bacterial strain. The strain SNM31 was cultivated in 50 mL of YEME medium (4 g yeast extract, 10 g malt extract, and 4 g glucose in 1 L artificial seawater) in a 125 mL Erlenmeyer flask. After cultivation for 3 days on a rotary shaker at 160 rpm at 30 °C, 10 mL of the culture was inoculated directly to 1 L of YEME liquid medium in 2.8 L Erlenmeyer flasks (12 ea × 1 L, total volume 12 L). After the bacteria were incubated for 4 days, the 12 L culture of the SNM31 strain was extracted with 18 L of EtOAc. The EtOAc layer was separated, and anhydrous sodium sulfate was added to remove residual water. The extraction procedure was repeated four times (total culture volume: 48 L). The extract in EtOAc was concentrated *in vacuo* to yield 4 g of dried

material in total.

Isolation of mohangic acids (20–24). The organic extract of SNM31 was filtered with a syringe filter and injected directly onto a semi-preparative reversed-phase HPLC column (Kromasil C_{18} (2): 250 × 10 mm, 5 μm) with a gradient solvent system (30% MeOH/H_2O to 80% MeOH/H_2O over 60 min, UV 280 nm detection, flow rate: 2 mL/min). Five major peaks at retention times of 44 min, 45 min, 48 min, 50 min, 54 min were observed. Each compound was further purified under gradient solvent conditions (10% CH_3CN/H_2O to 100% CH_3CN over 40 min, UV 280 nm detection, flow rate: 2 mL/min) using a reversed-phase C_{18} HPLC column (Kromasil C_{18} (2): 250 × 10 mm, 5 μm). Mohangic acids A–E (**20**–**24**) were obtained in pure form at retention times of 24.0 (72 mg), 22.5 (12 mg), 23.5 (15 mg), 25 (13 mg), and 18.5 min (8 mg), respectively.

Mohangic acid A (**20**): Yellow gum; $[\alpha]^{25}_{D}$ -6.9 (*c* 0.5, MeOH); UV (MeOH) λ_{max} (log ε) 270 (4.46) nm, 325 (4.15) nm; ECD (*c* 4.3 × 10^{-4} M, MeOH) λ_{max} ($\Delta\varepsilon$) 218 (-39.5), 257 (-5.5) nm; IR (neat) ν_{max} 3392, 2958, 1672, 1588, 1541 cm^{-1}; ^{1}H and ^{13}C NMR data, Table 1; HRFABMS *m*/*z* 482.2517 [M + Na]$^{+}$ (calcd for $C_{26}H_{37}NO_6Na$, 482.2519).

Mohangic acid B (**21**): Yellow gum; $[\alpha]^{25}_{D}$ -16.7 (*c* 0.5, MeOH); UV (MeOH) λ_{max} (log ε) 270 (4.57) nm, 325 (4.26) nm; ECD (*c* 4.2 × 10^{-4} M, MeOH) λ_{max} ($\Delta\varepsilon$) 218 (-39.5) nm; IR (neat) ν_{max} 3410, 2964, 1602, 1546, 1395 cm^{-1}; ^{1}H and ^{13}C NMR data, Table 1; HRFABMS *m*/*z* 496.2681 [M + Na]$^{+}$ (calcd for $C_{27}H_{39}NO_6Na$, 496.2675).

Mohangic acid C (**22**): Yellow gum; $[\alpha]^{25}_{D}$ -7.1 (*c* 0.5, MeOH); UV (MeOH) λ_{max} (log ε) 270 (4.63) nm; 325 (4.32) nm; ECD (*c* 4.0 × 10^{-4} M, MeOH) λ_{max} ($\Delta\varepsilon$) 218 (-39.1), 269 (-7.5), 275 (-6.2), 282 (-9.2) nm; IR (neat) ν_{max} 3402, 2967, 1675, 1593, 1536 cm^{-1}; ^{1}H and ^{13}C NMR data, Table 1; HRFABMS *m*/*z* 524.2629 $[M + Na]^+$ (calcd for $C_{28}H_{39}NO_7Na$, 524.2624).

Mohangic acid D (**23**): Yellow gum; $[\alpha]^{25}_{D}$-11.7 (*c* 0.5, MeOH); UV (MeOH) λ_{max} (log ε) 270 (4.46) nm; ECD (*c* 4.0 × 10^{-4} M, MeOH) λ_{max} ($\Delta\varepsilon$) 217 (-39.9), 259 (-4.4), 268 (-5.5), 280 (3.7) nm; IR (neat) ν_{max} 3452, 2958, 1737, 1598, 1366 cm^{-1}; ^{1}H and ^{13}C NMR data, Table 1; HRFABMS *m*/*z* 526.2784 $[M + Na]^+$ (calcd for $C_{28}H_{41}NO_7Na$, 526.2781).

Mohangic acid E (**24**): Yellow gum; $[\alpha]^{25}_{D}$ -25.7 (*c* 0.5, MeOH); UV (MeOH) λ_{max} (log ε) 270 (4.19) nm, 325 (3.91) nm; ECD (*c* 3.2 × 10^{-4} M, MeOH) λ_{max} ($\Delta\varepsilon$) 218 (-41.3), 292 (-3.5), nm; IR (neat) ν_{max} 3368, 2968, 1737, 1599, 1373 cm^{-1}; ^{1}H and ^{13}C NMR data, Table 1; HRFABMS *m*/*z* 644.3052 $[M + Na]^+$ (calcd for $C_{32}H_{47}NO_{11}Na$, 644.3047).

Hydrogenation of mohangic acid D. Mohangic acid D (**23**) (4 mg) was lyophilized for 24 h and subsequently suspended, along with a 10% Pd/C catalyst, in absolute EtOH (1.5 mL). The mixture solution of **23** was stirred for 2 h under 1 atm of H_2 at rt. The reaction mixture in EtOH was filtered using a PTFE syringe filter and evaporated *in vacuo* to yield the hydrogenation product (**25**) of **23**. The product was isolated in pure form by reversed-phase HPLC (Phenomenex Luna 5 μm C_{18} (2) 250 × 10.0 mm,

flow rate 2 mL/min, UV 254 nm detection) using a gradient solvent system (10% to 100% ACN/H_2O over 40 min). The hydrogenate product (**6**) was obtained at a retention time of 27 min (3 mg, 75 %) under HPLC conditions. The molecular formula of product (**25**) was confirmed as $C_{28}H_{47}NO_7$ on the basis of ESIMS data ($[M + H]^+$ *m*/*z* at 510).

Hydrogenation product (**25**). ^1H NMR (600 MHz, CD_3OD) δ_H 7.49 (d, *J* = 8.0 Hz, 2H), 7.30 (d, *J* = 8.0 Hz, 2H), 4.58 (m, 1H), 3.95 (m, 1H), 3.75 (m, 1H), 3.04 (dd, *J* = 7.5 Hz, 4.5 Hz, 1H), 2.42 (dd, *J* = 15.5 Hz, 5.5 Hz, 1H), 2.34 (dd, *J* = 15.5 Hz, 5.5 Hz, 1H), 2.10 (s, 3H), 1.75–1.72 (m, 2H), 1.66–1.62 (m, 3H), 1.56 (m, 1H), 1.47–1.42 (m, 4H), 1.38–1.30 (m, 5H), 1.24–1.20 (m, 2H), 1.12–1.05 (m, 2H), 0.88 (d, *J* = 6.5 Hz, 3H), 0.84 (d, *J* = 6.5 Hz, 3H), 0.82 (d, *J* = 6.5 Hz, 3H).

Preparation of acetonide derivative of 25 (26). The hydrogenation product of **23** (**25**) (3 mg) was prepared in a 40 mL vial and dried under high vacuum for 24 h. After adding pyridinium *p*-toluenesulfonate (1 mg), the mixture was dissolved in anhydrous MeOH (200 μL) and anhydrous CH_2Cl_2 (2 mL) at rt. Then, 2,2-dimethoxypropane (4 mL) was added to the reaction vial. The solution was stirred at rt under argon for 48 h. To quench the reaction, a saturated $NaHCO_3$ aqueous solution was added. The reaction mixture was fractionated by flash column reversed-phase chromatography using a gradient solvent system of MeOH/H_2O (20%, 40%, 60%, 80%, and 100%). The acetonide derivative (**26**) was eluted in the 80% and 100% MeOH/H_2O fractions. The final product (**26**) was purified by reversed-phase

HPLC (Phenomenex Luna 5 μm C_{18} (2) 250 × 10.0 mm, flow rate 2 mL/min, UV 254 nm detection) with a gradient solvent system (10% to 100% MeOH/H_2O) for 40 min. The acetonide product (**7**) eluted at a retention time of 35 min (2.5 mg, 83%) under the HPLC conditions. The molecular formula of **26** was confirmed as $C_{31}H_{51}NO_7$ by ESIMS analysis ($[M + H]^+$ *m*/*z* at 550).

Acetonide product (**26**). ^{1}H NMR (600 MHz, CD_3OD)) δ_H 7.52 (d, *J* = 8.0 Hz, 2H), 7.32 (d, *J* = 8.0 Hz, 2H), 3.95 (dd, *J* = 10.0 Hz, 6.0 Hz, 1H), 3.92 (m, 1H), 3.74 (m, 1H), 3.06 (dd, *J* = 7.0 Hz, 4.0 Hz, 1H), 2.38 (dd, *J* = 15.0 Hz, 5.0 Hz, 1H), 2.30 (dd, *J* = 15.0 Hz, 8.5 Hz, 1H), 2.12 (s, 3H), 1.98 (m, 1H), 1.87 (m, 1H), 1.77 (m, 1H), 1.69-1.67 (m, 2H), 1.57-1.55 (m, 2H), 1.47–1.42 (m, 4H), 1.39 (s, 6H), 1.38–1.30 (m, 5H), 1.22 (m, 1H), 1.12-1.06 (m, 2H), 0.89 (d, *J* = 6.5 Hz, 3H), 0.88 (d, *J* = 6.5 Hz, 3H), 0.84 (d, *J* = 6.5 Hz, 3H).

Analysis of the absolute configuration of the glucose in mohangic acid E (24). Mohangic acid E (3 mg) was dissolved in 3 N HCl (0.5 mL) and stirred at 80 °C for 2 h. After the solution cooled to rt, the HCl was evaporated *in vacuo* to yield the hydrolysate. HMDS and TMSCl (50 μL, v/v = 2:1) were added to the hydrolysate with pyridine (0.5 mL). After being stirred at 60 °C for 30 min, the mixture was dried *in vacuo* and separated using H_2O and CH_2Cl_2 (1 mL, v/v = 1:1). The CH_2Cl_2 layer was injected into a GC equipped with an HP5 column (0.32 mm × 30 m). The temperature of the injector and the detector in the GC was maintained at 200 °C. During

analysis, the temperature of the GC column was controlled (60 °C for 3 min, 60–200 °C at 4 °C/min, and 200 °C for 3 min). The glucose derivative from the hydrolysate of **24** was detected at a retention time of 32.65 min. The authentic D-glucose and L-glucose samples were treated and analyzed using the same procedures. The derivatives of D-glucose and L-glucose were detected at 32.67 min and 32.85 min, respectively. Co-injection of the silylated derivative of the hydrolysate and authentic D-glucose gave a single peak at 32.64 min, thereby determining the absolute configuration of the glucose in **24** as the D-form.

Synthesis of bidentate chiral NMR solvents. *N*-Bromosuccinimide (2.2 mmol) was added to a mixture of 2-methyl-1,3-propanediol (1.0 mmol) and triphenylphosphine (2.2 mmol) in CH_2Cl_2 (10.0 mL) at 0 °C. The reaction mixture was stirred at rt for 30 min. The solvent was removed, and the dibromopropane was purified by column chromatography (silica gel, 40–63 μm, pentane). With the acquired dibromopropane, bidentate chiral solvents (*R*,*R*)-and (*S*,*S*)-bis-α-methylbenzylamine-*p*-Me (BMBA) were synthesized according to previously reported procedures.[43]

Quinone reductase (QR) assay. QR activities were determined spectrophotometrically according to a modified microtiter method.[44] Hepa-1c1c7 cells were plated at a density of 20,000 cells/mL and cultured for 24 h in a humidified incubator containing 5% CO_2 at 37 °C. The cells were then exposed to mohangic acids (**20**–**24**) and incubated for an additional 24 h. The media was subsequently decanted, and the cells in each well were lysed

by incubation at 37 °C for 10 min with 250 µL of a solution containing 10 mM Tris-HCl pH 8.0, 140 mM NaCl, 15 mM $MgCl_2$, and 0.5 % NP-40 (IGEPAL CA-630) (Sigma-Aldrich). The plates were then agitated on an orbital shaker for additional 10 min at 25 °C, after which 1 mL of the complete reaction mixture containing 12.5 mM Tris-HCl pH 7.4, 0.67 mg/mL bovine serum albumin (BSA), 0.01% Tween-20, 50 µM flavin adenine dinucleotide (FAD), 1 mM glucose-6-phosphate, 2 U/mL glucose-6-phosphate dehydrogenase, 30 µM NADP, 50 µg/mL 3-(4,5-dimethylthiazo-2-yl)-2,5-diphenyltetrazolium bromide (MTT), and 50 µM menadione were added. A blue color developed, and the reaction was stopped after 10 min. The rate of the NADPH-dependent, menadiol-mediated reduction of MTT was measured at 610 nm. Protein was detected by crystal violet staining of an identical set of test plates. The specific activity (SA) of quinone reductase (nmol/min/mg of protein) was calculated from the equation:

$$SA = [MTTabs/CVabs] \times 3{,}345,$$

where MTTabs is the change in the absorbance of MTT per min, CVabs is the absorbance of crystal violet, and 3,345 is the ratio of the proportionality constant determined for crystal violet and the extinction coefficient of MTT and has units of nmol/mg.

II. III. Experimental section

Isolation of bacteria, cultivation, and extraction. A sediment sample was obtained from the southern area of Jeju Island in a 40-mL sterilized plastic tube. The sample (1 g) was dried at room temperature (rt) for 3 h and diluted in 4 mL of sterilized distilled water. The mixture was spread on actinomycete isolation agar, chitin-based agar, SC medium (1 L of distilled water, 10 g of starch, 0.3 g of casein, 2.0 g of KNO_3, 2.0 g of K_2HPO_4, 0.05 g of $MgSO_4 \cdot 7H_2O$, 0.02 g of $CaCO_3$, 0.01 g of $FeSO_4 \cdot 7H_2O$, 16 g of agar, and 100 mg/L cycloheximide), and A4 medium (1 L of distilled water, 18 g of agar, and 100 mg/L cycloheximide). The strain SAK1 was isolated on SC medium. Based on the analysis of the 16S rDNA sequence, SAK1 was clarified to be most closely related to *Streptomyces flavogriseus* (99% identity, GenBank accession number: KY484916). For the production of the succinilenes, the strain SAK1 was initially cultivated in 50 mL of YEME media (4 g of yeast extract, 10 g of malt extract, and 4 g of glucose in 1 L of distilled water) in a 125 mL Erlenmeyer flask. This seed culture was cultivated for 3 days on a rotary shaker at 200 rpm at 30 °C. Ten milliliters of the seed culture was inoculated into 1 L of YEME medium in 2.8-L Fernbach flasks (12 ea × 1 L, total volume of 12 L). After 2 days of incubation, the whole culture (12 L) was extracted twice with 18 L of ethyl acetate. The ethyl acetate layer was separated by a fractionating funnel and dried over anhydrous sodium sulfate. The ethyl acetate extract was concentrated *in vacuo* to yield 2 g of dried material. This procedure was

repeated 6 times (72 L of culture; total amount of extract: 12 g) to obtain a sufficient amount of the succinilenes for the structure elucidation and bioassays.

Isolation of succinilenes A–D. The organic extract of the bacterial strain SAK1 culture was adsorbed on Celite, and the extract-Celite mixture was loaded onto a 2-g Sep-Pak C_{18} cartridge for flash column chromatography. Then, the mixture was fractionated with 20 mL each of 20%, 40%, 60%, 80%, and 100% MeOH in water and 1:1 MeOH/dichloromethane. Succinilenes A–D (**27**–**30**) were detected in the 80% and 100% MeOH/water fractions by LC/MS analysis. To obtain pure succinilenes A-D (**27**–**30**), the fractions bearing **27**–**30** were subjected to reversed-phase HPLC (Kromasil C_{18} (2): 250 × 10 mm, 5 μm) with gradient elution (30% acetonitrile/water to 65% acetonitrile/water over 40 min; UV detection at 280 nm; flow rate: 2 mL/min). Four major HPLC peaks were collected at retention times of 20 min, 28 min, 29 min, and 35 min. These major compounds were further purified under isocratic solvent conditions (65% methanol/water; UV detection at 280 nm; flow rate: 2 mL/min) on a reversed-phase HPLC column (Kromasil C_{18} (2): 250 × 10 mm, 5 μm). Finally, succinilenes A–D (**27**–**30**) were isolated as pure compounds at retention times of 33 min (12 mg), 31 min (11 mg), 36 min (5 mg), and 14 min (2 mg), respectively.

Succinilene A (**27**) $[\alpha]_D$ -5 (c 0.05, MeOH); UV (MeOH) λ_{max} (log ε) 270 (3.92) nm; IR (neat) ν_{max} 3405, 2935, 1647, 1450 cm^{-1}; for ^1H and ^{13}C NMR data, see Table 11; HRFABMS *m/z* 437.2550 $[M-H]^-$ (calcd for $C_{24}H_{37}O_7$ 437.2539).

Succinilene B (**28**) $[\alpha]_D$ -8, (c 0.05, MeOH); UV (MeOH) λ_{max} (log ε) 270 (3.89) nm; IR (neat) ν_{max} 3410, 2930, 1652, 1452 cm^{-1}; for ^1H and ^{13}C NMR data, see Table 11; HRFABMS *m/z* 437.2550 $[M-H]^-$ (calcd for $C_{24}H_{37}O_7$ 437.2539).

Succinilene C (**29**) $[\alpha]_D$ -3, (c 0.05, MeOH); UV (MeOH) λ_{max} (log ε) 270 (3.94) nm; IR (neat) ν_{max} 3392, 2944, 1647, 1452 cm^{-1}; for ^1H and ^{13}C NMR data, see Table 2; HRFABMS *m/z* 437.2545 $[M+H]^+$ (calcd for $C_{24}H_{37}O_7$ 437.2562).

Succinilene D (**30**) $[\alpha]_D$ -6, (c 0.05, MeOH); UV (MeOH) λ_{max} (log ε) 270 (3.85) nm; IR (neat) ν_{max} 3407, 2924, 1650, 1454 cm^{-1}; for ^1H and ^{13}C NMR data, see Table 12; HRFABMS *m/z* 361.2347 $[M+Na]^+$ (calcd for $C_{20}H_{34}O_4Na$ 361.2355).

Methanolysis of succinilenes A–C. Succinilene A (**27**) (5 mg) was dissolved in 2 mL of MeOH, and 28 mg of NaOMe was added to the vial to prepare a 0.5 M NaOMe solution. The mixture was stirred at room temperature for 5 h. The reaction was quenched by the addition of 1 N HCl. The methanolysis product was extracted by water-ethyl acetate partitioning after evaporating the MeOH *in vacuo*. After removing the solvent, the

methanolysis product (**31**) was purified by HPLC using gradient elution conditions (10% – 100% acetonitrile/water over 40 min; UV detection at 280 nm; flow rate: 2 mL/min) and a reversed-phase HPLC column (Kromasil C_{18} (2): 250 × 10 mm, 5 μm). The methanolysis product (**31**) eluted at a retention time of 25 min. The structure of **31** was confirmed by analysis of its ^{1}H and 2D NMR spectral data and ESI mass spectra ($[M+H]^+$ *m*/*z* at 339; molecular formula, $C_{20}H_{35}O_4$). The same procedures were repeated for succinilenes B and C (**32** and **33**). The structures of the methanolysis products of **28** and **29** (**32** and **33**) were also assigned based on the analysis of ^{1}H and 2D NMR spectral data and ESI mass spectra (for **32**, $[M+H]^+$ *m*/*z* at 339 and molecular formula of $C_{20}H_{33}O_4$; for **33**, $[M+H]^+$ *m*/*z* at 337 and molecular formula of $C_{20}H_{33}O_4$).

MTPA esterification of succinilenes A–C. The methanolysis products of succinilenes A–C (**31**–**33**) were prepared individually in 40-mL vials (two 1-mg samples for each compound) and dried completely under high vacuum overnight. After adding catalytic amounts of crystalline dimethylaminopyridine (DMAP) to each reaction vial, freshly distilled anhydrous pyridine (1 mL) was added under argon gas. The reaction mixtures were stirred at room temperature for 5 min. After 5 min, *R*- and *S*-□-methoxy trifluoromethyl-phenylacetic acid (MTPA) chloride (20 μL) were added, respectively. The reactions were carried out for 3 h at room temperature with stirring. The reactions were quenched by adding 50 μL of MeOH. The reaction products were purified by HPLC using gradient elution

conditions of 40% to 100% aqueous acetonitrile over 20 min with a reversed-phase C_{18} column (Kromasil C_{18} (2): 250 × 10 mm, 5 μm; flow rate: 2 mL/min; UV detection at 280 nm). The tetra-*S*- and -*R*-MTPA esters (**34** and **35**) of **31** eluted at 34.3 and 35.2 min, respectively. The tetra-*S*- and -*R*-MTPA esters (**36** and **37**) of **32** eluted at 33.5 and 34.7 min. The tetra-*S*- and -*R*-MTPA esters (**38** and **39**) of **33** were isolated at 36.1 and 37.3 min. The $\Delta\delta_{S-R}$ values around the stereogenic centers of the MTPA esters were assigned based on the analysis of ^{1}H and ^{1}H-^{1}H COSY NMR spectra.

Tetra *S*-MTPA Ester (**34**) of methanolysis product (**31**) of succinilene A (**27**)

^{1}H NMR (600 MHz, pyridine-d_5) δ 7.83–7.81 (m, 4H), 7.78–7.75 (m, 4H), 7.48–7.45 (m, 12H), 6.32–6.17 (m, 4H), 5.73 (m, 1H), 5.67–5.60 (m, 4H), 5.41 (d, J = 6.5, 1H), 5.26 (m, 1H), 3.67 (s, 3H), 3.62 (s, 9H), 2.75 (m, 1H), 2.63–2.54 (m, 2H), 2.51–2.46 (m, 2H), 1.76 (s, 3H), 1.72 (m, 1H), 1.58 (m, 1H), 1.32 (d, J = 6.5, 3H), 0.93 (d, J = 6.5, 3H), 0.88 (t, J = 6.5, 3H). The molecular formula of **34** was confirmed as $C_{60}H_{62}F_{12}O_{12}Na$ ($[M+Na]^+$ at m/z 1227).

Tetra-*R*-MTPA Ester (**35**) of methanolysis product (**31**) of succinilene A (**27**)

^{1}H NMR (600 MHz, pyridine-d_5) δ 7.82–7.81 (m, 4H), 7.79–7.76 (m, 4H), 7.49–7.44 (m, 12H), 6.30–6.22 (m, 4H), 5.75–5.71 (m, 2H), 5.67 (t, J = 7.0, 1H), 5.63 (d, J = 7.0, 1H), 5.56 (d, J = 9.5, 1H), 5.50 (t, J = 7.0, 1H), 5.25 (m, 1H), 3.65 (s, 3H), 3.63 (s, 3H), 3.62 (s, 3H), 3.59 (s, 3H), 2.77 (m, 1H), 2.68 (m, 1H) 2.64–2.61 (m, 2H), 2.55 (m, 1H), 1.80–1.74 (m, 2H), 1.63 (s,

3H), 1.25 (d, J = 6.5, 3H), 1.00 (d, J = 6.5, 3H), 0.86 (t, J = 6.5, 3H). The molecular formula of **35** was confirmed as $C_{60}H_{62}F_{12}O_{12}Na$ ($[M+Na]^+$ at m/z 1227).

Tetra-*S*-MTPA ester (**36**) of methanolysis product (**32**) of succinilene B (**28**)

^{1}H NMR (600 MHz, pyridine-d_5) δ 7.81–7.77 (m, 8H), 7.48–7.45 (m, 12H), 6.32–6.25 (m, 3H), 6.19 (dd, J = 14.5, 10.5, 1H), 5.80–5.75 (br, 3H), 5.65 (m, 1H), 5.64 (m, 1H), 5.61 (m, 1H), 5.58 (br, 1H), 3.67 (s, 6H), 3.61 (s, 6H), 2.74 (br, 1H), 2.68–2.66 (m, 2H), 2.58 (m, 1H), 2.49 (m, 1H), 1.73 (m, 3H), 1.67–1.62 (m, 2H), 0.94 (d, J = 6.5, 3H), 0.89 (d, J = 6.5, 3H), 0.86 (t, J = 7.5, 3H). The molecular formula of **36** was confirmed as $C_{60}H_{62}F_{12}O_{12}Na$ ($[M+Na]^+$ at m/z 1227).

Tetra-*R*-MTPA Ester (**37**) of methanolysis product (**32**) of succinilene B (**28**)

^{1}H NMR (600 MHz, pyridine-d_5) δ 7.75–7.73 (m, 8H), 7.46–7.44 (m, 12H), 6.30–6.29 (m, 2H), 6.24 (m, 1H), 6.17 (m, 1H), 5.76–5.72 (br, 3H), 5.67 (m, 1H), 5.63 (m, 1H), 5.58 (br, 1H), 5.56 (d, J = 9.5, 1H), 3.66 (s, 3H), 3.63 (s, 6H), 3.58 (s, 3H), 2.77 (br, 1H), 2.67 (m, 1H) 2.56–2.54 (m, 2H), 2.45 (m, 1H), 1.76 (m, 2H), 1.68 (s, 3H), 0.98 (d, J = 6.5, 3H), 0.90 (t, J = 7.5, 3H), 0.84 (d, J = 6.5, 3H). The molecular formula of **37** was confirmed as $C_{60}H_{62}F_{12}O_{12}Na$ ($[M+Na]^+$ at m/z 1227).

Tetra-*S*-MTPA Ester (**38**) of methanolysis product (**33**) of succinilene C (**29**)

^{1}H NMR (600 MHz, pyridine-d_5) δ 7.81–7.78 (m, 6H), 7.50–7.47 (m, 9H), 6.25–6.15 (m, 3H), 6.02 (dd, J = 15.0, 9.5, 1H), 5.73 (m, 1H), 5.67–5.62 (m, 2H), 5.57 (m, 1H), 5.55 (d, J = 9.5, 1H), 5.28 (m, 1H), 3.67 (s, 3H), 3.65 (s, 3H), 3.63 (s, 3H), 2.92 (m, 1H), 2.82–2.73 (m, 2H), 2.69 (m, 1H), 2.58–2.50 (m, 3H), 1.69 (s, 3H), 1.13 (d, J = 6.5, 3H), 1.05 (t, J = 7.5, 3H), 0.89 (d, J = 6.5, 3H). The molecular formula of **38** was confirmed as $C_{50}H_{53}F_9O_{10}Na$ ($[M+Na]^+$ at m/z 1007).

Tetra-*R*-MTPA Ester (**39**) of methanolysis product (**33**) of succinilene C (**29**)

^{1}H NMR (600 MHz, pyridine-d_5) δ 7.82–7.80 (m, 6H), 7.51–7.48 (m, 9H), 6.23–6.15 (m, 4H), 5.74 (m, 1H), 5.66–5.60 (m, 2H), 5.58 (t, J = 6.5, 1H), 5.42 (m, 1H), 5.26 (m, 1H), 3.69 (s, 3H), 3.65 (s, 3H), 3.63 (s, 3H), 2.91 (m, 1H), 2.84–2.75 (m, 2H), 2.62 (m, 1H), 2.57–2.51 (m, 3H), 1.65 (s, 3H), 1.18 (d, J = 6.5, 3H), 1.06 (t, J = 7.5, 3H), 0.85 (d, J = 6.5, 3H). The molecular formula of **39** was confirmed as $C_{50}H_{53}F_9O_{10}Na$ ($[M+Na]^+$ at m/z 1007).

Evaluation of antiproliferative activity. The effects of succinilenes A–D (**27**–**30**) on cell proliferation were evaluated by the sulforhodamine B (SRB) cellular protein-staining assay, with slight modifications. Briefly, A549 (lung cancer), SNU638 (gastric cancer), and HCT116 (colon cancer) cells (1×10^4 cells in 190 μL of complete RPMI 1640 medium) were seeded in a 96-well plate with various concentrations of **27**–**30** and incubated at 37 °C in a humidified atmosphere containing 5% CO_2. After 72 h of treatment with succinilenes A–D (**27**–**30**), the cells were fixed with a 10%

TCA solution for 1 h, and cellular proteins were stained with 0.4% SRB in a 1% acetic acid solution. The stained cells were dissolved in 10 mM Tris buffer (pH 10.0). The effects of **27**–**30** on cell viability were calculated as percentages relative to the solvent-treated control. The IC_{50} values were calculated using nonlinear regression analysis (percent survival versus concentration).

Evaluation of i-NOS Assay

Materials

Dulbecco's modified Eagle's medium (DMEM), fetal bovine serum (FBS), sodium pyruvate, L-glutamine, antibiotics-antimycotics solution, and trypsin-EDTA were purchased from Invitrogen Co. (Grand Island, NY, USA). Lipopolysaccharide (LPS, E. coli 0111:B4), 3-(4,5-dimethylthiazol-2-yl)-2,5-diphenyltetrazolium bromide (MTT), and other chemicals were purchased from Sigma (St. Louis, MO, USA).

Cell culture

Mouse macrophage RAW 264.7 cells, provided from the American Type Culture Collection (ATCC, Rockville, MD, USA), were cultured in DMEM supplemented with 10% heat-inactivated fetal bovine serum (FBS) and antibiotics-antimycotics (PSF; 100 units/ml penicillin G sodium, 100 μg/ml streptomycin, and 250 ng/mL amphotericin B). Cells was incubated in humidified atmosphere containing 5 % CO_2 at 37°C.

Nitrite Assay

To evaluate the inhibitory activity of succinilenes A-D (**27**-**30**) on LPS-induced NO production, RAW 264.7 cells were cultured in 10 % FBS-DMEM without phenol red, plated in 24-well plates (3 × 105 cells/mL), and incubated for 24 h. Cells were washed with PBS, fresh medium was added, and the cells were incubated with 1 μg/mL LPS in the presence or absence of test compounds. After additional 20 h of incubation, the media were collected and analyzed for nitrite accumulation as an indicator of NO production by the Griess reaction. Briefly, 180 μL of Griess reagents (0.1 % N-(1-naphthyl) ethylenediamine dihydrochloride in H_2O and 1 % sulfanilamide in 5 % H_3PO_4) was added to 100 μL of each supernatant from LPS or sample-treated cells in 96-well plates. The absorbance was measured at 540 nm, and nitrite concentration was determined by comparison with a sodium nitrite standard curve. Percent inhibition was expressed as [1-(NO level of test samples / NO levels of vehicle-treated control)] × 100.

Statistical Analysis

Data are presented as the means ± SD for the indicated number of independently performed experiments. Statistical significance ($p<0.05$) was assessed by a one-way analysis of variation (ANOVA) coupled with the Dunnett's *t*-test.

Computer-aided NMR spectral analysis. The PERCH NMR software package (ver. 2013.1, PERCH Solutions Ltd., Kuopio, Finland) was used for

HiFSA, as previously described.[52,53,54] The final optimized NMR parameters of compounds **27 - 30** are provided as PERCH parameter text files (*.pms).

Conclusions. Succinilenes A–D (**27**–**30**) were discovered from a marine-derived *Streptomyces* sp. through chemical profiling of a marine actinomycete strain collection. Spectroscopic analysis of **27**-**30** was used to assign their structures as new polyene polyol compounds, each bearing a conjugated triene moiety. These compounds were biologically evaluated for inhibitory effects on LPS-induced NO production, indicating their anti-inflammatory significance. Succinilenes A-C, commonly incorporating a succinic acid moiety, displayed significant inhibitory effects on NO production whereas succinilene D without succinic acid did not inhibit NO production, thus proposing that the succinic moiety is important for the inhibitory effects on LPS-induced NO production. Microbial metabolites having succinic acid are not common but a few microbial polyketide compounds are known to bear succinic acid in their structures such as macrolactin T from the marine bacterium *Bacillus marinus*,[55] reveromycin A from *Streptomyces* sp.,[56] and macrocyclic lactone A26771B from the fungus *Penicillium turbatum*.[57] These succinic acid-bearing compounds have not been tested for the inhibitory activities on LPS-induced NO production. Because the chemical shifts of the olefinic protons belonging to the triene moieties, and thus coupling with each other, are close enough to generate second-order peaks, the triene geometries of the succinilenes could not be determined using conventional methods. My application of the spin

simulation of QM-HiFSA enabled us to calculate the ^{1}H-^{1}H coupling constants of these double bond protons and successfully determine the triene geometries. These results suggest that the QM-HiFSA technique is a useful tool for the detailed structural elucidation of complicated natural products displaying highly overlapped ^{1}H NMR spectra.

III. II. Experimental section

Bacterial isolation. A mud sample was collected from the sediment in Ul-lengdo, Republic of Korea. The sample was dried at room temperature for (rt) 3 h, and the dry sediment (1 g) was diluted in 4 mL of sterilized artif icial seawater. The mixture was spread onto actinomycete isolation agar, A4 medium (1 L seawater, 18 g agar, 100 mg/L cycloheximide), A5 medium (750 mL seawater, 250 mL distilled water, 18 g agar, 100 mg/L cycloheximide), and chitin-based agar (1 L seawater, 18 g agar, 5 g chitin powder, 100 mg/L cycloheximide) by stamping, spreading, or both. The single-strain SUD119 was isolated on A5 medium.

Cultivation and extraction of the bacterial strain. The strain SUD119 was cultivated in 50 mL of YEME medium (4 g yeast extract, 10 g malt extract, and 4 g glucose in 1 L artificial seawater) in a 125 mL Erlenmeyer flask. After cultivation for 3 days on a rotary shaker at 160 rpm at 30 °C, 10 mL of the culture was inoculated directly to 1 L of YEME liquid medium in 2.8 L Erlenmeyer flasks (12 ea × 1 L, total volume 12 L). After the bacteria were incubated for 4 days, the 12 L culture of the SUD119

strain was extracted with 18 L of EtOAc. The EtOAc layer was separated, and anhydrous sodium sulfate was added to remove residual water. The extraction procedure was repeated twelve times (total culture volume: 144 L). The extract in EtOAc was concentrated *in vacuo* to yield 12 g of dried material in total.

Isolation of ullengacenes A and B (40 and 41). The organic extract of SUD119 was filtered with a syringe filter and injected directly onto a semi-preparative reversed-phase HPLC column (Kromasil C_{18} (2): 250 × 10 mm, 5 μm) with a gradient solvent system (20% MeOH/H_2O to 80% MeOH/H_2O over 40 min, UV 280 nm detection, flow rate: 2 mL/min). Two major peaks at retention times of 41.6 min, 43.5 min were observed. Each compound was further purified under gradient solvent conditions (35% CH_3CN/H_2O to 60% CH_3CN over 40 min, UV 280 nm detection, flow rate: 2 mL/min) using a reversed-phase C_{18} HPLC column (Kromasil C_{18} (2): 250 × 10 mm, 5 μm). Ullengacenes A and B (**40** and **41**) were obtained in pure form at retention times of 37.2 (6.5 mg), and 24.6 min (3.3 mg), respectively.

Ullengacene A (**40**): Yellow gum; $[\alpha]^{25}_{D}$ -6.9 (*c* 0.5, MeOH); UV (MeOH) λ_{max} (log ε) 270 (4.12) nm; ECD (*c* 4.3 × 10^{-4} M, MeOH) λ_{max} ($\Delta\varepsilon$) 285 (-3.92), 321 (+0.2) nm, 350 (-1.8); IR (neat) ν_{max} 3282, 2978, 1656, 1592, 1555 cm^{-1}; ^{1}H and ^{13}C NMR data, Table 13; HRFABMS *m/z* 761.2394 [M + Na]$^{+}$ (calcd for $C_{42}H_{42}O_{10}SNa$, 761.2396).

Ullengacene B (**41**): Yellow gum; $[\alpha]^{25}_{D}$ +5.4 (*c* 0.5, MeOH); UV (MeOH) λ_{max} (log ε) 270 (4.21) nm; ECD (*c* 4.2 × 10^{-4} M, MeOH) λ_{max} ($\Delta\varepsilon$) 285 (-

4.6) nm, 310 (+3.8) nm, 375 (+0.6) nm; IR (neat) ν_{max} 3369, 2982, 1687, 1588, 1546 cm^{-1}; ^{1}H and ^{13}C NMR data, Table 13; HRFABMS *m*/*z* 723.2275 $[M + H]^+$ (calcd for $C_{41}H_{39}O_{10}S$, 723.2264).

MTPA Esterification of ullengacene A. Ullengacene A (**40**) were prepared individually in 40-mL vials (two 1-mg samples for each compound) and dried completely under high vacuum overnight. After adding catalytic amounts of crystalline dimethylaminopyridine (DMAP) to each reaction vial, freshly distilled anhydrous pyridine (1 mL) was added under argon gas. The reaction mixtures were stirred at room temperature for 5 min. After 5 min, *R*- and *S*-α-methoxy trifluoromethyl-phenylacetic acid (MTPA) chloride (20 μL) were added, respectively. The reactions were carried out for 3 h at room temperature with stirring. The reactions were quenched by adding 50 μL of MeOH. The reaction products were purified by HPLC using gradient elution conditions of 40% to 100% aqueous acetonitrile over 20 min with a reversed-phase C_{18} column (Kromasil C_{18} (2): 250 × 10 mm, 5 μm; flow rate: 2 mL/min; UV detection at 280 nm). The di-*S*- and -*R*-MTPA esters (**42** and **43**) of **40** eluted at 32.6 and 33.4 min, respectively. The $\Delta\delta_{S-R}$ values around the stereogenic centers of the MTPA esters were assigned based on the analysis of ^{1}H and ^{1}H-^{1}H COSY NMR spectra.

Di-*S*-MTPA Ester (**42**) of ullengacene A (**40**)

^{1}H NMR (600 MHz, pyridine-d_5) δ 7.87 (s, 2H), 7.78 (t, J = 7.5, 2H), 7.57–7.44 (m, 4H), 7.42-7.35 (m, 4H), 7.33-7.26 (m, 4H), 7.17-7.07 (m, 2H), 6.28 (s, 2H), 6.22 (s, 2H), 5.91 (m, 2H), 5.85 (m, 2H), 3.84 (s, 6H), 3.22 (s, 6H), 3.09 (s, 6H), 2.75 (m, 2H), 2.58-2.53 (m, 4H), 1.24 (d, J = 6.5, 6H). The molecular formula of **42** was confirmed as $C_{62}H_{56}F_6O_{14}Na$ ($[M+Na]^+$ at m/z 1193).

Di-*R*-MTPA Ester (**43**) of ullengacene A (**40**)

^{1}H NMR (600 MHz, pyridine-d_5) δ 8.00 (s, 2H), 7.78 (t, J = 7.5, 2H), 7.50–7.42 (m, 4H), 7.34-7.30 (m, 4H), 7.26-7.21 (m, 4H), 7.13-7.06 (m, 2H), 6.28 (s, 2H), 6.26 (s, 2H), 5.94 (m, 2H), 5.92 (m, 2H), 3.89 (s, 6H), 3.25 (s, 6H), 3.13 (s, 6H), 2.83 (m, 2H), 2.71-2.63 (m, 4H), 1.23 (d, J = 6.5, 6H). The molecular formula of **43** was confirmed as $C_{62}H_{56}F_6O_{14}Na$ ($[M+Na]^+$ at m/z 1193).

Computational analysis. The ground-state geometries were optimized with density functional theory (DFT) calculations, using Turbomole 6.5 at the basis set def-SV(P) for all atoms and functional B3LYP/DFT level, the ground states were further confirmed by the harmonic frequency calculation. The calculated ECD data corresponding to the optimized structures were obtained with TDDFT at the functional B3LYP/DFT level at the basis set def2-TZVPP for all atoms. The CD spectra were simulated by overlapping for each transition, where σ is the width of the band at 1/e height. ΔE_i and R_i

are the excitation energies and rotatory strengths for transition *i*, respectively. In the current work a value of σ was 0.10 eV.

DP4 analysis. For the DP4 application, conformers of diastereomers of four models within 10 kJ/mol found in the MMFF force field were regarded and the geometry of the conformers was optimized at the B3LYP/6-31G++ level in the gas phase. The shielding tensor values of the optimized conformers were computed at the B3LYP/6-31++ level. These values were averaged based on the Boltzmann population in the associated Gibbs free energy and utilized for DP4 analysis facilitated by an Excel sheet provided by the original authors.

***In vitro* capillary tube formation assay.** Matrigel (70 μl/well) was coated on 96-well plate and polymerized for 30 min at 37 ℃. HUVECs (1.5 × 10^4 cells/well) and WS9326A-E, WS9326F-I (**7-10**) (0-20μM) were seeded onto each well of the Matrigel-coated 96-well plate with EBM-2 medium . Then, cells were incubated for 8hrs. The formation of endothelial cell tubular structure was visualized under an inverted microscope and photographed. Furthermore, tube formation was quantified by calculating the tube number and was expressed as a percentage by normalization with untreated control cells.

Quinone reductase (QR) assay. QR activities were determined spectrophotometrically according to a modified microtiter method.[42] Hepa-1c1c7 cells were plated at a density of 20,000 cells/mL and cultured for 24 h in a humidified incubator containing 5% CO_2 at 37 °C. The cells were then

exposed to mohangic acids (**20**–**24**) and incubated for an additional 24 h. The media was subsequently decanted, and the cells in each well were lysed by incubation at 37 °C for 10 min with 250 μL of a solution containing 10 mM Tris-HCl pH 8.0, 140 mM NaCl, 15 mM $MgCl_2$, and 0.5 % NP-40 (IGEPAL CA-630) (Sigma-Aldrich). The plates were then agitated on an orbital shaker for additional 10 min at 25 °C, after which 1 mL of the complete reaction mixture containing 12.5 mM Tris-HCl pH 7.4, 0.67 mg/mL bovine serum albumin (BSA), 0.01% Tween-20, 50 μM flavin adenine dinucleotide (FAD), 1 mM glucose-6-phosphate, 2 U/mL glucose-6-phosphate dehydrogenase, 30 μM NADP, 50 μg/mL 3-(4,5-dimethylthiazo-2-yl)-2,5-diphenyltetrazolium bromide (MTT), and 50 μM menadione were added. A blue color developed, and the reaction was stopped after 10 min. The rate of the NADPH-dependent, menadiol-mediated reduction of MTT was measured at 610 nm. Protein was detected by crystal violet staining of an identical set of test plates. The specific activity (SA) of quinone reductase (nmol/min/mg of protein) was calculated from the equation:

$$SA = [MTTabs/CVabs] \times 3{,}345,$$

where MTTabs is the change in the absorbance of MTT per min, CVabs is the absorbance of crystal violet, and 3,345 is the ratio of the proportionality constant determined for crystal violet and the extinction coefficient of MTT and has units of nmol/mg.

Summary

In this thesis for the degree of doctor of philosophy, I described two parts of studies. In part A, I focused on new bioactive non-ribosomal peptides from marine *Streptomyces* spp., including three kinds of novel peptides. Mohangamides A and B were discovered from a marine Streptomyces sp. collected in an intertidal mud flat. The structures of the compounds were elucidated as novel dilactone-tethered pseudo-dimeric peptides bearing two unusual acyl chains and 14 amino acid residues based on comprehensive spectroscopic analysis. The absolute configurations of the mohangamides were determined by multiple step chemical derivatizations (Figure 1). In particular, for the stereochemistry of the dihydropyridine-bearing acyl chain, the double bond in the dihydropyridine ring was oxidized to yield diol functionality by using OsO_4. The introduced diol in the ring was further derivatized with 4-(dimethylamino) benzoyl chloride (DMAB-Cl), which induced exciton coupling in circular dichroism enabling to establish the absolute stereochemistry of the ring. Mohangamide A displayed strong inhibitory activity against *Candida albicans* isocitrate lyase.

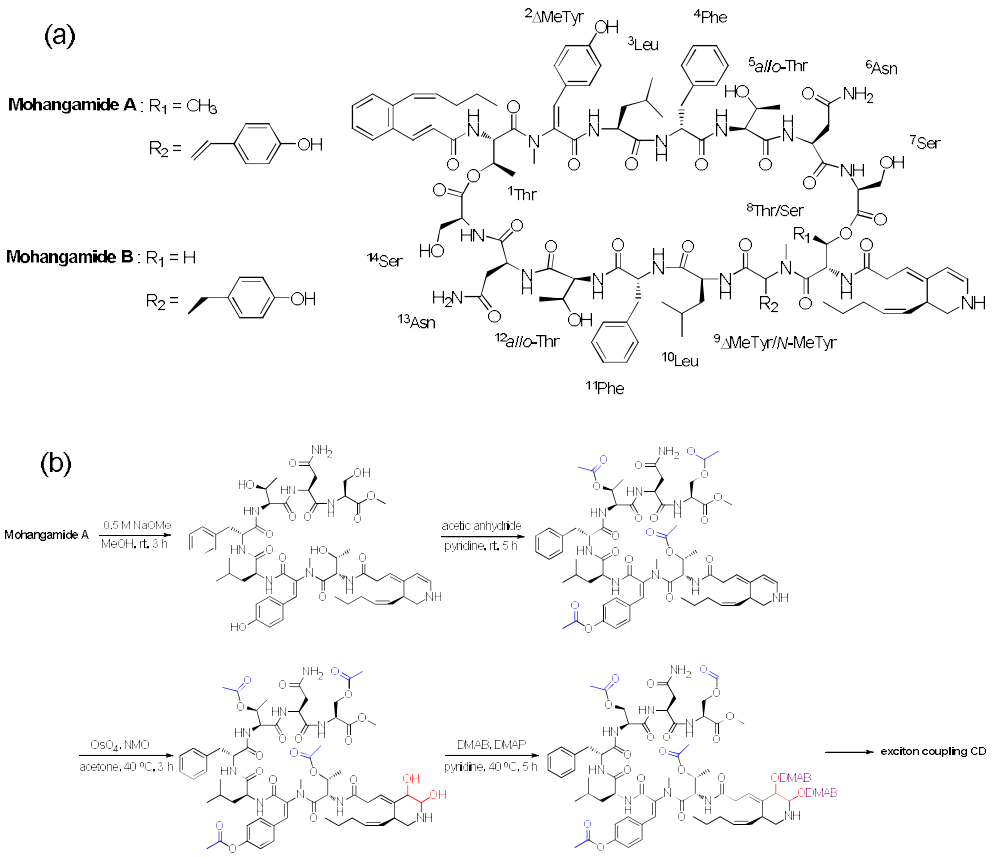

Figure 1. (a) The structures of mohangamides A and B. (b) Four-step derivatization scheme to determine the absolute configuration of dihydropyridine in mohangamide A by exciton coupling CD.

A continuous chemical study of the mohangamide producer (*Streptomyces* sp. SNM55) led to the discovery of four new peptides, WS9326F-I, belonging to the WS9326 class. The planar structures of WS9326s were established by 1D and 2D NMR, mass, UV, and IR analyses. These compounds bear 6~7 amino acid units with a unique acyl chain. Interestingly, WS9326I incorporates an unprecedented 4-amino-2,4-dihydro-3H-pyarzol-3-one and a sugar-derived moiety. The structure of the pyrazole-derived ring was further confirmed by comprehensive analysis of

the ^{15}NHSQC spectrum of WS9326I. In addition, the analysis of COSY and HMBC spectra after selective hydrogenation of the carbon-nitrogen double bond in the ring by using $NaBH_3CN$ clearly supported the structure of 4-amino-2,4-dihydro-3H-pyarzol-3-one. The absolute configurations of amino acids of WS9326F-I were established by advanced Marfey's analysis. The determination of the absolute configuration of extreamly modified starting unit in WS9326I was established by four-step of chemical derivatizations and DP4 calculations (Figure 4). WS9326F-I displayed significant antiangiogenic activity with moderate cytotoxicity against human cancer cells.

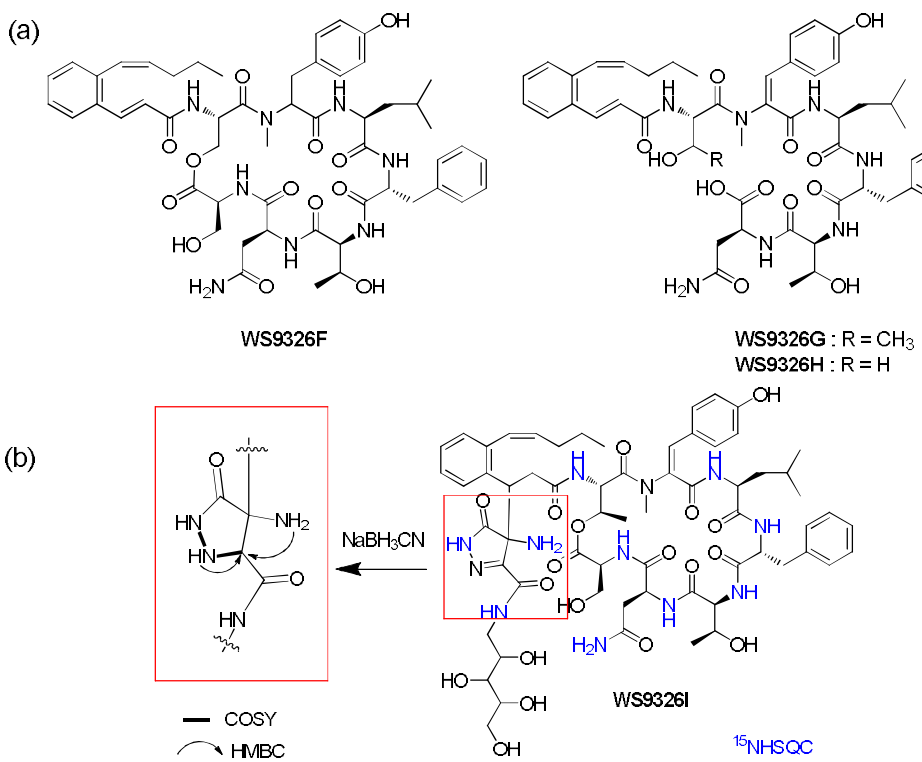

Figure 3. (a) The structures of WS9326F-H. (b) The structure of WS9326I and the elucidation of the 4-amino-2,4-dihydro-3H-pyarzol-3-one ring by ^{15}NHSQC and imine-selective reduction followed by COSY and HMBC

experiments.

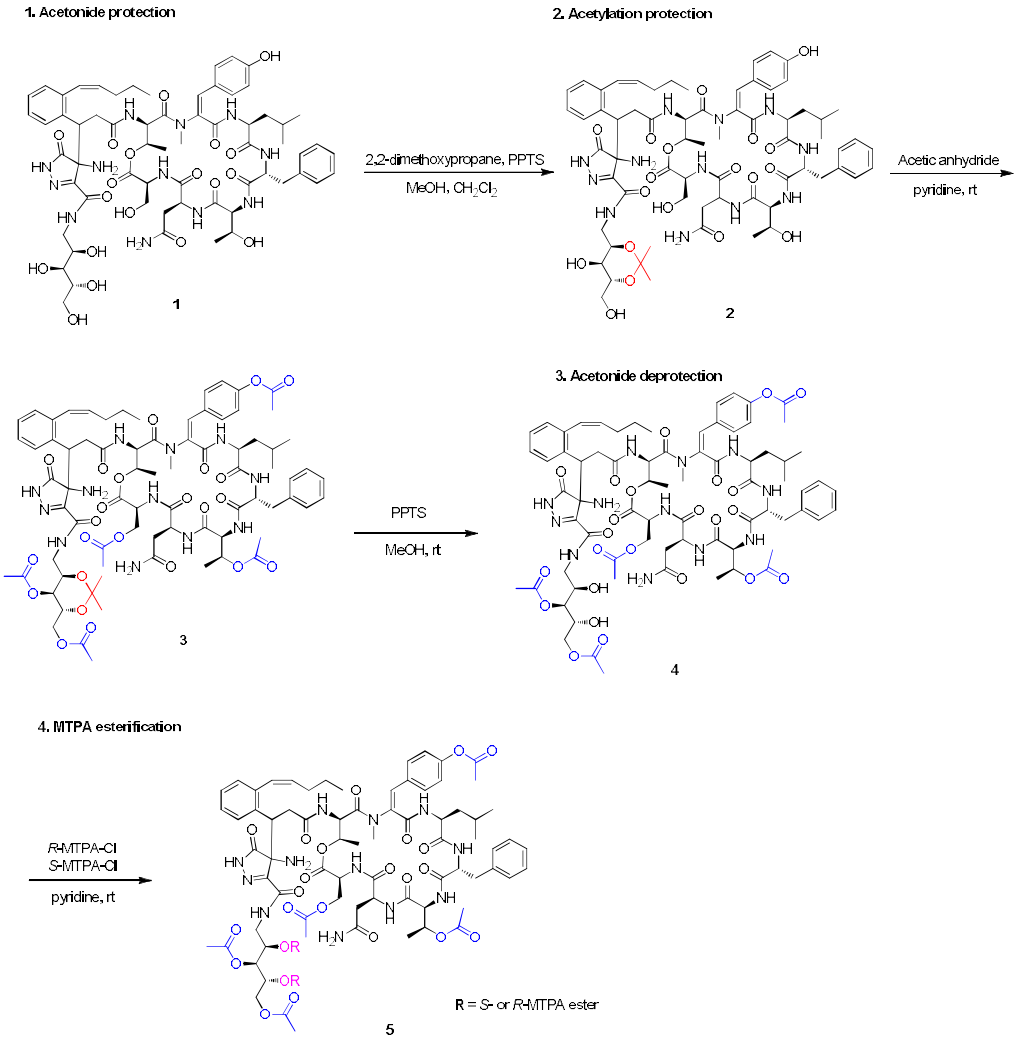

Figure 4. Four-step derivatization scheme to determine the absolute configuration of 4-amino-2,4-dihydro-3H-pyarzol-3-one with sugar moiety in WS9326I.

Alterations in microbial culture conditions may trigger the production of diverse bioactive secondary metabolites. While applying various culture conditions and monitoring secondary metabolite profiles using LC/MS, hormaomycins B and C were discovered from a marine mudflat-derived actinomycete, *Streptomyces* sp., collected in Mohang, Republic of Korea.

The planar structures of the hormaomycins, which bear structurally unique units, such as 4-(*Z*)-propenylproline, 3-(2-nitrocyclopropyl)alanine, 5-chloro-1-hydroxypyrrol-2-carboxylic acid, and β-methylphenylalanine, were established as the first natural analogues belonging to the hormaomycin peptide class (Figure 5). The absolute configurations of hormaomycins B and C were deduced by comparing their CD spectra with that of hormaomycin. These hormaomycins exhibited significant inhibitory effects against various pathogenic Gram-positive bacteria including *Staphylococcus aureus* ATCC 25923, *Bacillus subtilis* ATCC 6633, *Kocuria rhizophila* NBRC 12708, and *Streptococcus pyogenes* ATCC 19615. Further investigation revealed that these hormaomycins displayed remarkable activity against *Salmonella enterica* ATCC 14028 and *Proteus hauseri* NBRC 3851 belonging to Gram-negative bacteria.

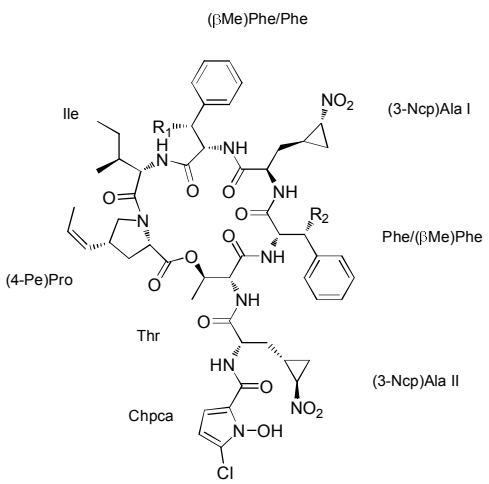

Hormaomycin B : $R_1 = CH_3$, $R_2 = H$
Hormaomycin C : $R_1 = H$, $R_2 = CH_3$

Figure 5. The structures of hormaomycins B and C.

In part B, I focused on new bioactive non-ribosomal peptides from marine *Streptomyces* spp. including three of novel polyketides. Mohangic acids A–E were isolated from a marine *Streptomyces* sp. collected from a mudflat in Buan, Republic of Korea. Comprehensive spectroscopic analysis revealed that the mohangic acids are new members of the p-aminoacetophenonic acid class (Figure 6). The relative and absolute configurations of the mohangic acids were determined by *J*–based configuration analysis and by the application of bidentate chiral NMR solvents, (*R*,*R*)- and (*S*,*S*)-bis-α-methylbenzylamine-*p*-Me (BAMA), followed by ^{13}C NMR analysis, chemical derivatization, and circular dichroism spectroscopy. Mohangic acid E, which is the first glycosylated compound in the p-aminoacetophenonic acid family, displayed significant quinone reductase induction activity.

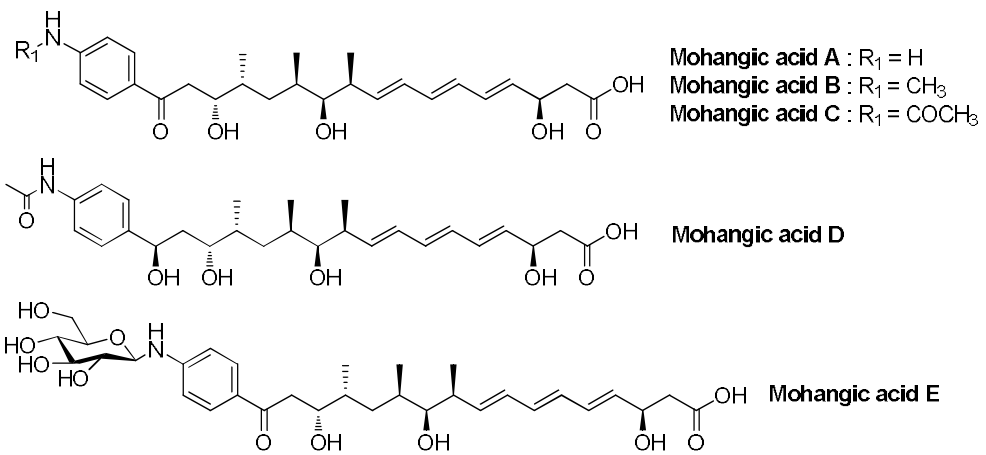

Figure 6. The structures of mohangic acids A-E.

Based on profiles of secondary metabolites produced by marine bacteria obtained using LC/MS, succinilenes A-D, new triene polyols, were discovered from a culture of a *Streptomyces* strain SAK1, which was

collected in the southern area of Jeju Island, Republic of Korea. The gross structures of succinilenes were primarily determined through analysis of NMR spectra. The double bond geometries of the succinilenes, which could not be established from conventional ^{1}H NMR spectra because of the highly overlapped olefinic signals, were successfully deciphered using the recently developed quantum-mechanics-driven ^{1}H iterative full spin analysis (Figure 7). Succinilenes A-C displayed inhibitory effects against lipopolysaccharide (LPS)-induced nitric oxide (NO) production, indicating their significance as anti-inflammatory agents. The absolute configurations of succinilenes A-D were established through *J*-based configuration analysis, the modified Mosher's method following methanolysis, and CD spectral analysis.

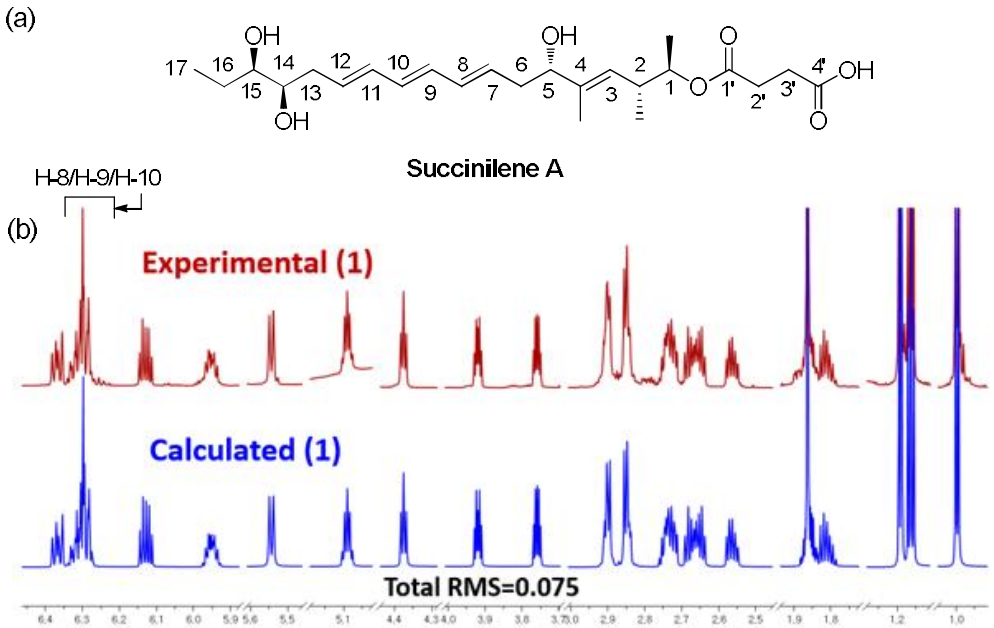

Figure 7. (a) The structure of succinilene A. (b) ^{1}H NMR fingerprints of succinilene A generated by HiFSA. Comparison of the observed (red, obtained in pyridine-d_5) and calculated (blue) ^{1}H spectra.

The chemical analysis of *Streptomyces* strain SUD119, which was isolated from a sediment sample collected in Ul-leung Island, a Korean volcanic island, resulted in the discovery of new benz[*a*]anthracene dimers linked by a sulfide bond. The planar structure of uleungacenes A and B were clarified based on NMR, MS, UV, and EDX (energy dispersive X-ray) spectroscopic data (Figure 8). The stereochemistry of uleungacenes A and B were determined by the analysis of MTPA derivati-zations, DP4 calculation, and ROESY correlations with ECD calculations based on density functional theory. Uleungacenes A exhibited significant quinone reductase induction activity whereas uleungacenes B displayed remarkable anti-angiogenesis activity.

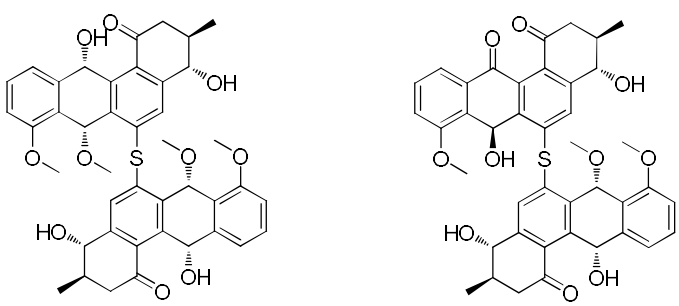

Figure 8. The structures of ulleungacenes A and B.

References

1. Bérdy, J. *J. Antibiot.* **2012**, *65*, 385-395.
2. Fenical, W.; Jensen, P. R. *Nat. Chem. Biol.* **2006**, *2*, 666-673.
3. Haefner, B. *Drug Discov. Today* **2003**, *8*, 536-544.
4. Feling, R. H.; Buchanan, G. O.; Mincer, T. J.; Kauffman, C. A.; Jensen, P. R.; Fenical, W. *Angew. Chem.-Int. Edit.* **2003**, *42*, 355-357.
5. Perez Baz, J.; Canedo, L. M.; Fernandez Puentes, J. L.; Silva Elipe, M. V. *J. Antibiot.* **1997**, *50*, 738-741.
6. Pittenger, R. C.; Brighani, R. B.; *Antibiotics and Chemotherapy*, **1956**, *6*, 642.
7. Petcher, T. J.; Weber, H. P.; Rűegger, A. *Helv. Chim. Acta* **1976**, *59*, 1480.
8. (a) Maggi, S. N.; Fűresz, S.; Maffii, G. *Antimicr. Agents and Chemoth.* **1966**, 699. (b) Prelog, V.; Oppolzer, W. *Helv. Chim. Acta* **1973**, *56*, 2279.
9. Wiley, P. F.; Gerzon, K.; Flynn, E. H.; Sigal Jr. M. V.; Weaver, O.; Quarch, U. C.; Chauvette, R. R.; Monahan, R. *J. Am. Chem. Soc.* **1957**, *79*, 6062.
10. Dehydrotyrosine was previously reported in cyclo(L-arginine) dehydrotyrosine from a marine sponge. See Sugumaran, M.; Robinson, W. E. *Mar. Drugs* **2010**, *8*, 2906-2935.
11. The same moiety was reported in pepticinnaminsa and its short version was discovered in skyllamycin.b See (a) Shiomi, K.; Yang, H.;

Inokoshi, J.; Van Der Pyl, D.; Nakagawa, A.; Takeshima, H.; Omura, S. *J. Antibiot*. **1993**, *46*, 229-234; (b) Schubert, V.; Di Meo, F.; Saaidi, P.; Bartoschek, S.; Fiedler, H.; Trouillas, P.; Süssmuth, R. D. *Chem. Eur. J*. **2014**, *20*, 4948-4955.

12. The 63*Z* geometry was deduced by the ROESY correlation between H-63 and H-64 in compound **5** because these protons were almost overlapped in **1**.

13. Fujii, K.; Ikai, Y.; Mayumi, T.; Oka, H.; Suzuki, M.; Harada, K. *Anal. Chem*. **1997**, *69*, 3346-3352.

14. (a) Hess, S.; Gustafson, K. R.; Milanowski, D. J.; Alvira, E.; Lipton, M. A.; Pannell, L. K. *J. Chromatogr. A* **2004**, *1035*, 211-219; (b) It was previously reported that L-*allo*-Thr is biosynthesized from glycine and acetaldehyde via L-*allo*-threonine aldolase. See Kataoka, M.; Wada, M.; Nishi, K.; Yamada, H.; Shimizu, S. *FEMS Microbiol. Lett*. **1997**, *151*, 245-248.

15. Matsumori, N.; Kaneno, D.; Murata, M.; Nakamura, H.; Tachibana, K. *J. Org. Chem.* **1999**, *64*, 866-876.

16. Wilson, M. C.; Nam, S.-J.; Gulder, T. A. M.; Kauffman, C. A.; Jensen, P. R.; Fenical, W.; Moore, B. S. *J. Am. Chem. Soc*. **2011**, *133*, 1971-1977..

17. Harada, N.; Nakanishi, K. *Circular Dichroic Spectroscopy – Exciton Coupling in Organic Stereochemistry*; University Science Books: Mill Valley, 1983; pp. 32-54.

18. Dawson, S.; Malkinson, J. P.; Paumier, D.; Searcey, M. *Nat. Prod. Rep*. **2007**, *24*, 109-126.

19. Sato, M.; Nakazawa, T.; Tsunematsu, Y.; Hotta, K.; Watanabe, K. *Curr. Opin. Chem. Biol*. **2013**, *17*, 537-545.

20. Lemay, M.; Ogilvie, W. W. *Org*. *Lett*. **2005**, *7*, 4141-4144.

21. Rychnovsky, S. D.; Rogers, B. N.; Richardson, T. I. *Acc*. *Chem*. *Res*. **1998**, *31*, 9-17.

22. Smith, S. G.; Goodman, J. M. *J. AM. CHEM. SOC*. **2010**, *132*, 12946-12959.

23. Yu, Z.; Vodanovic-Jankovic, S.; Kron, M.; Shen, B. *Org*. *Lett*. **2012**, *14*, 4946-4949.

24. (a) Zhan, J.; Burns, A. M.; Liu, M. X.; Faeth, S. H.; Gunatilaka, A. A. L. *J. Nat*. *Prod*. **2007**, *70*, 227–232. (b) Fukai, M.; Suzuki, T.; Nagasawa, I.; Kinoshita, K.; Takahashi, K.; Koyama, K. *J. Nat*. *Prod*. **2014**, *77*, 1065-1068.

25. Carmeliet, P.; Jain, R. K. *Nature* **2000**, *407*, 249-257.

26. Hayashi, K.; Hashimoto, M.; Shegematsu, N.; Nishikawa, M.; Ezaki, M.; Yamashita, M.; Kiyoto, S.; Okuhara, M.; Kohsaka, M.; Imanaka, H. *J. Antibiot*. **1992**, *45*, 1055-1063.

27. Toki, S.; Agatsuma, T.; Ochiai, K.; Saitoh, Y.; Ando, K.; Nakanishi, S.; Lokker, N. A.; Giese, N. A.; Matsuda, Y. *J. Antibiot*. **2001**, *54*, 405-414.

28. Pretsch, E.; Bùhlmann, P.; Affolter, C. Springer: New York, NY, USA,

2000; p. 104.

29. Zlatopolskiy, B. D.; de Meijere, A. *Chem. Eur. J.* **2004**, *10*, 4718-4727.

30. Cai, X.; Teta, R.; Kohlhaas, C.; Cruesemann, M.; Ueoka, R.; Mangoni, A.; Freeman, M. F.; Piel, J. *Chem. Biol.* **2013**, *20*, 839-846.

31. Andres, N.; Wolf, H.; Zähner, H. *Naturforsch.* **1990**, *45*, 851-855.

32. Pretsch, E.; Bühlmann, P.; Badertscher, M. *Structure Determination of Organic Compounds*; Springer-Verlag: Berlin Heidelberg, 2009; p. 149.

33. Moon, K.; Ahn, C.-H.; Shin, Y.; Won, T. H.; Ko, K.; Lee, S. K.; Oh, K.-B.; Shin, J.; Nam, S.-I.; Oh, D.-C. *Mar. Drugs* **2014**, *12*, 2526-2538.

34. Kurz, M.; Schmieder, P.; Kessler, H. *Angew. Chem., Int. Ed.* **1991**, *103*, 1341−1342.

35. Ohtani, I.; Kusumi, T.; Kashman, Y.; Kakisawa, H. *J. Am. Chem. Soc.* **1991**, *113*, 4092-4096.

36. Kobayashi, Y.; Hayashi, N.; Kishi, Y. *Org. Lett.* **2002**, *4*, 411-414.

37. Hong, W. K.; Sporn, M. B. *Science* **1997**, *278*, 1073-1077.

38. Cuendet, M.; Oteham, C. P.; Moon, R. C.; Pezzuto, J. M. *J. Nat. Prod.* **2006**, *69,* 460-463.

39. Ross, D.; Kepa, J. K.; Winski, S. L.; Beall, H. D.; Anwar, A.; Siegel, D. *Chem. Biol. Interact.* **2000**, *129*, 77-97.

40. Wang, F.; Xu, M.; Li, Q.; Sattler, I.; Lin, W. *Molecules* **2010**, *15*, 2782-2790.

41. Guan, S.-H.; Sattler, I.; Lin, W.-H.; Guo, D.-A.; Grabley, S. *J. Nat. Prod.* **2005**, *68,* 1198-1200.

42. Szwarc, K.; Szczeblewski, P.; Sowiński, P.; Borowski, E.; Pawlak, J. *J. Antibiot.* **2015**, *68*, 504-510.

43. Westerbeek, A.; Leeuwen, J. G. E. V.; Szymański, W.; Feringa, B. L.; Janssen, D. B. *Tetrahedron Lett*. **2012**, *68*, 7645-7650.

44. Park, H. J.; Lee, Y. W.; Park, H. H.; Lee, Y. S.; Kwon, I. B.; Yu, J. H. *Eur. J. Cancer Prev*. **1998**, *7*, 465-471.

45. Napolitano, J. G.; Gödecke, T.; Rodriguez-Brasco, M. F.; Jaki, B. U.; Chen, S.-N.; Lankin, D. C.; Pauli, G. F. *J. Nat. Prod*. **2012**, *75*, 238−248.

46. Félix, F.; Seco, J. M.; Quiñoá, E.; Riguera. R. *J. Org. Chem*. **2005**, *70*, 3778-3790.

47. Pauli, G. F.; Chen, S.-N.; Lankin, D. C.; Bisson, J.; Case, R. J.; Chadwick, L. R.; Gödecke, T.; Inui, T.; Krunic, A.; Jaki, B. U.; McAlpine, J. B.; Mo, S.; Napolitano, J. G.; Orjala, J.; Lehtivarjo, J.; Korhonen, S.-P.; Niemitz, M. *J. Nat. Prod*. **2014**, *77*, 1473-1487.

48. Friebolin, H. *Basic one- and two- dimensional NMR spectroscopy*. 4th ed.; Wiley-VCH: 2011.

49. Fujihara, M.; Muroi, M.; Tanamoto, K.; Suzuki, T.; Azuma, H.; Ikeda, H. *Pharmacol. Ther*. **2003**, *100*, 171−194.

50. Rietschel, E. T.; Brade, H. *Sci. Am*. **1992**, *267*, 54−61.

51. Sweet, M. J.; Hume, D. A. *J. Leukoc. Biol*. **1996**, *60*, 8−26.

52. Napolitano, J. G.; Lankin, D. C.; Graf, T. N.; Friesen, J. B.; Chen, S.-N.; McAlpine, J. B.; Oberlies, N. H.; Pauli, G. F. *J. Org. Chem.* **2013**, *78*, 2827-2839.

53. Napolitano, J. G.; Lankin, D. C.; McAlpine, J. B.; Niemitz, M.; Korhonen, S.-P.; Chen, S.-N.; Pauli, G. F. *J. Org. Chem.* **2013**, *78*, 9963-9968.

54. Nam, J.-W.; Phansalkar, R. S.; Lankin, D. C.; Bisson, J.; McAlpine, J. B.; Leme, A. A.; Vidal, C. M. P.; Ramirez, B.; Niemitz, M.; Bedran-Russo, A.; Chen, S.-N.; Pauli, G. F. *J. Org. Chem.* **2015**, *80*, 7495-7507.

55. Xue, C.; Tian, L.; Xu, M.; Deng, Z.; Lin, W. A. *J. Antibiot.* **2008**, *61*, 668-674.

56. Osada, H.; Koshino, H.; Isono, K.; Takahashi, H.; Kawanishi, G. Reveromycin A. *J. Antibiot.* **1991**, *44*, 259-261.

57. Michel, K. H.; Demarco, P. V.; Nagarajan, R. *J. Antibiot.* **1977**, *30*, 571-575.

APPENDIX A:

NMR Spectroscopic Data

List of Figures

Figure A1. ^{1}H and ^{13}C NMR spectra of compound **1** 138

Figure A2. ^{1}H and ^{13}C NMR spectra of compound **2** 139

Figure A3. ^{1}H and ^{13}C NMR spectra of compound **7** 140

Figure A4. ^{1}H and ^{13}C NMR spectra of compound **8** 141

Figure A5. ^{1}H and ^{13}C NMR spectra of compound **9** 142

Figure A6. ^{1}H and ^{13}C NMR spectra of compound **10** 143

Figure A7. ^{1}H and ^{13}C NMR spectra of compound **18** 144

Figure A8. ^{1}H and ^{13}C NMR spectra of compound **19** 145

Figure A9. ^{1}H and ^{13}C NMR spectra of compound **20** 146

Figure A10. ^{1}H and ^{13}C NMR spectra of compound **21** 147

Figure A11. ^{1}H and ^{13}C NMR spectra of compound **22**..... 148

Figure A12. ^{1}H and ^{13}C NMR spectra of compound **23** 149

Figure A13. ^{1}H and ^{13}C NMR spectra of compound **24** 150

Figure A14. ^{1}H and ^{13}C NMR spectra of compound **27** 151

Figure A15. ^{1}H and ^{13}C NMR spectra of compound **28** 152

Figure A16. ^{1}H and ^{13}C NMR spectra of compound **29** 153

Figure A17. ^{1}H and ^{13}C NMR spectra of compound **30** 154

Figure A18. ^{1}H and ^{13}C NMR spectra of compound **40** 155

Figure A19. ^{1}H and ^{13}C NMR spectra of compound **41** 156

Figure A1. ^{1}H and ^{13}C NMR spectra of compound **1**.

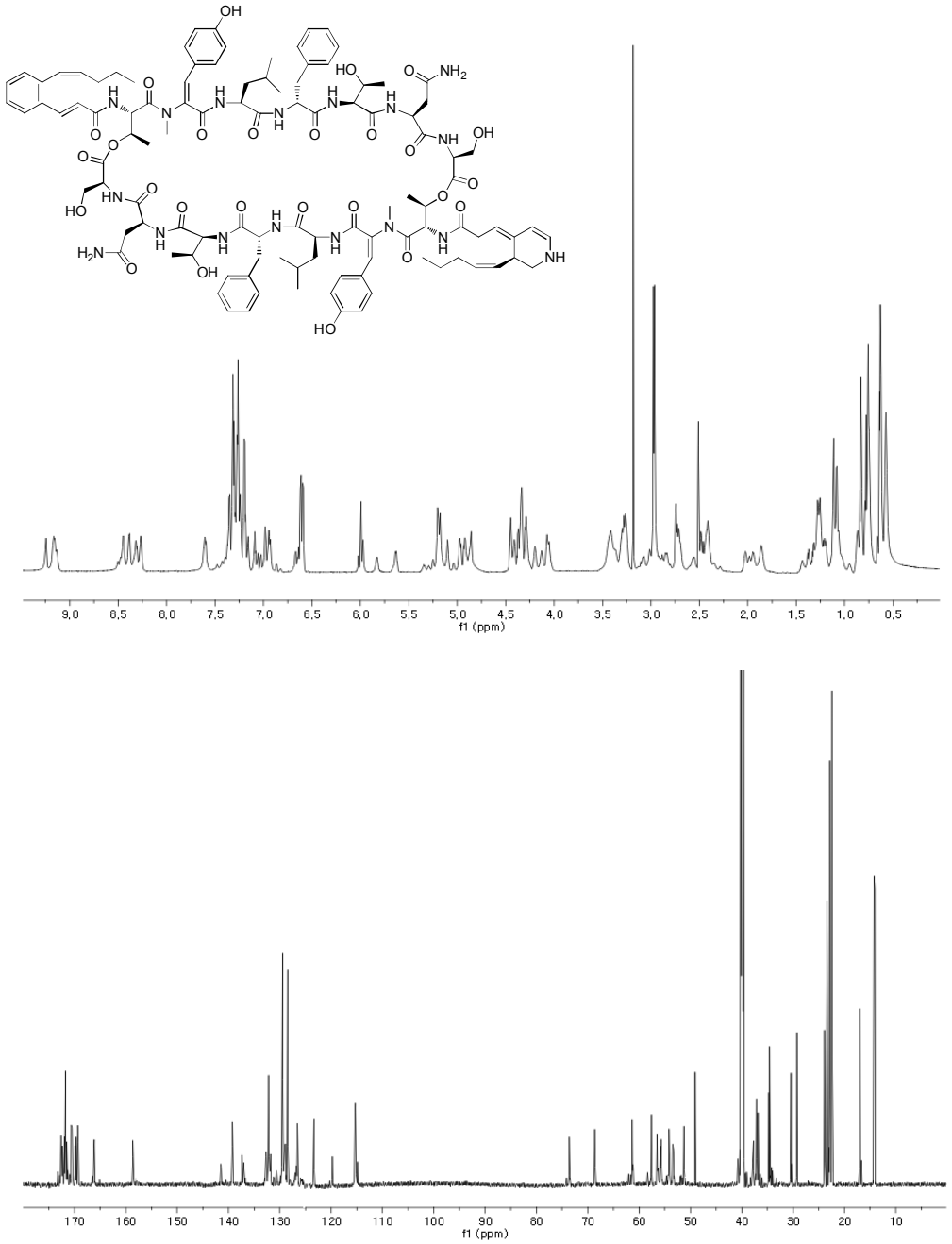

Figure A2. ^{1}H and ^{13}C NMR spectra of compound **2**.

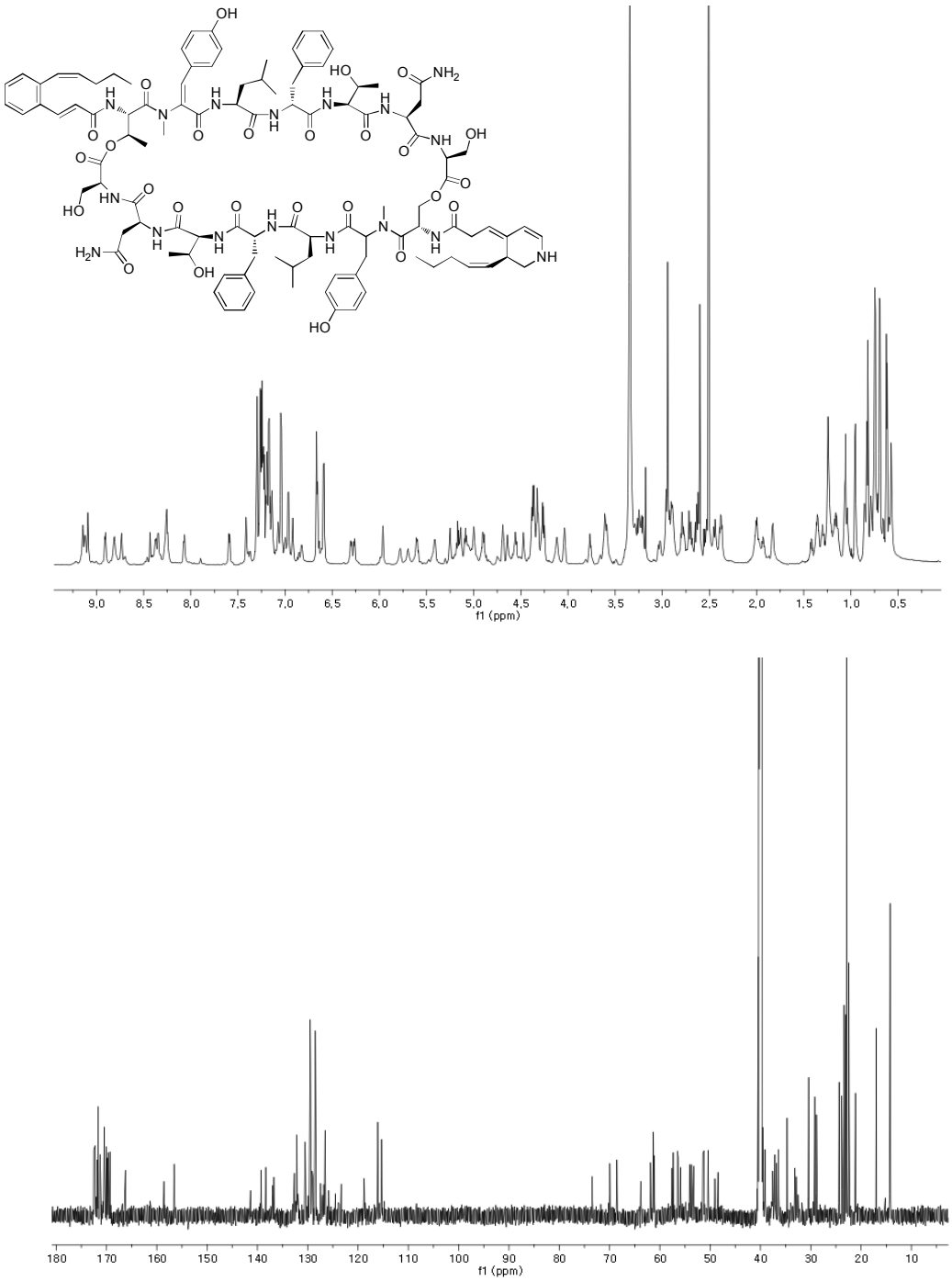

Figure A3. ^{1}H and ^{13}C NMR spectra of compound **7**.

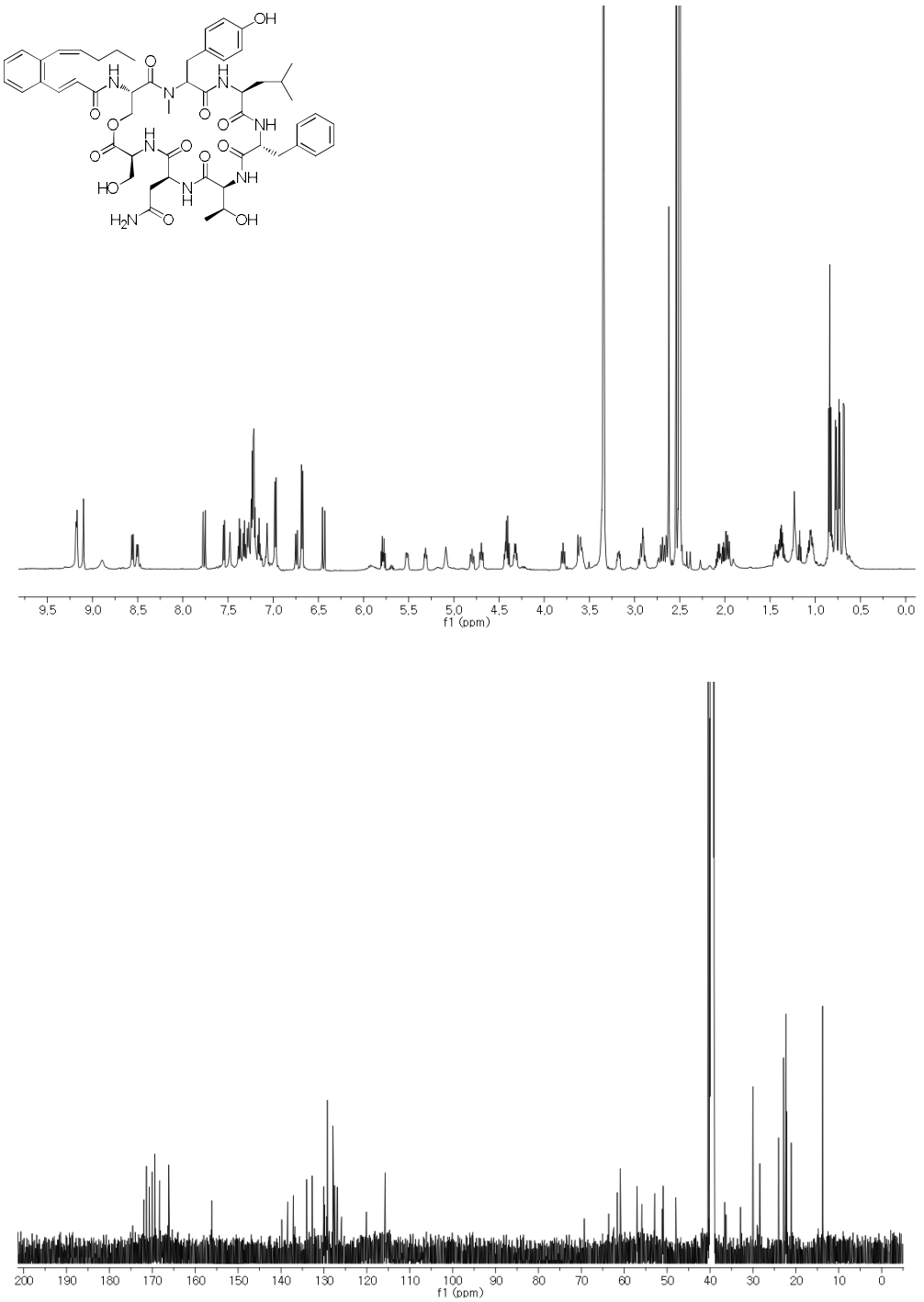

Figure A4. ^{1}H and ^{13}C NMR spectra of compound **8**.

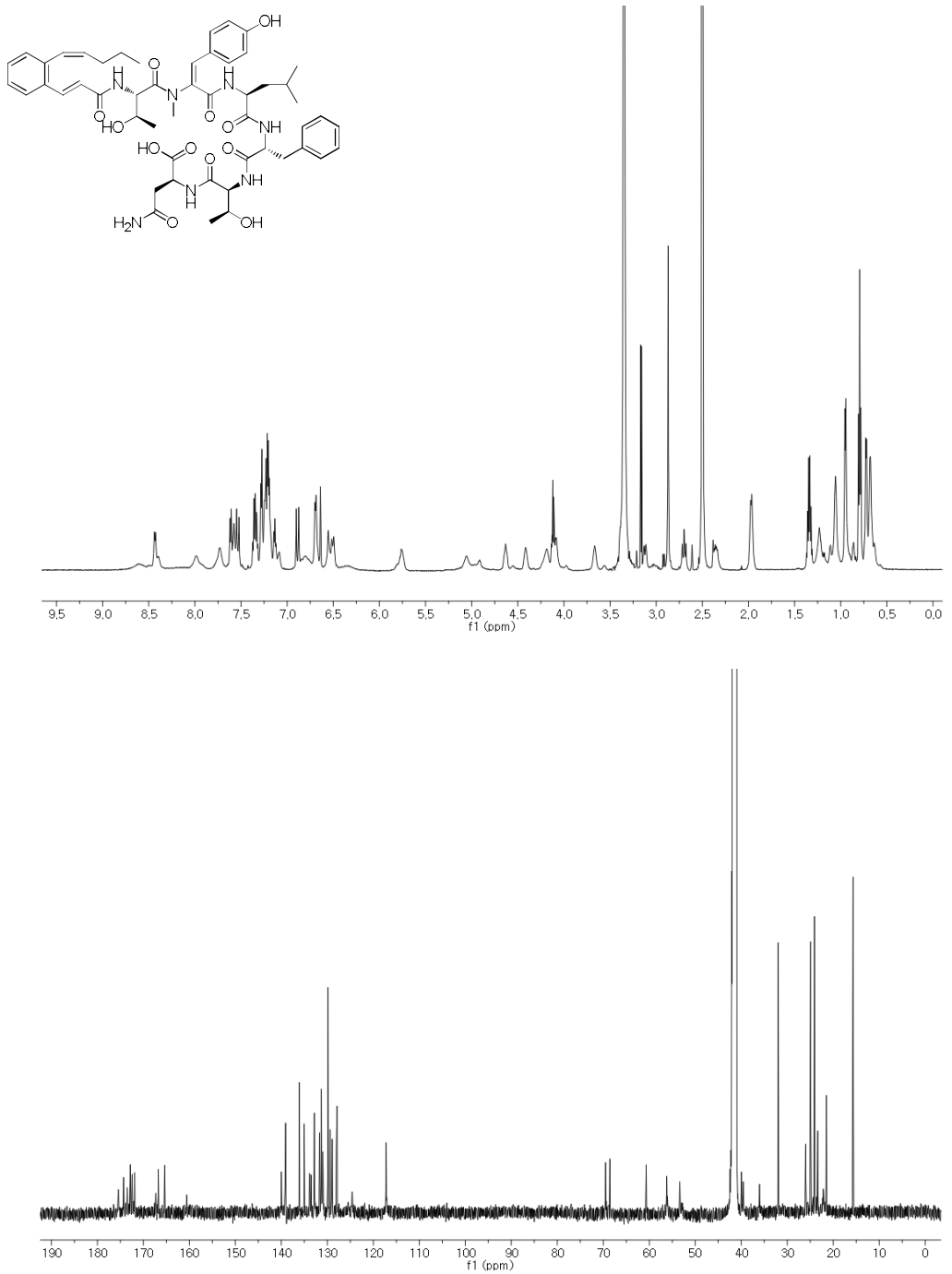

Figure A5. ^{1}H and ^{13}C NMR spectra of compound **9**.

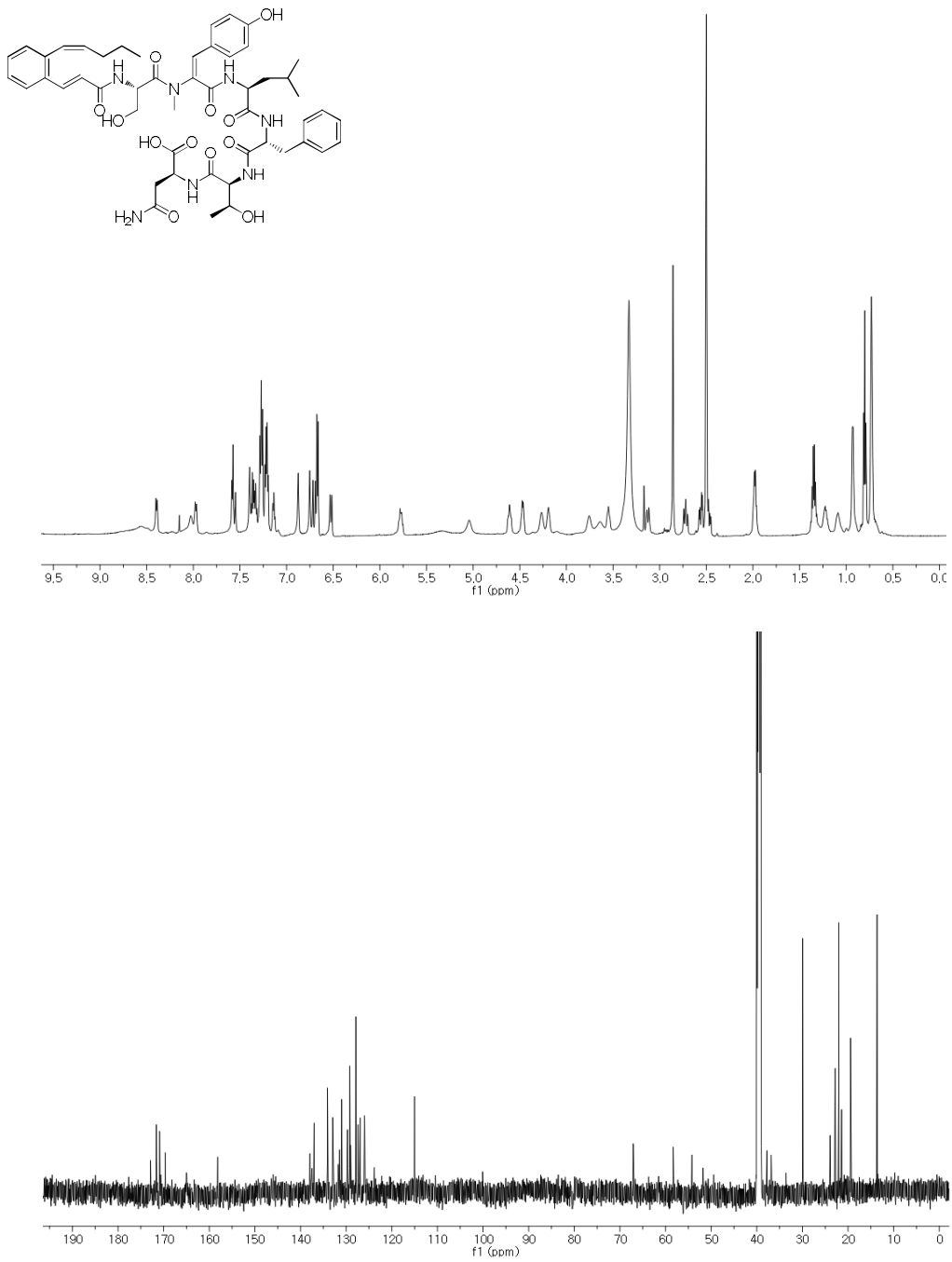

Figure A6. ^{1}H and ^{13}C NMR spectra of compound **10**.

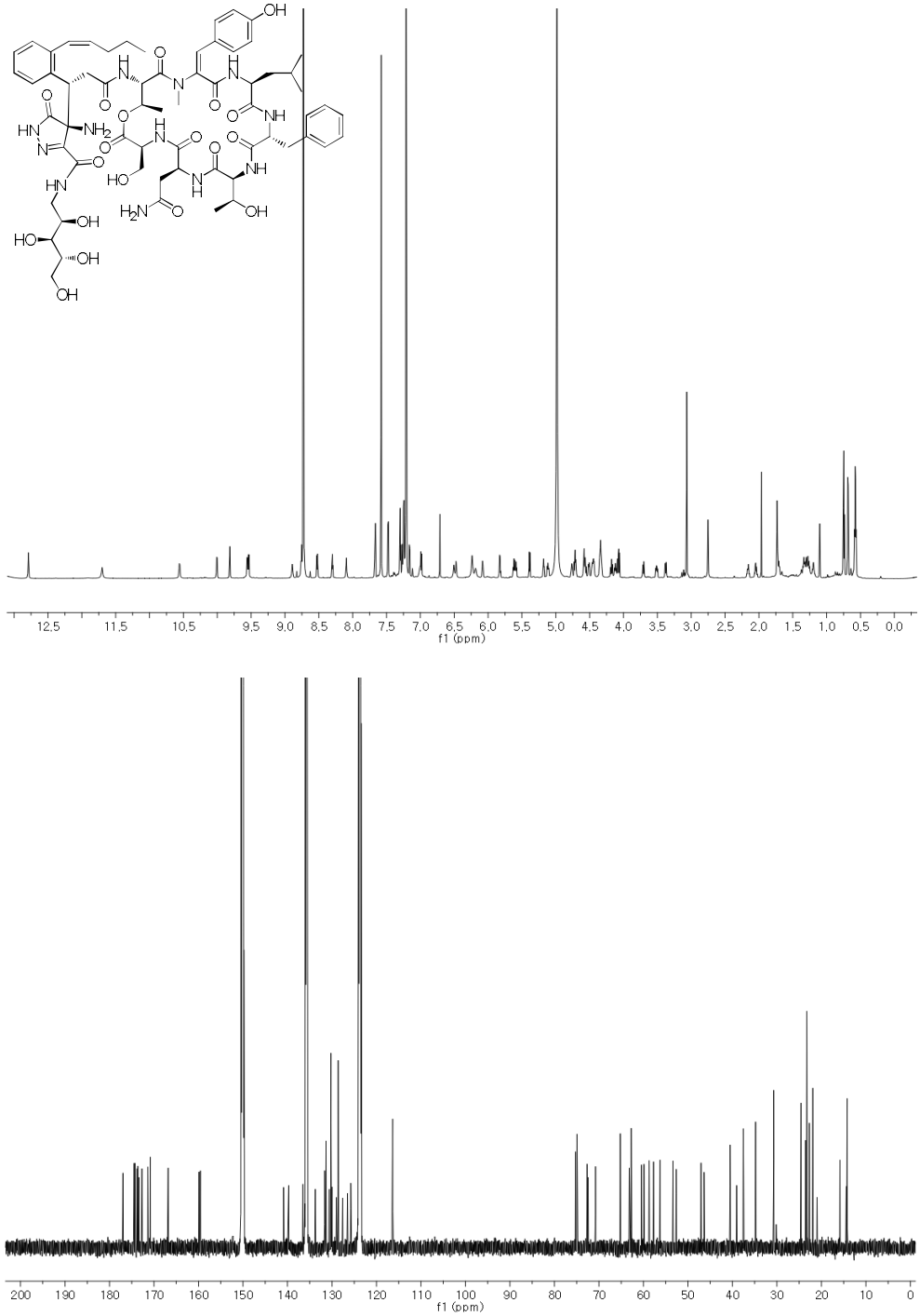

Figure A7. ^{1}H and ^{13}C NMR spectra of compound **18**.

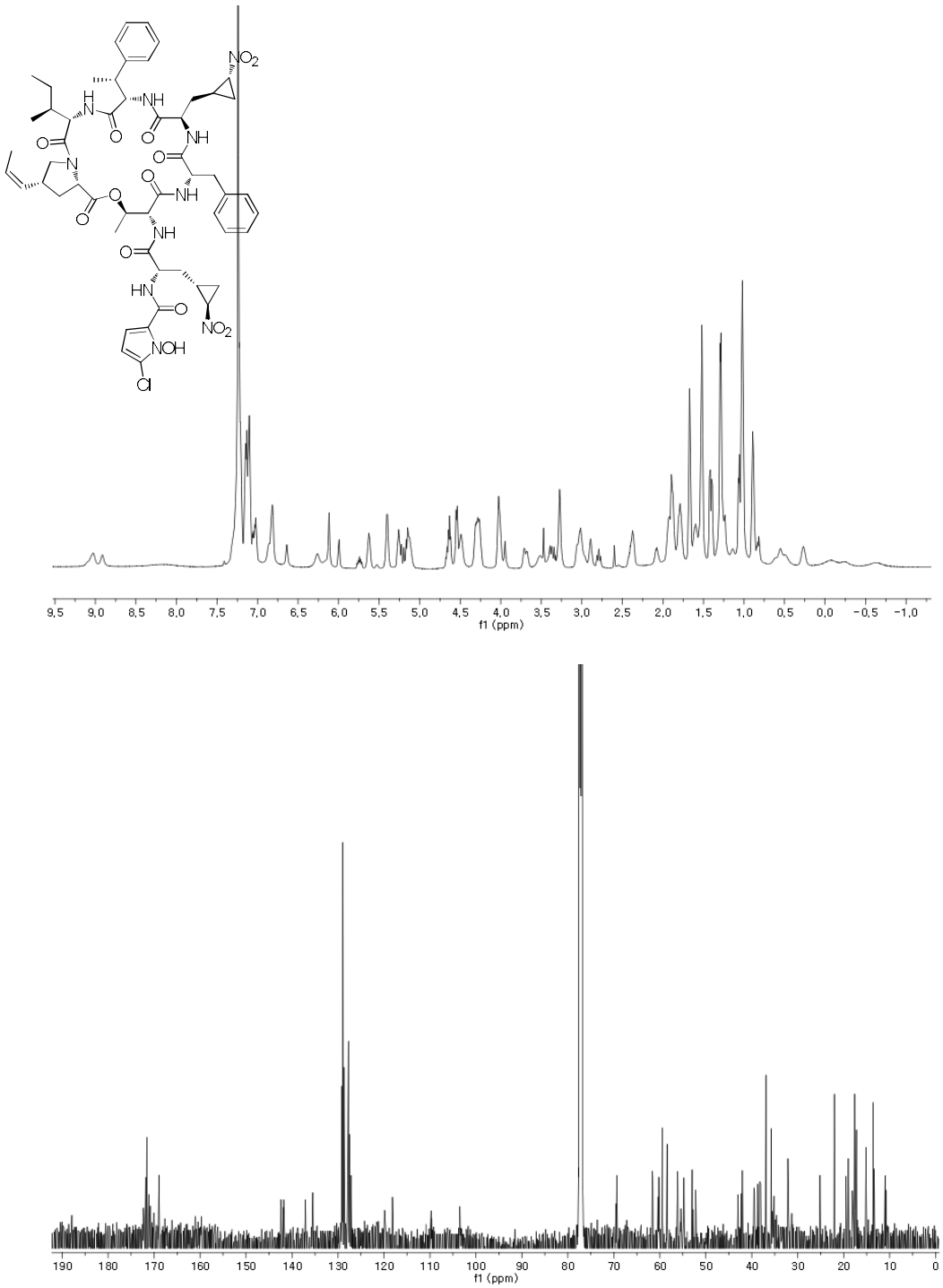

Figure A8. ^{1}H and ^{13}C NMR spectra of compound **19**.

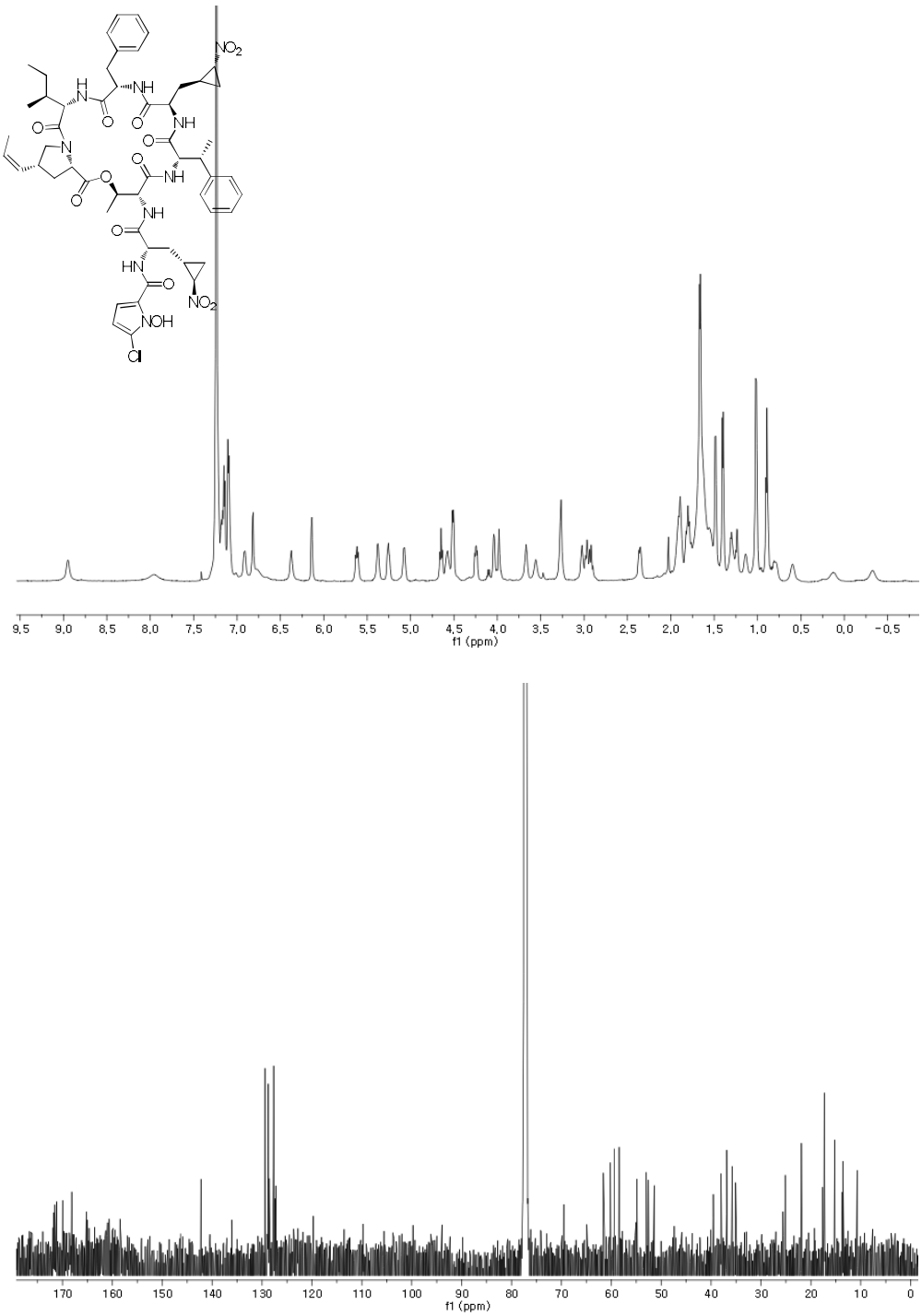

Figure A9. ^{1}H and ^{13}C NMR spectra of compound **20**.

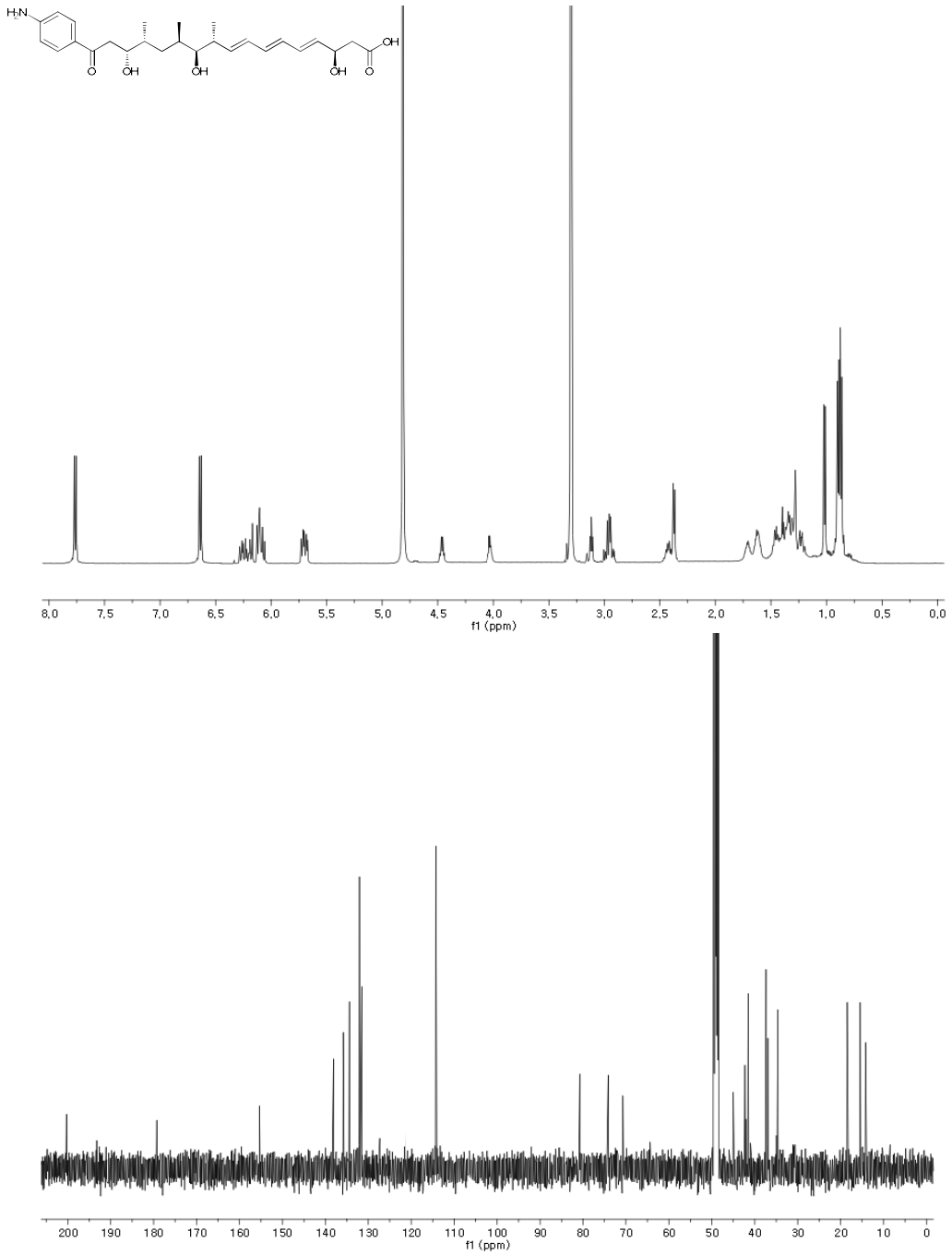

Figure A10. ^{1}H and ^{13}C NMR spectra of compound **21**.

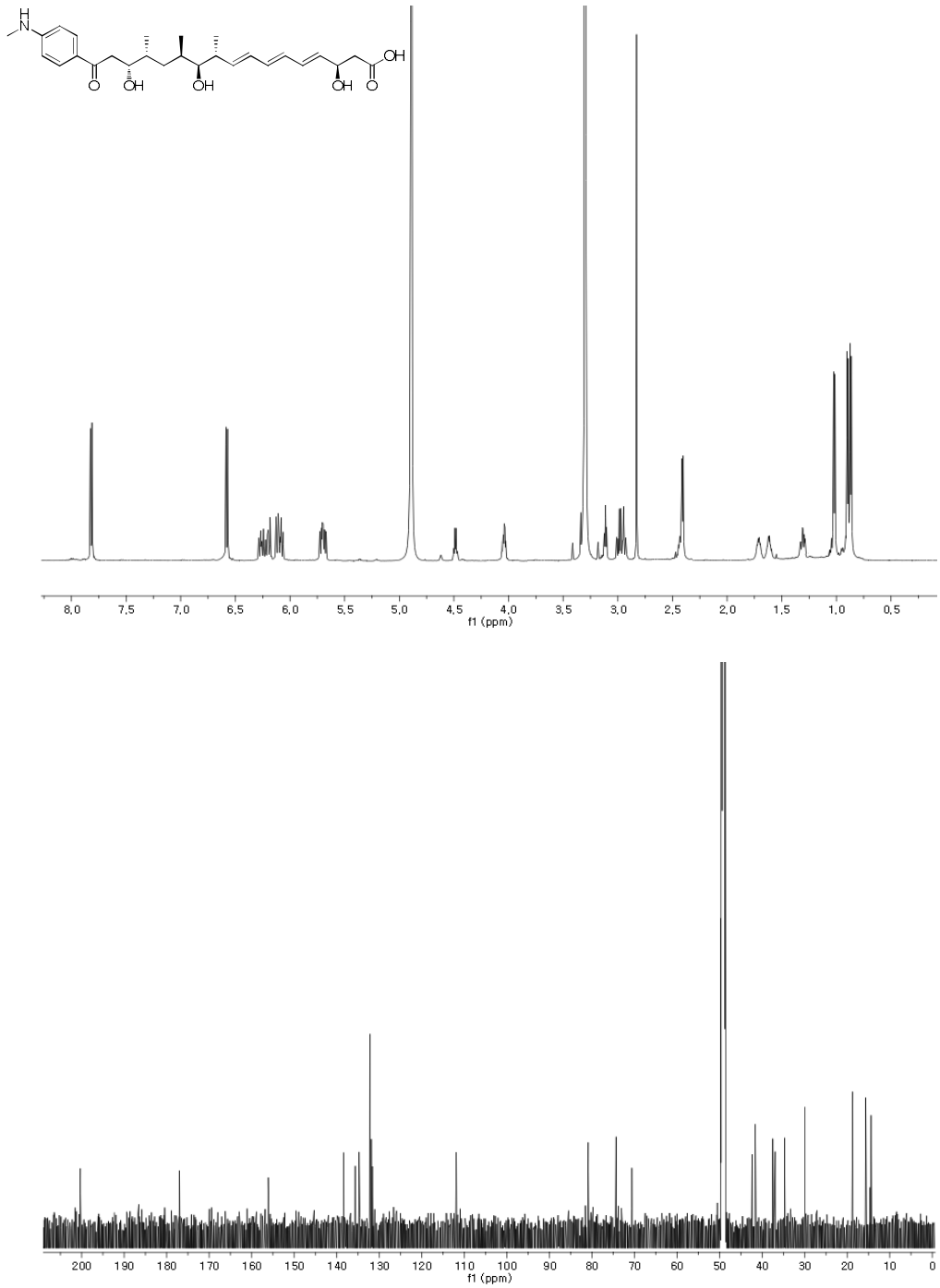

Figure A11. ^{1}H and ^{13}C NMR spectra of compound **22**.

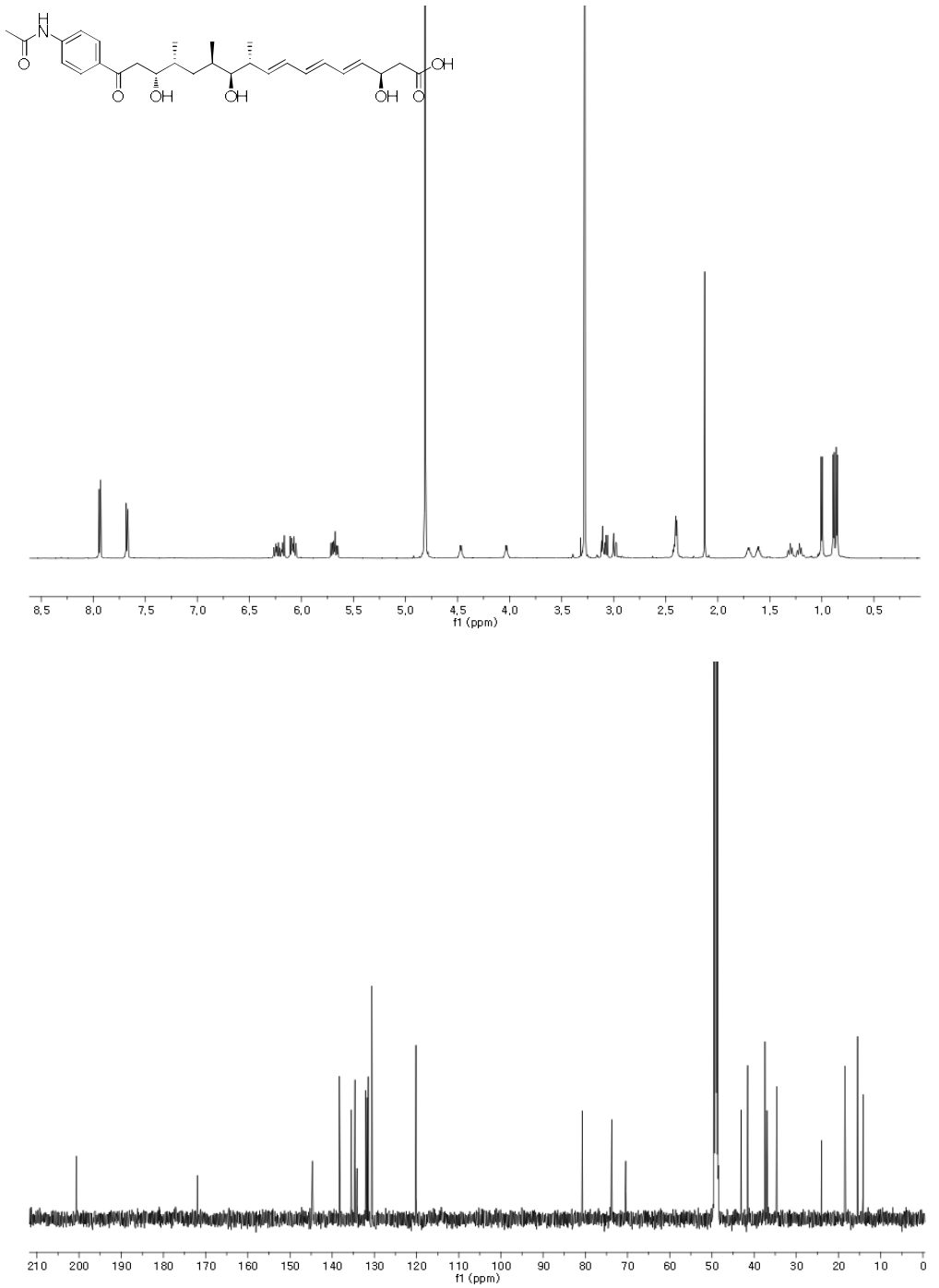

Figure A12. ^{1}H and ^{13}C NMR spectra of compound **23**.

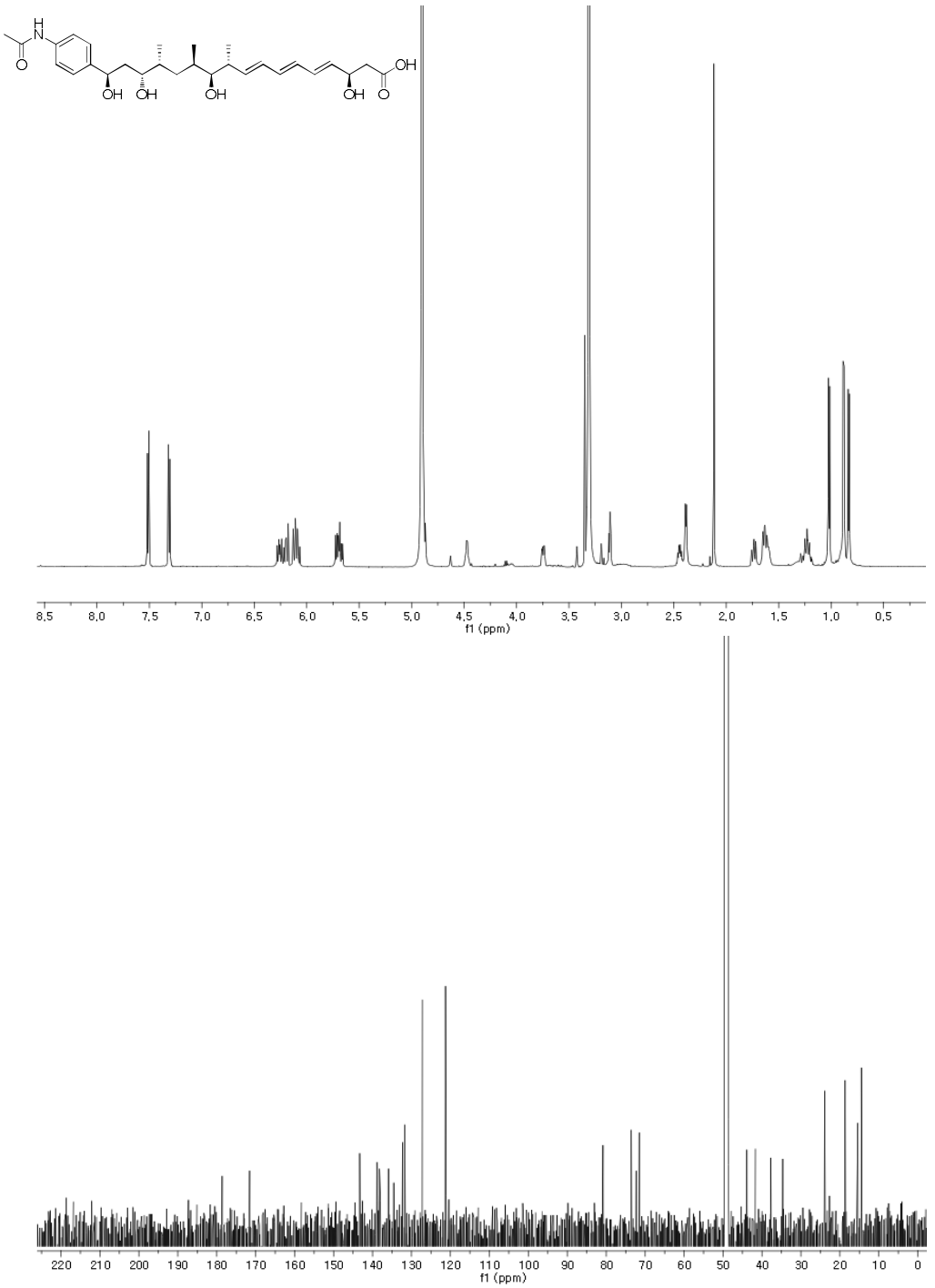

Figure A13. ^{1}H and ^{13}C NMR spectra of compound **24**.

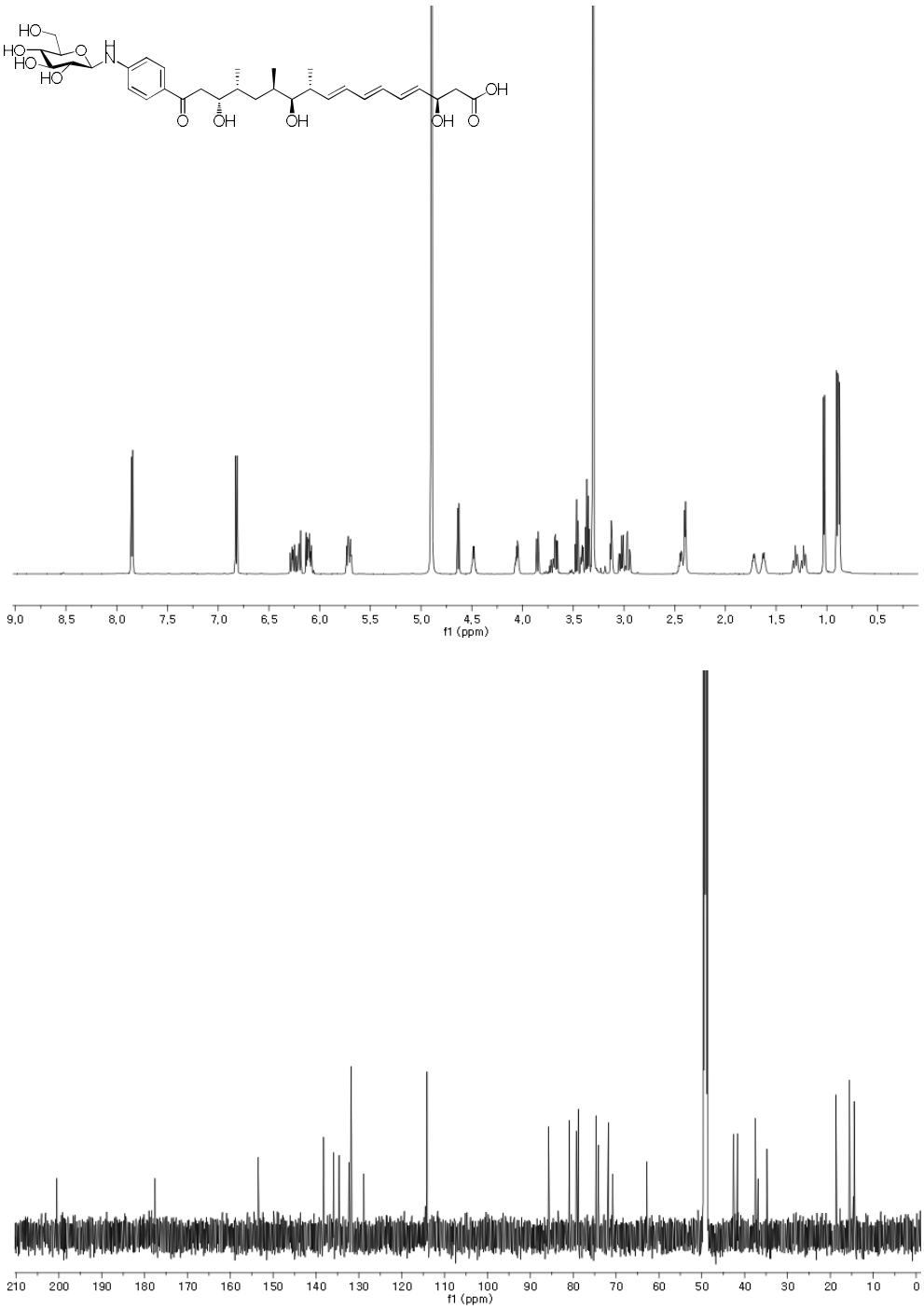

Figure A14. ^{1}H and ^{13}C NMR spectra of compound **27**.

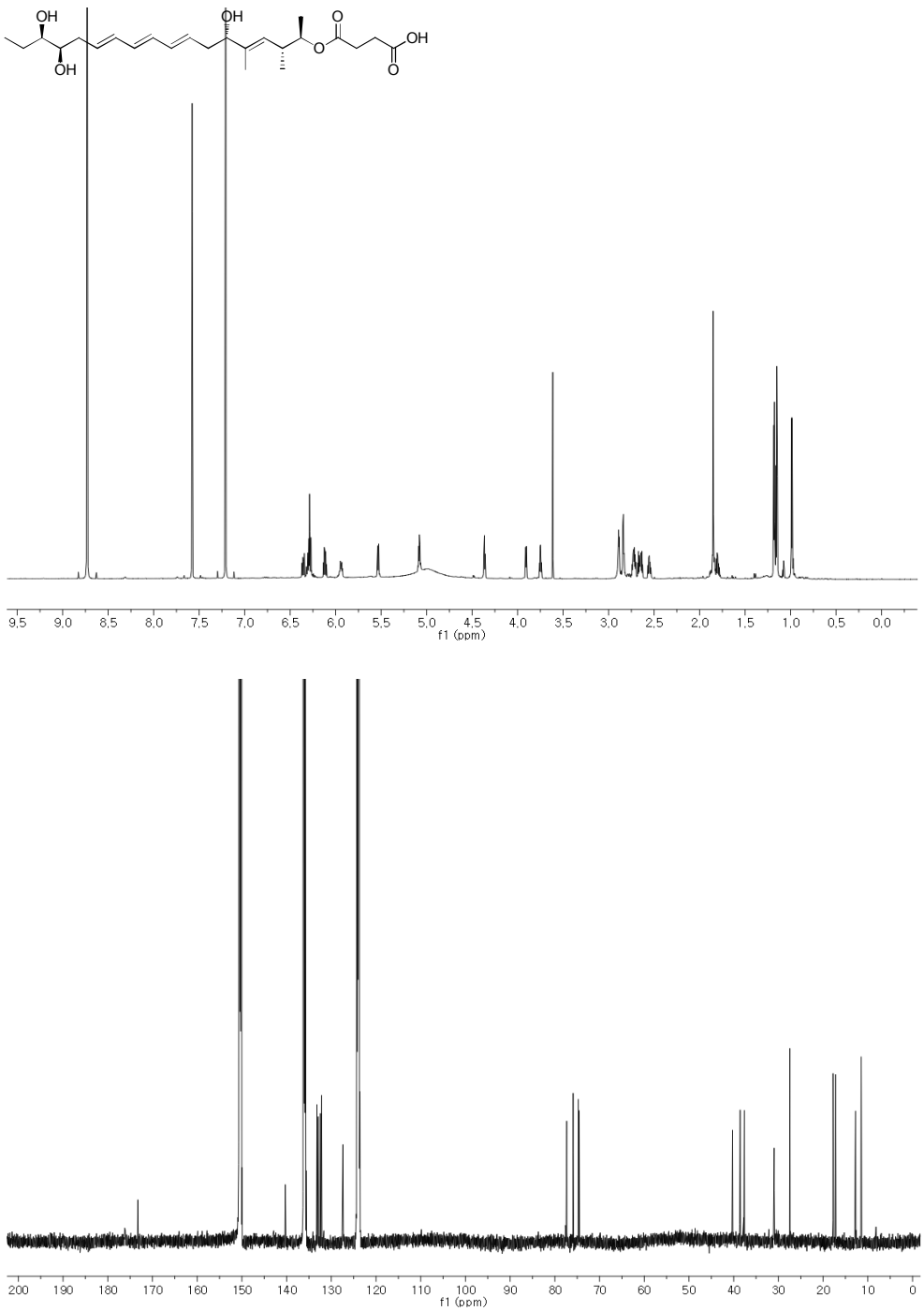

Figure A15. ^{1}H and ^{13}C NMR spectra of compound **28**.

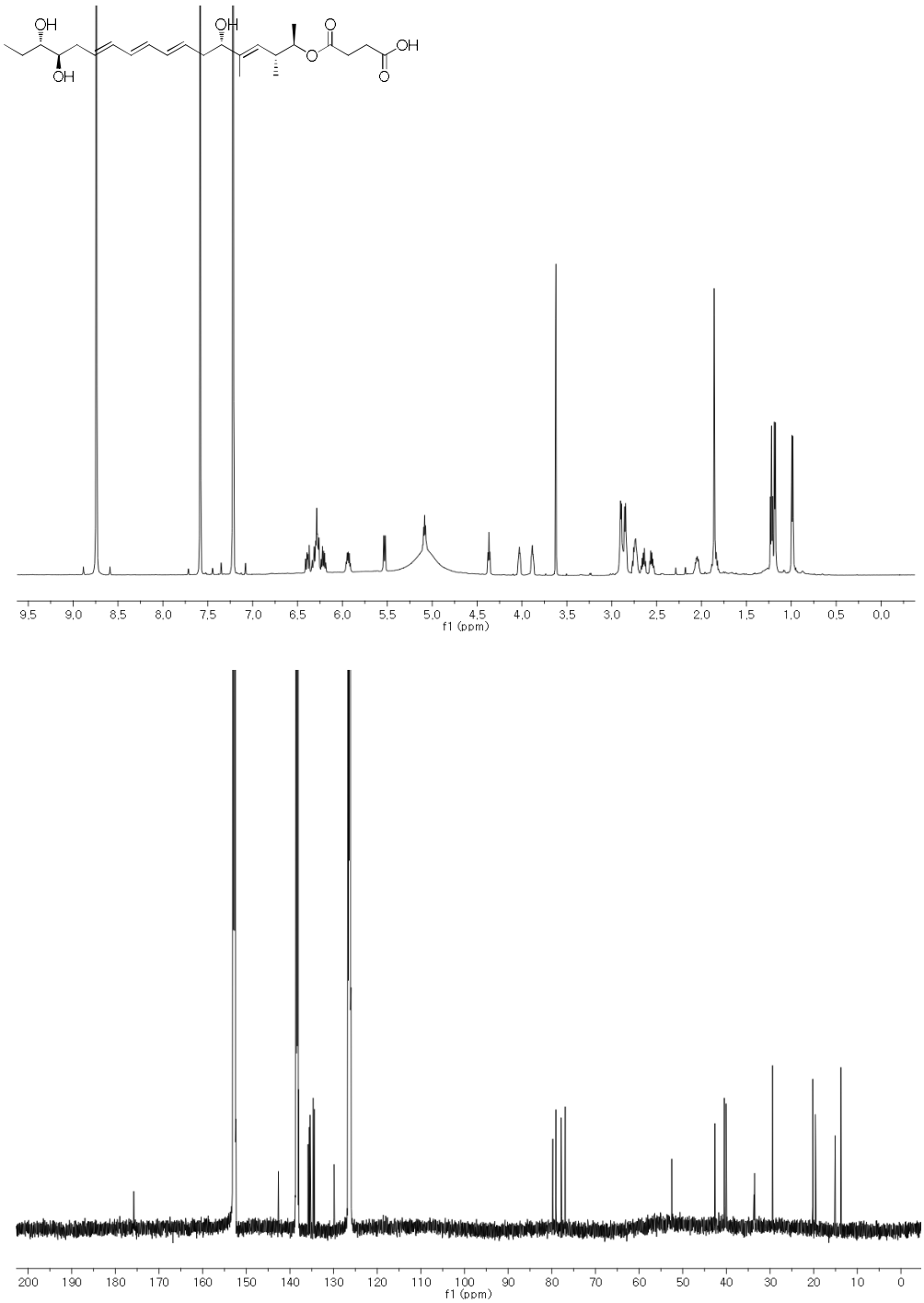

Figure A16. ^{1}H and ^{13}C NMR spectra of compound **29**.

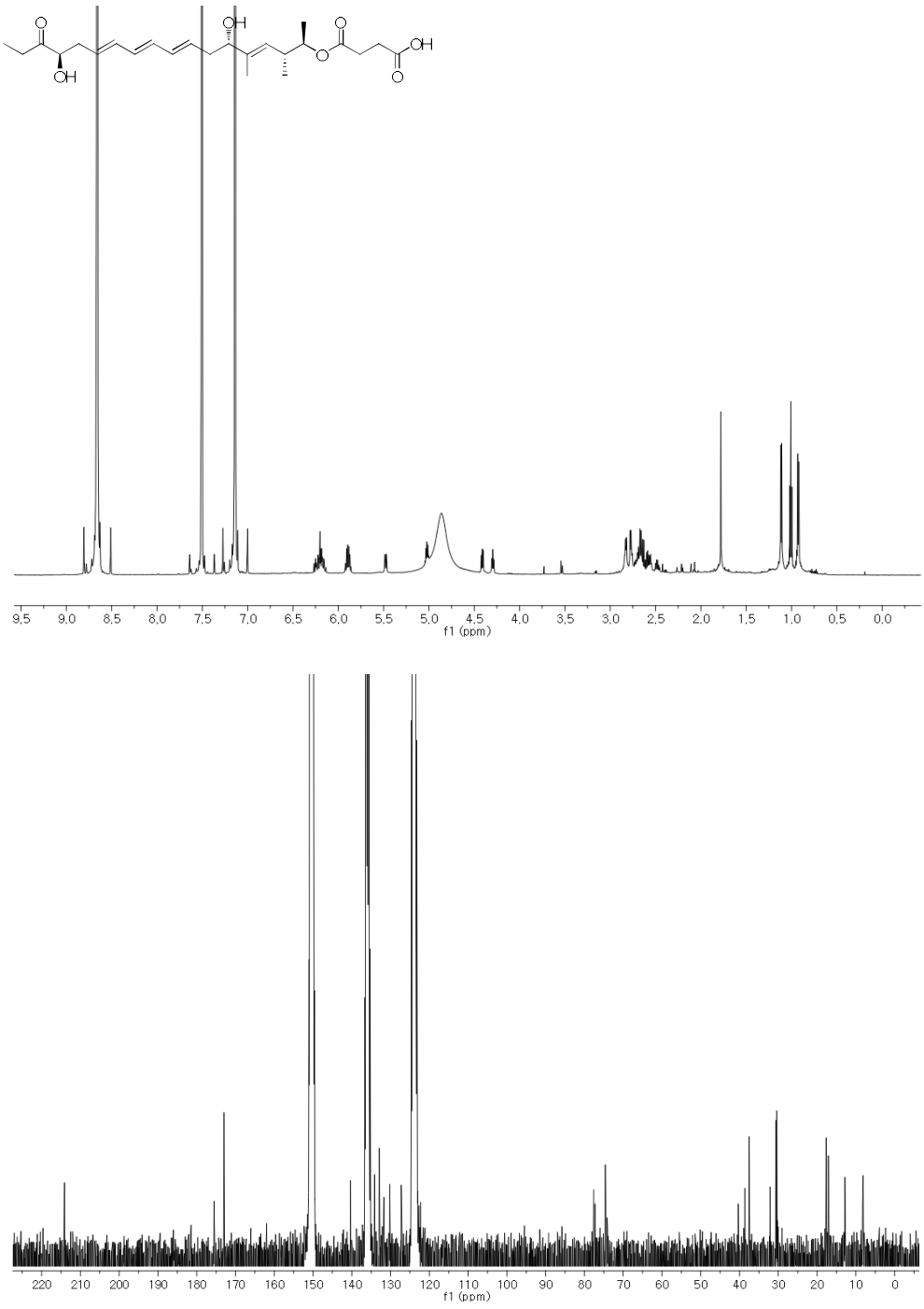

Figure A17. ^{1}H and ^{13}C NMR spectra of compound **30**.

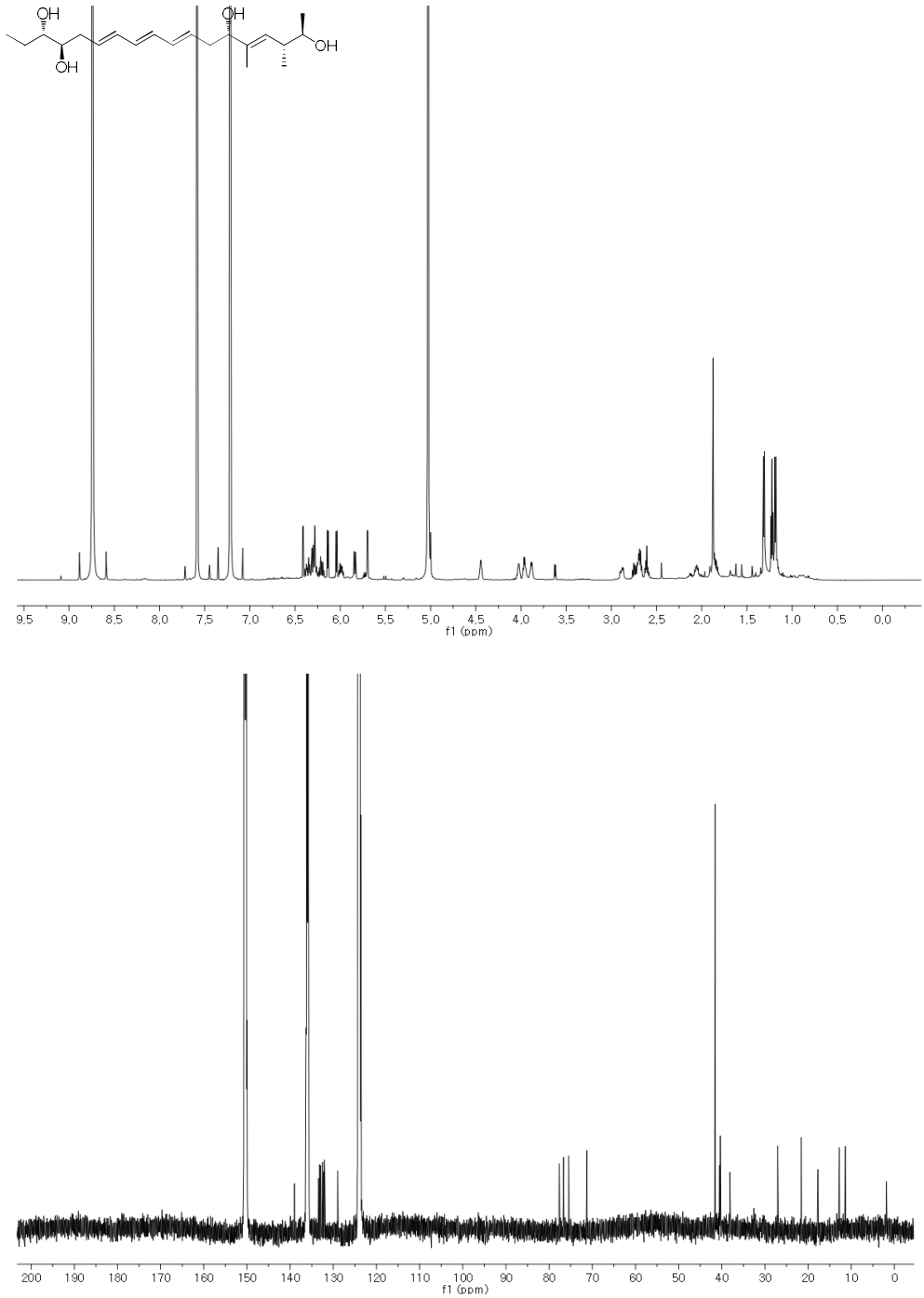

Figure A18. ^{1}H and ^{13}C NMR spectra of compound **40**.

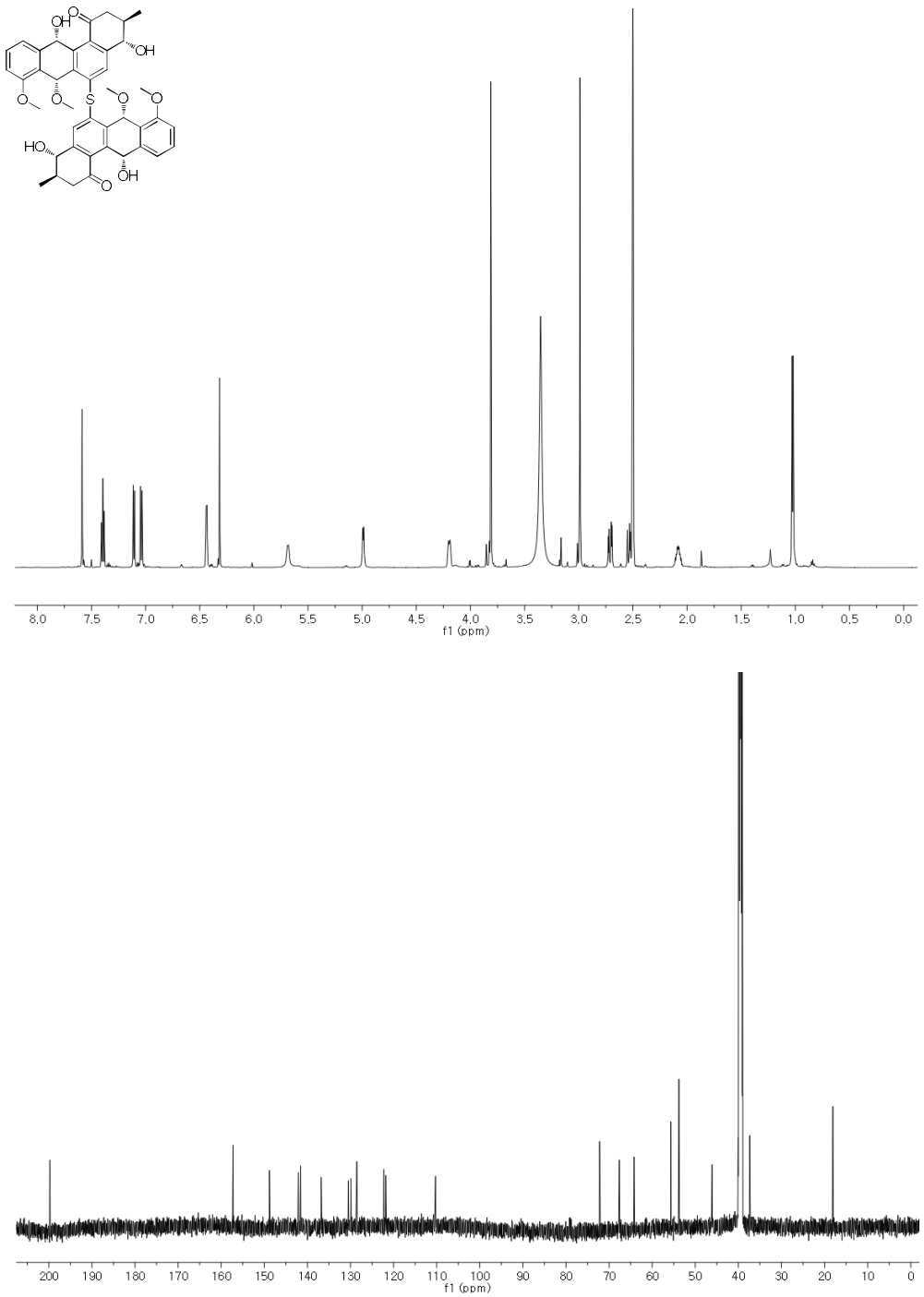

Figure A19. ^{1}H and ^{13}C NMR spectra of compound **41**.

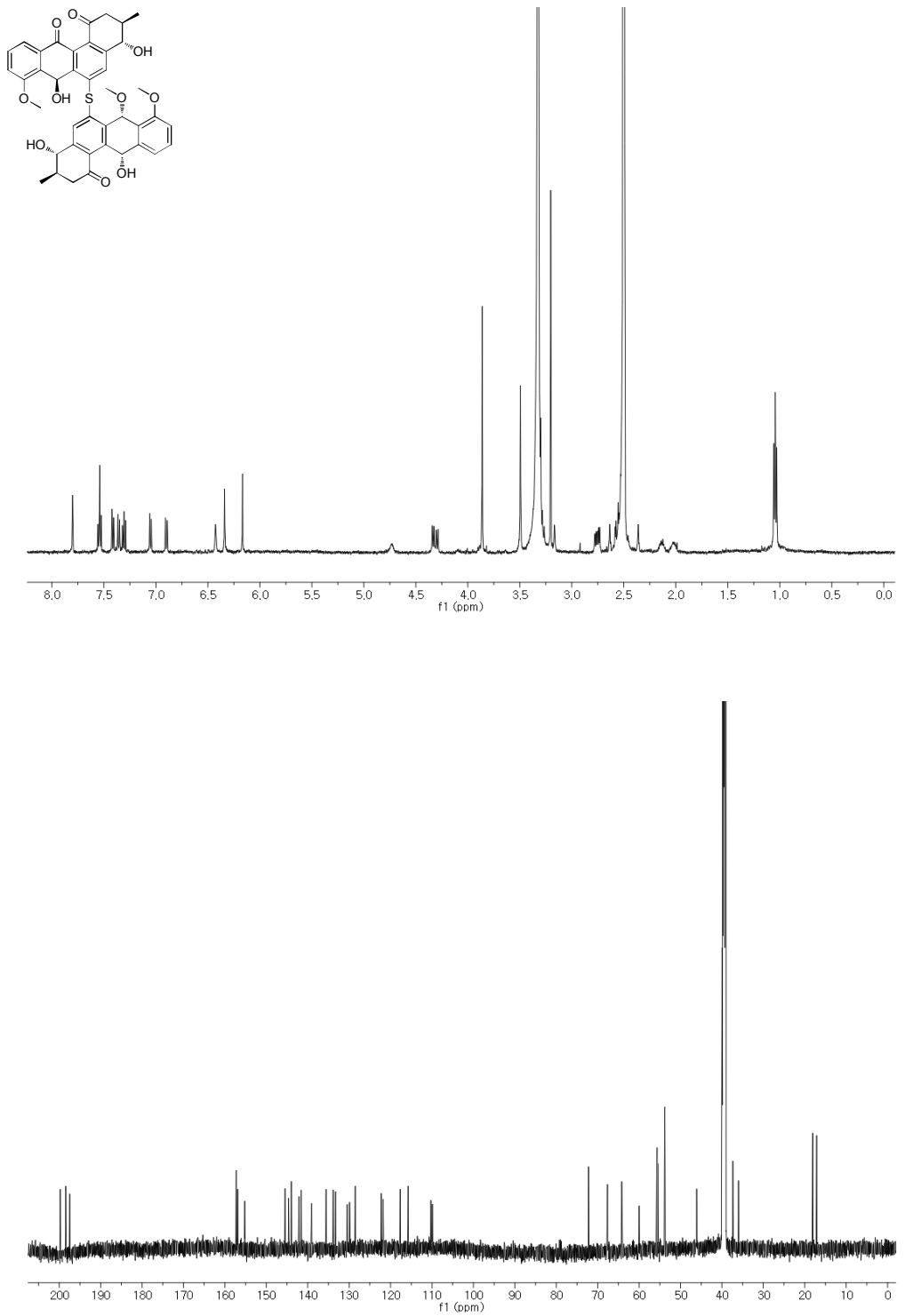

국문초록

해양 유래 방선균에서 분리한 peptides와 polyketides 신규 활성 물질에 대한 연구

배문형
서울대학교 약학대학 대학원
천연물과학전공

해양 유래 미생물로부터 신규 활성 물질을 발견하고자 하는 노력의 일환으로 생물학적 다양성의 집합지인 갯벌과 독특한 고유의 특성을 지닌 화산섬 지역에서 유력한 이차대사산물 생산 균주들을 분리하였다.

Part A. 기존에 연구가 충분히 이루어 지지 않았던 갯벌 유래 스트렙토마이시스 균주들로부터 분리한 신규 펩타이드 생리활성 물질의 탐색에 집중하여 총 8 개의 신규 펩타이드와 6 개의 기지 물질을 발견하였다. 이들의 구조는 분광학적 분석과 다양한 화학 반응 및 컴퓨터를 이용한 계산을 통해 규명 및 동정하였고 분리된 물질은 dilactone 으로 연결된 pseudo-dimeric peptide 2 종, WS9326 물질군에 속하는 peptide 4 종, cyclic depsipeptide 2 종인 것으로 밝혀졌다. 해당 물질들은 다양한 생리활성 실험을 실시하여 주목할만한 효소 저해활성, 혈관생성억제활성, 항박테리아 활성 결과를 얻었다.

Part B. 바다에 둘러쌓인 화산섬인 제주도 및 울릉도 지역에서 분리한 스트렙토마이시스 균주로부터 총 11 개의 신규 폴리케타이드 생리활성 물질을 발견하였다. 이들의 평면구조 및 입체구조는 분광학적 분석과 화학 반응 및 컴퓨터를 이용한 계산을 통해 규명하였고 분리된 물질은 *p*-aminophenonic acid 신규물질 5 종, succinic acid 를 포함하는

triene polyol 4 종, dimeric benz[*a*]anthracene 2 종인 것으로 밝혀졌다. 이들 중 몇몇은 주목할만한 항염증 활성과 혈관생성억제 활성을 보였다.

주요어 : 스트렙토마이시스, 펩타이드, 폴리케타이드
학번 : 2013-30506

Publication List

1. Sengupta, S.*; Bae, M.*; Oh, D.-C.; Dash, U.; Kim, H. J.; Song, W. Y.; Shin, I.; Sim, T. “Total synthesis of baulamycin A: Stereochemical revision, structure elucidation and structure-activity relationship” *J. Org. Chem* ASAP (*co-first author).

2. Bae, M.; Park, S.; Kwon, Y.; Lee, S. K.; Shin, J.; Nam, J.-W.*; Oh, D.-C.* "QM-HiFSA-aided structure determination of succinlilens A-D, new triene polyols from a marine-derived *Streptomyces* sp." *Mar. Drugs* **2017**, *15*, 38 (*co-corresponding author).

3. Bae, M.; Chung, B.; Oh, K.-B.; Shin, J.; Oh, D.-C. “Hormaomycins B and C: new antibiotic cyclic depsipeptides from a marine mudflat-derived *Streptomyces* sp.” *Mar. Drugs* **2017**, *13*, 5187-5200.

4. Kim, C. S.; Bae, M.; Oh, J.; Subedi, L.; Suh, W. S.; Choi, S.-Z.; Son, M. W.; Kim, S. Y.; Choi, S. U.; Oh, D.-C.; Lee, K. R. “Anti-neurodegenerative biflavonoid glycosides from *Impatiens balsamina*” *J. Nat. Prod.* **2017**, *80*, 471-478

5. Bae, M.; Moon, K.; Kim, J.; Park, H.-J.; Lee, S. K.; Shin, J.; Oh, D.-C. “Mohangic acids A-E, *p*-aminoacetophenonic acids from a marine mudflat-derived *Streptomyces* sp.” *J. Nat. Prod.* **2016**, *79*, 332-339.

6. Human, Z. R.; Moon, K.; Bae, M.; de Beer, Z. W.; Cha, S.; Wingfield, M. J.; Slippers, B.; Oh, D.-C.*; Venter, S. N.* "Antifungal *Streptomyces* spp. associated with the infructescences of two *Protea* spp. in South Africa" *Front*. *Microbiol*. **2016**, *7*, 1657 (*co-corresponding author).

7. Bae, M.; Kim, H.; Moon, K.; Nam, S.-J.; Shin, J.; Oh, K.-B.; Oh, D.-C. "Mohangamides A and B, new dilactone-tethered pseudo-dimeric peptides inhibiting *Candida albicans* isocitrate lyase" *Org*. *Lett*. **2015**, *17*, 712-715.

8. Kwon, Y.; Kim, S.-H.; Shin, Y.; Bae, M.; Kim, B.-Y.; Lee, S. K.; Oh, K.-B.; Shin, J.; Oh, D.-C. "A new benzofuran glycoside and indole alkaloids from a sponge-associated rare actinomycete, *Amycolatopsis* sp." *Mar*. *Drugs* **2014**, *12*, 2326-2340.

9. Bae, M.; Kim, H.; Shin, Y.; Kim, B. Y.; Lee, S. K.; Oh, K.-B.; Shin, J.; Oh, D.-C. "Separacenes A-D, novel polyene polyols from the marine actinomycete, *Streptomyces* sp." *Mar*. *Drugs* **2013**, *11*, 2882-2893.

Reproduced from [Bae, M.; Kim, H.; Moon, K.; Nam, S.-J.; Shin, J.; Oh, K.-B.; Oh, D.-C. *Org. Lett.* **2015**, *17*, 712-715.]

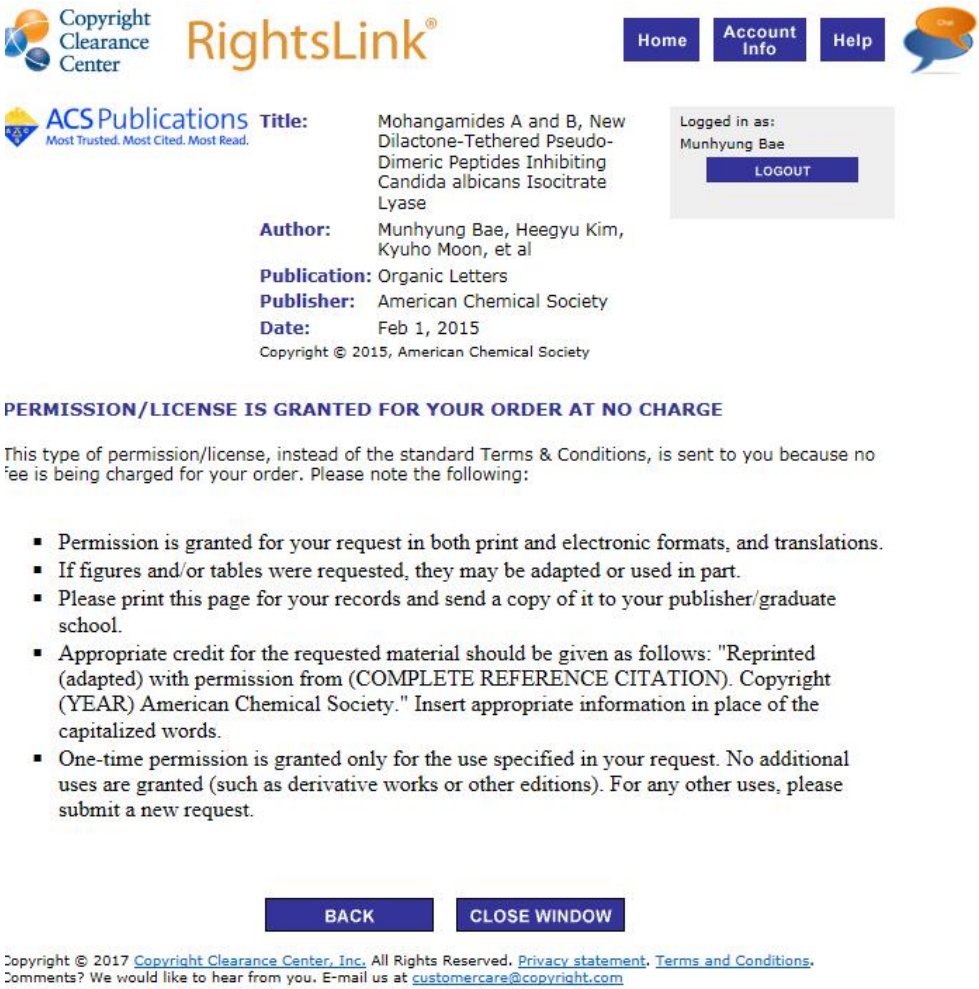

Copyright Clearance Center RightsLink®

Home | Account Info | Help

ACS Publications Most Trusted. Most Cited. Most Read.

Title: Mohangamides A and B, New Dilactone-Tethered Pseudo-Dimeric Peptides Inhibiting Candida albicans Isocitrate Lyase

Author: Munhyung Bae, Heegyu Kim, Kyuho Moon, et al

Publication: Organic Letters

Publisher: American Chemical Society

Date: Feb 1, 2015

Copyright © 2015, American Chemical Society

Logged in as: Munhyung Bae

LOGOUT

PERMISSION/LICENSE IS GRANTED FOR YOUR ORDER AT NO CHARGE

This type of permission/license, instead of the standard Terms & Conditions, is sent to you because no fee is being charged for your order. Please note the following:

- Permission is granted for your request in both print and electronic formats, and translations.
- If figures and/or tables were requested, they may be adapted or used in part.
- Please print this page for your records and send a copy of it to your publisher/graduate school.
- Appropriate credit for the requested material should be given as follows: "Reprinted (adapted) with permission from (COMPLETE REFERENCE CITATION). Copyright (YEAR) American Chemical Society." Insert appropriate information in place of the capitalized words.
- One-time permission is granted only for the use specified in your request. No additional uses are granted (such as derivative works or other editions). For any other uses, please submit a new request.

BACK | CLOSE WINDOW

Copyright © 2017 Copyright Clearance Center, Inc. All Rights Reserved. Privacy statement. Terms and Conditions.
Comments? We would like to hear from you. E-mail us at customercare@copyright.com

Reproduced from [Bae, M.; Moon, K.; Kim, J.; Park, H.-J.; Lee, S. K.; Shin, J.; Oh, D.-C. *J. Nat. Prod.* **2016**, *79*, 332-339.]

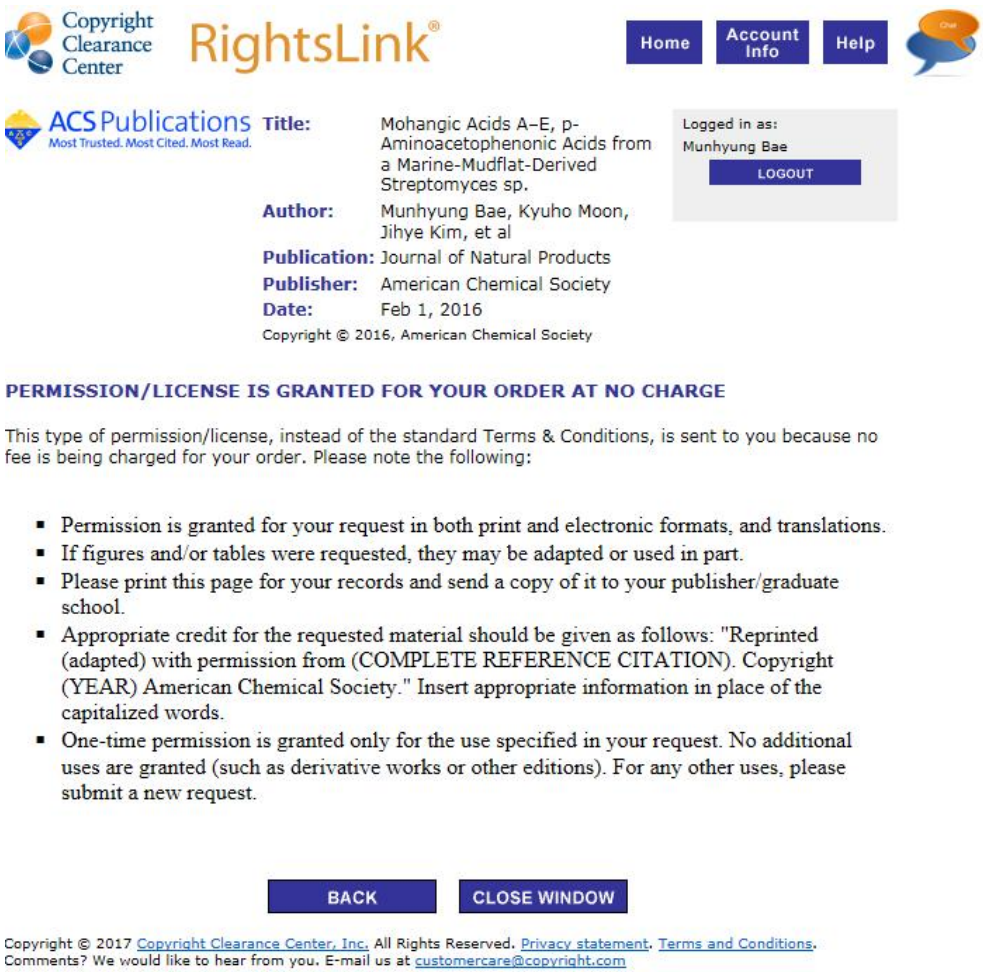

Copyright Clearance Center RightsLink®

Home | Account Info | Help

ACS Publications
Most Trusted. Most Cited. Most Read.

Title: Mohangic Acids A–E, p-Aminoacetophenonic Acids from a Marine-Mudflat-Derived Streptomyces sp.

Author: Munhyung Bae, Kyuho Moon, Jihye Kim, et al

Publication: Journal of Natural Products

Publisher: American Chemical Society

Date: Feb 1, 2016

Copyright © 2016, American Chemical Society

Logged in as:
Munhyung Bae
LOGOUT

PERMISSION/LICENSE IS GRANTED FOR YOUR ORDER AT NO CHARGE

This type of permission/license, instead of the standard Terms & Conditions, is sent to you because no fee is being charged for your order. Please note the following:

- Permission is granted for your request in both print and electronic formats, and translations.
- If figures and/or tables were requested, they may be adapted or used in part.
- Please print this page for your records and send a copy of it to your publisher/graduate school.
- Appropriate credit for the requested material should be given as follows: "Reprinted (adapted) with permission from (COMPLETE REFERENCE CITATION). Copyright (YEAR) American Chemical Society." Insert appropriate information in place of the capitalized words.
- One-time permission is granted only for the use specified in your request. No additional uses are granted (such as derivative works or other editions). For any other uses, please submit a new request.

BACK | CLOSE WINDOW

Copyright © 2017 Copyright Clearance Center, Inc. All Rights Reserved. Privacy statement. Terms and Conditions.
Comments? We would like to hear from you. E-mail us at customercare@copyright.com